SACLANTCEN
Conference Proceedings No. 5

PART II

SESSIONS 4 – 6
INFORMAL PRESENTATIONS,
CONCLUSIONS AND RECOMMENDATIONS
OF THE CONFERENCE

GEOMETRICAL ACOUSTICS (RAY TRACING)

Proceedings of a Conference held at SACLANTCEN
on 27–30 September 1971

Organized by

BRIAN W. CONOLLY and RICHARD H. CLARKE

15 DECEMBER 1971

VIALE SAN BARTOLOMEO 400
I – 19026 – LA SPEZIA, ITALY

SACLANTCEN

CONFERENCE PROCEEDINGS NO. 5

NORTH ATLANTIC TREATY ORGANIZATION
SACLANT ASW RESEARCH CENTRE
Viale San Bartolomeo 400
I 19026 - La Spezia, Italy

GEOMETRICAL ACOUSTICS (RAY TRACING)

Proceedings of a Conference held at SACLANTCEN
on 27-30 September 1971

PART II

Sessions 4-6.
Informal Presentations,
Conclusions and Recommendations
of the Conference

Organized by

Brian W. Conolly and Richard H. Clarke

15 December 1971

ATTENDEES — AUTHOR INDEX (page numbers in parentheses)

ATTENDEES — AUTHOR INDEX (Cont'd)

L.B. Palmer	(307)	NRL, Washington, U.S.
G. Pazienza		USEA, San Terenzo, La Spezia, Italy
E. Pichon	(49)	LDSM, Le Brusc, France
R.H. Prager		SACLANTCEN
R.L. Reeves	(114) & (323)	NSSC, Washington D.C., U.S.
J.G. Schothorst		NDRO, TNO, The Hague, Netherlands
L.P. Solomon	(114)	Tetra Techn. Inc., Arlington, Va., U.S.
C.W. Spofford	(228)	Bell Telephone Labs., Whippany N.J., U.S.
J.H. Stockhausen		SACLANTCEN
T. Strarup	(108)	DDRE, Copenhagen, Denmark
G. Tacconi		MARIPERMAN, La Spezia, Italy
P.R. Tatro		ONR, Washington D.C., U.S.
R Thiele		Forschungsanstalt der Bundeswehr für Wasserschall und Geophysik, Kiel, Germany
M. Thompson	(37)	SACLANTCEN
S. Toft		DDRE, Copenhagen, Denmark
M.J. van der Scheur	(345)	NDRO, TNO, The Hague, Netherlands
W.S. van Langeweyde	(302)	Forschungsanstalt der Bundeswehr für Wasserschall und Geophysik, Kiel, Germany
G.C. Vettori	(150)	SACLANTCEN
H. Weinberg	(77)	NUSC, New London, Conn., U.S.
T.D. Westrup		SACLANTCEN
W. Wijmans	(37)	SACLANTCEN

AUTHORS NOT ATTENDING

I.M. Blatstein	(210)	NOL, Silver Spring, Md., U.S.
I. Roebuch	(243)	AUWE, Portland, Dorset, U.K.

TABLE OF CONTENTS

TABLE OF CONTENTS (Cont'd)

TABLE OF CONTENTS (Cont'd)

SESSION 4

EXTENSIONS OF RAY TRACING TO CAUSTICS, CONVERGENCE AND SHADOW ZONES

Session Chairman : M.J. Daintith

Session Secretary : R.H. Clarke

4.1 Status of Ray Theory Development at Naval Undersea Research and Development Center

by D.F. Gordon

4.2 A Theoretical Method for the Prediction of Underwater Explosion Pulses at Caustics

by I.M. Blatstein (read by R.M. Barash)

4.3 Intensity at Caustics

by C.W. Spofford

4.4 Special Formulation of Modified Ray Analysis for Machine Computation

by E.L. Murphy and J.A. Davis

4.5 The Effect of Gravity-Forced Oscillations at the Base of the Duct on its Effective Depth as a Channel for Acoustic Rays

by I. Roebuck (read by G. Murdoch)

STATUS OF RAY THEORY DEVELOPMENT AT NAVAL UNDERSEA RESEARCH AND DEVELOPMENT CENTER

by

D.F. Gordon
Naval Undersea Research and Development Center
San Diego, California, U.S.

INTRODUCTION

The first part of this paper discusses NUC (Naval Undersea Research and Development Center) work on the accuracy and validity of ray theory. By comparing the range to convergence zones as indicated by experiment and by theory, we have found which techniques are required to make accurate ray computations.

By comparing computations done by ray theory and normal-mode or wave theory, we can determine the limits to the accuracy of ray theory at low frequencies.

The final portion of this paper discusses new developments in ray theory.

CONVERGENCE ZONE RANGE

The range to the leading edge of the convergence zone can be determined very accurately experimentally. This is partly because the average travel time to the leading edge of the zone is very insensitive to minor variations in the velocity profile and can be used to measure range accurately, and partly because of the rather abrupt increase in sound pressure at the zone. The range

at which the propagation loss decreases to less than 95 dB has been used to indicate the leading edge of the zone because at frequencies of a few kiloHertz this loss is clearly distinguishable from bottom returns. It is, therefore, interesting to compare this range with the range to the first zonal caustic of ray theory.

Pedersen and Anderson gave a paper on this topic at the 28th Naval Symposium on Underwater Acoustics. Figure 1 is a summary of portions of that paper. The figure indicates average results from a number of Pacific locations. The jagged line indicates a possible experimentally observed convergence zone edge. The three vertical lines represent computed losses at caustics with their characteristic shape and indicate the range relative to the true zone. This leading caustic is formed by rays which travel downward from the source and upward to the receiver.

Early attempts to compute the range to this caustic, used sound velocities computed from Kuwahara's tables. Several trials gave ranges which averaged 1.5 kyd short of the zone, as indicated in fig. 1. Altering the profile to simulate the effect of earth curvature shortened the range an additional 600 yd as shown.

The advent of Wilson's equations for the computation of sound velocity increased the range to computed caustics and the correction for earth curvature became an asset rather than a liability The caustic line labelled "Wilson" indicates the average relative position of computed caustics from 12 different locations in the Pacific. This average position is about 500 yd beyond the true convergence zone. However, by applying a caustic correction taken from Brekhovskikh, the difference between theory and experiment is reduced by half.

The final step in Pedersen and Anderson's investigation was to make an adjustment in sound velocities to fit a portion of Wilson's data which includes those ranges of temperature, salinity, and pressure

found in the Pacific. This gave sound velocities which were smaller at shallow depths and larger at greater depths than those obtained from Wilson's equations by amounts up to 1 ft/s. The median difference between computed and experimental convergence zone ranges became zero. This is shown by the diffraction curve labelled "Wilson adjusted". These results indicate in a statistical sense that the current methods for computing convergence zone ranges have no significant bias. Although the average of the differences is zero, their scatter is not. Fifty percent of the differences were less than 360 yd. The largest difference was over 4 kyd.

RAY AND NORMAL-MODE THEORY

Figure 2 shows two profiles of special form for which both ray and normal-mode computations can be made. Comparisons will be made between computations made by the two theories. On the left is an Epstein layer which is a five-parameter function of hyperbolic cosines and tangents. It has been fitted to an Indian Ocean velocity profile. The curve has two vertical asymptotes, one at 1636 and one at 1753 yd/s. To simplify certain aspects of the problem, computations were done without the surface, so the profile is shown extending above the surface.

On the right side of the figure is a four-layer approximation to an Atlantic profile in which the squared index of refraction is linear in each layer. Normal-mode computations for this profile at 10 Hz and 30 Hz were published by Tolstoy and Clay in JASA in 1960.

Figure 3 compares propagation loss as computed in three different ways for the Epstein layer. Since no surface or bottom is included in this profile model, only energy trapped in the duct by diffraction is seen at the zones. Only two caustics appear at each zone. With surface reflection, three additional caustics would appear. The source and receiver are at depths of 33 yd and 100 yd and the frequency is 30 Hz. The channel axis is at 1589-yd depth.

The normal-mode theory gives the most accurate solution for this idealized duct. The inability of the simple ray theory to compute diffraction effects is apparent. In the modified ray theory Brekhovskikh's caustic correction has been applied to each caustic and the results, which are Airy functions, have been added in random phase. A possible explanation for the difference between the mode and modified ray theory results is that the caustic corrections were not added in phase.

The next four figures will compare ray and mode theory for the four-layer Atlantic profile. Mode theory will be shown for 10 Hz, 30 Hz, and 100 Hz. Figure 4 is a ray diagram for a source at 500-yd depth and the upper 500 yd is shown. Rays are drawn at each 1° in source angle with the rays that just penetrate into the surface duct and just graze the bottom included. The range is to 100 kyd and includes one convergence zone.

The leading caustic runs from 54 upward to 62-kyd range before it encounters the surface. A similar caustic is formed by the rays which start upward at the source. Three additional caustics are formed by the surface-reflected rays, the last between 70 kyd and 73 kyd.

Figure 5 shows propagation loss contours as computed by normal modes for precisely the same situation as was used on the ray diagram, except that an extra 100 yd in depth is shown. The frequency is 10 Hz. The two refracted caustics and the final surface-reflected caustic from the previous figure are shown by broken lines. Note that the leading caustic from the ray diagram from 54 kyd to 57 kyd approximately parallels the 80 and 90-dB contours. Note also the surface-image effect which depresses the 90-dB contour in the zone deeper than 50 yd from the surface.

The 110-dB contour appears to be influenced by the surface duct which has a depth of 153 yd. However, judging from the next figure, this is not a result of the surface duct which is too small at this frequency to have any large effect upon the loss.

Figure 6 is the same as Fig. 5 but for 30 Hz. Here the leading caustic lies partly within the 80-dB contour. The second refracted caustic lies near the string of 80-dB contours. The 90-dB contour comes within about 25 yd of the surface at this frequency.

At 10-Hz frequency the 110-dB contour in the near field extended to 28 kyd range. Here it reaches only 21 kyd. It seems more reasonable to attribute this difference to differences in diffraction into the shadow zone than to attribute it to propagation in the surface duct which should be stronger at the higher frequency.

Figure 7 shows the contoured field at 100 Hz. Here definite surface duct propagation is seen. This surface duct can trap one mode at 100 Hz so this propagation is not unexpected. The effect of the surface duct can be seen in the 90, 100, and 110-dB contours in and following the direct field and in the 100 and 110-dB contours following the zone. The zone itself, as outlined by the 90-dB contour, is only slightly larger than the ray theory zone bounded by the first refracted caustic and the last surface-reflected caustic between 54 and 73-kyd range.

Some phase interference or Lloyd-mirror beats can be seen near 10 kyd. They were at somewhat shorter range for the lower frequencies.

These figures have shown several limitations of ray theory at low frequencies. Diffraction from caustics and shadow zones is important as is the interaction between ducts such as the SOFAR duct and surface duct. This interaction between ducts can remain important at higher frequencies. The surface image or surface decoupling effect must be considered.

NEW TECHNIQUES

Three items under current development at NUC are generalized velocity functions, two-dimensional velocity variation, and numerical quadrature.

In March 1968, Pedersen published his generalized ray theory in JASA. This theory uses depth as a function of velocity to represent the velocity profile. The function can be a polynomial, a power series, or a series in non-integral powers of velocity. This makes it possible to fit velocity profiles directly with polynomials of any required degree or to use standard profile forms by expanding velocity as a power series in depth and then inverting the power series. By using non-integral powers of velocity, Pedersen was able to develop a theory of the axial ray published in JASA in January 1969. This ray theory requires the use of elliptic integrals. However, new developments have determined the range and travel time as a power series, making elliptic integrals unnecessary. A report by Pedersen and White on this development was given at the recent International Acoustic Congress in Budapest.

In another new development, White and Keir at NUC have developed a method of determining ray fields with two-dimensional velocity variations. This is done by transformations on the depth and range axes. This technique gives theoretical examples of two-dimensional velocity variation which can approximate various realistic situations and also can give models to test numerical ray tracing programs.

In May 1971, Mr Edward R. Floyd of NUC published an article in JASA on ray tracing by Gaussian quadrature. This method again allows a polynomial of arbitrary degree to be fitted to all given velocity points and thereby avoids false caustics. It is not yet clear whether this method can give sufficient accuracy for computing intensities from detailed velocity profiles. However, it appears to be well suited for quick approximations to range and travel time.

SUMMARY

The range to convergence zones can be accurately computed if accurate velocity profiles which are independent of range are known, and if earth curvature and diffraction from the caustic are taken into consideration.

The technique of comparing ray and mode solutions for identical velocity profiles gives valuable information on the validity of ray theory for finite wavelengths.

New work includes power series expansions for a general class of velocity profiles, velocity-depth transformations to simulate two-dimensional velocity variation, and numerical quadrature.

DISCUSSION

Bartberger had also encountered convergence difficulties using Gaussian quadrature even with 25 points. The author felt, however, that numerical techniques were now available which might make the method usable.

In reply to a question concerning the continued use of the random-phase addition of modes, the author said that certain results to be found in Brekhovskikh's work now made this unnecessary.

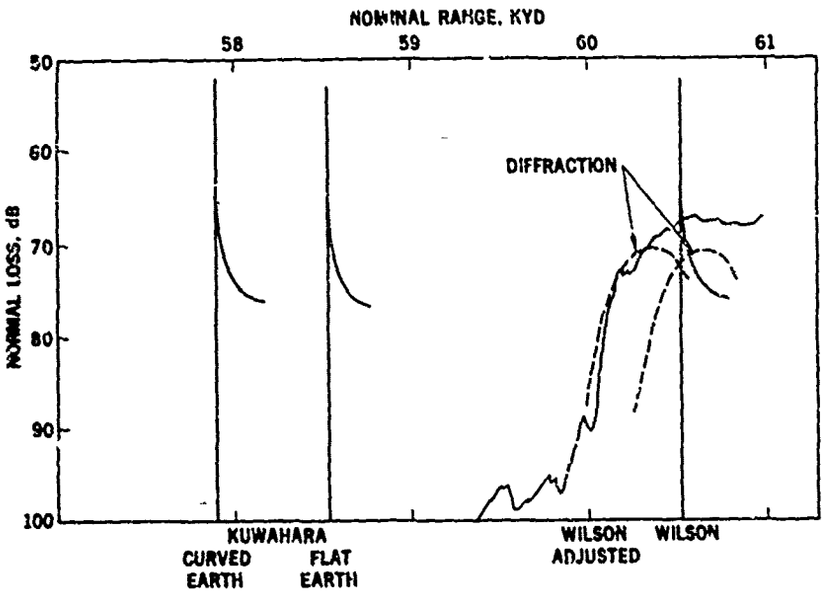

FIG. 1

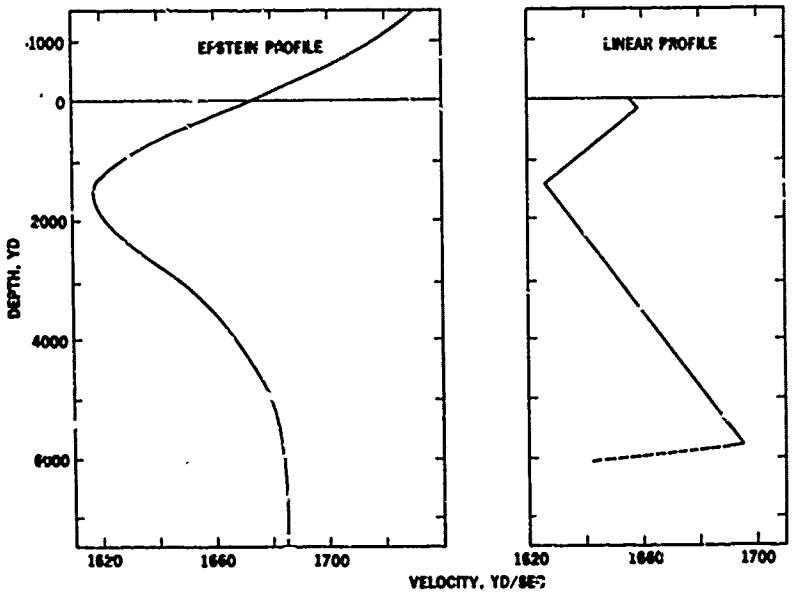

FIG. 2

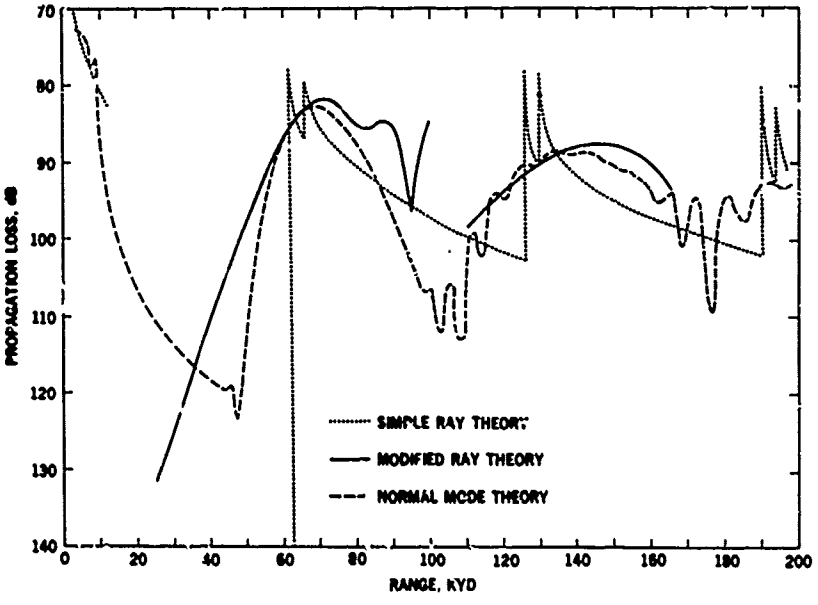

FIG. 3

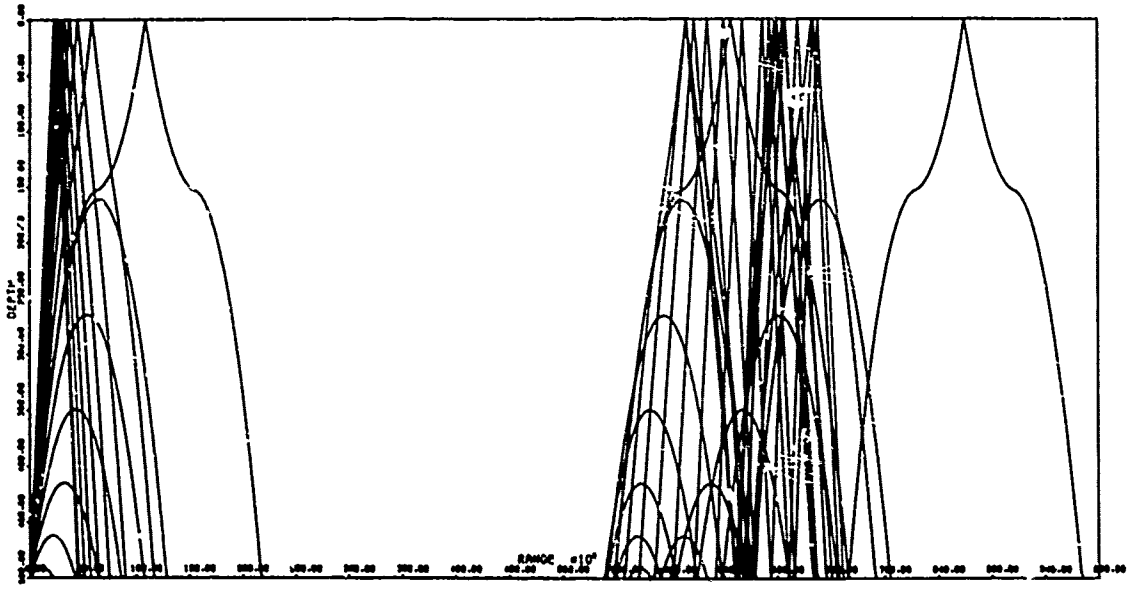

FIG. 4

FIG. 5

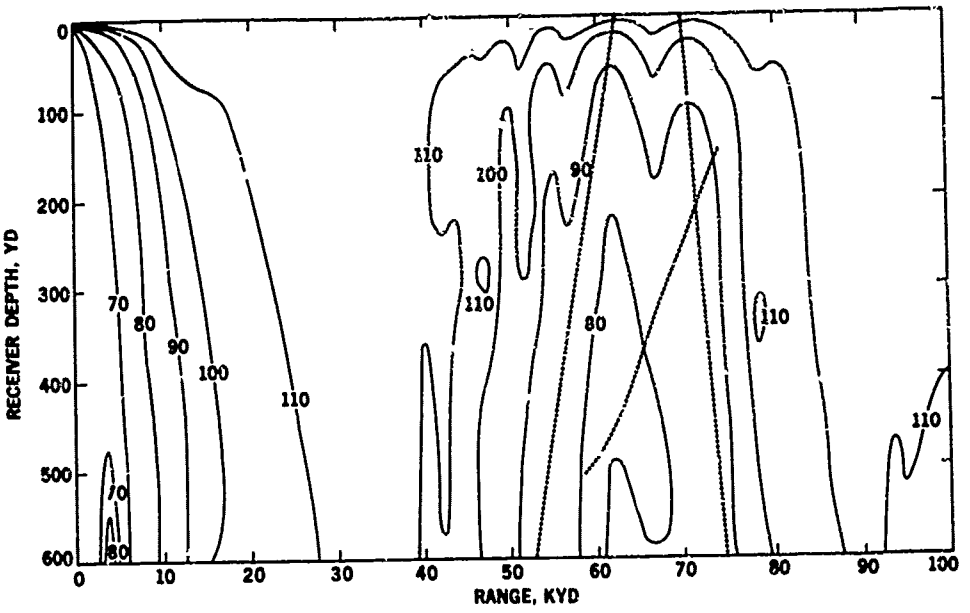

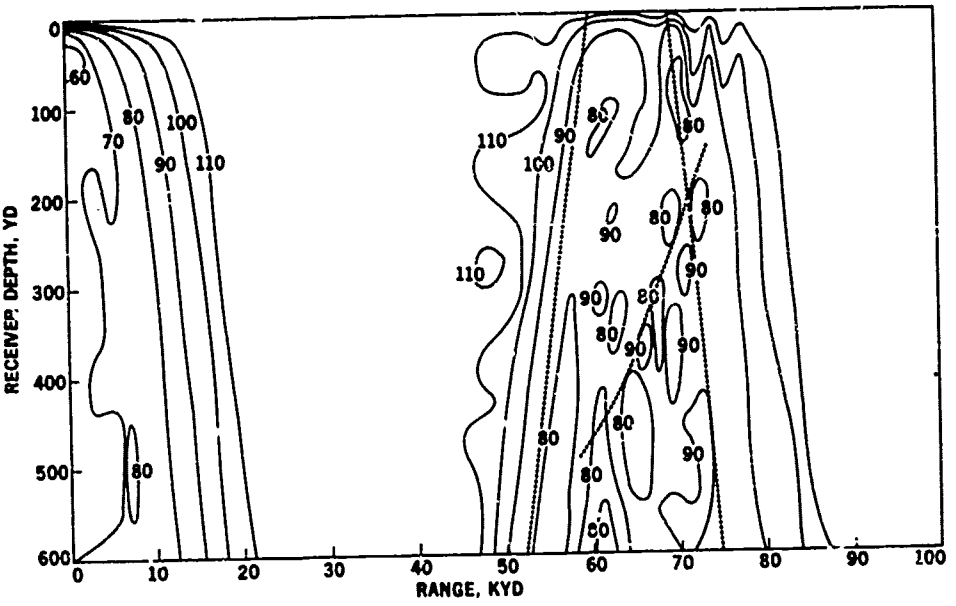

FIG. 6

FIG. 7

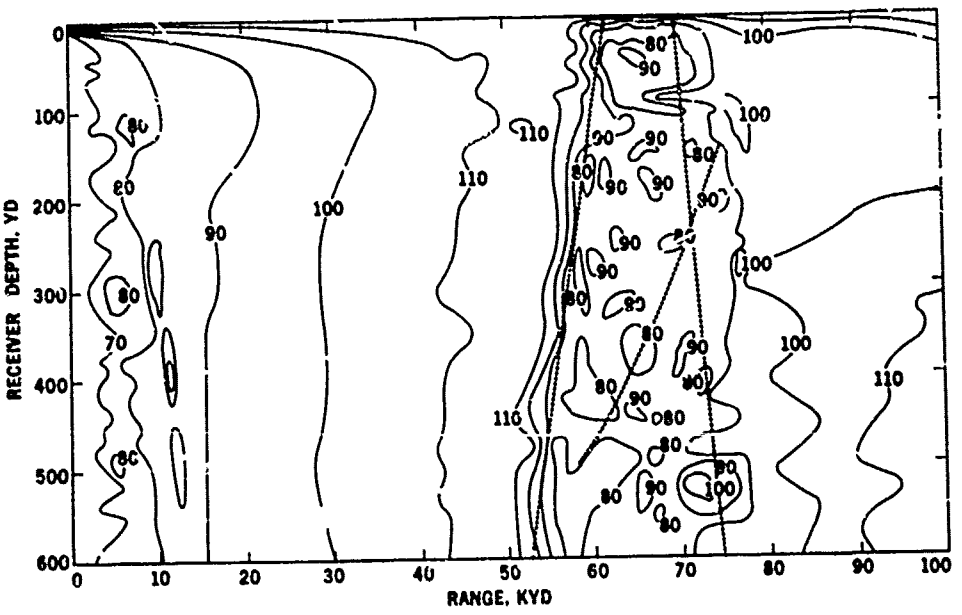

A THEORETICAL METHOD FOR THE PREDICTION OF UNDERWATER EXPLOSION PULSES AT CAUSTICS

by

I.M. Blatstein
(read by R.M. Barash)

Naval Ordnance Laboratory
White Oak, Silver Spring, Maryland, U.S.

Our concern [Refs. 1 and 2] is with the effect of refraction on the long range propagation of underwater explosion shock waves. Here, as with accustic sources, ray tracing can be used to predict refraction effects. From the divergence or convergence of rays, an amplification factor can be calculated. This is defined as the square root of the ratio of the cross sectional area between rays at a given point assuming spherical spreading to the cross sectional area between rays at the same point when the actual sound velocity profile is specified. We can then multiply the pressure history expected at a given point if no refraction occurred by the appropriate amplification factor. This then gives us the pressure history expected at that point when refraction is accounted for.

However, the amplification factor is inversely proportional to the square root of the cross sectional area between adjacent rays. So as we approach a caustic, where these rays cross, the amplification factor reaches infinity, and ray theory is invalid. Furthermore, in the shadow zone adjacent to the caustic, ray theory predicts zero energy penetration. This is due to the high frequency nature of the ray theory approximation. So if we are interested in the pressure near a caustic or in an adjacent shadow zone a method other than ray theory must be used.

In this paper, I will describe such a method for calculating shock wave pressure histories in and near caustic regions. This method involves the incorporation of various propagation effects into a Fourier series representation of the initial shock wave from an underwater explosion. I will then describe comparisons that have been made between calculated pressure histories and experimental results from ocean and flooded quarry tests. Figure 1 shows a typical ray diagram for the ocean case which we have considered. Here the source explosion is at a depth of 1000 ft. The convergence zone caustic then occurs at 20 mi to 30 mi from the source. If the source is deeper, in or just below the thermocline, a thermocline related caustic occurs. This shows up at 2 mi to 5 mi and is due to upward starting rays. The flooded quarry test that we have considered was intended to model this thermocline related caustic. For both cases, comparisons will be shown, agreement will be praised, and discrepancies will be sullenly discussed. Finally, I will talk about the accuracy of ray theory near the caustic, a region where it is known to break down.

A starting point for our work was a solution to the wave equation that has been done at various times in slightly different forms by Brekohvskikh [Ref. 3], Tolstoy [Ref. 4], and in this case, Sachs and Silbiger [Ref. 5], [Fig. 2]. The wave equation is solved for a harmonic source and an arbitrary depth dependent sound velocity profile. First they arrive at a ray solution, where each term in the sum corresponds to an arrival reaching the point of interest after leaving the source at a different initial angle. But as with any ray solution, this one breaks down on the caustic. So they do a further approximation and arrive at an expression valid at and near a caustic for a sinusoidal acoustic source. If we divide this expression by the pressure expected at that point assuming spherical spreading, we get an amplification factor valid at a caustic [Fig. 3].

Most of the quantities in the amplification factor are constants of the propagation path. These are determined once the sound velocity

profile, source depth, and point of interest are given. The expression also contains the Airy function, a function of both frequency through $k^{2/3}$ and distance off the caustic through Δr. For a given source frequency, the Airy function, and so the amplification factor, falls off exponentially as we move to the left of the caustic into the shadow zone. As we start moving to the right of the caustic, which is located at $\Delta r = 0$, the amplification factor at first increases. Further to the right we see an oscillating function. This is the result of two arrivals interfering in what is familiar to us in ray theory as the double arrival region. From an asymptotic expression for the Airy function, it can be shown that one arrival is approaching the caustic and has been amplified. The other arrival is receding from the caustic. It has been amplified and also phase shifted by 90°. While this information about phase shifts and amplitudes is difficult to verify in the resultant signal from a sinusoidal source, it is more readily seen in the resultant signal from a transient such as a shock wave. We will see this in some of the figures.

Now that we have a frequency dependent amplification factor, we need to apply it to a shock wave. Our next step is to describe the shock wave in a frequency dependent manner. This has to be done in such a way that we describe what the shock wave would look like at the range of the caustic if no refraction occurred. Then we can incorporate our amplification factor into the pressure history in order to account for refraction.

We represent the initial shock wave as an abrupt rise to a peak pressure followed by an exponential decay [Fig. 4]. We then write the Fourier series for the pulse. This way it is expressed in a frequency dependent manner. In this figure, the amplitude of the shock wave is normalized to one. In general, we will need both a peak pressure, P_1, and a decay constant, θ, to determine the pulse shape and series. We would like these parameters to be characteristic of the range of interest and also to take into account the finite amplitude effects that are present in the propagation of a shock wave.

We do this by using the similitude, or scaling, equations which were discussed in the companion paper by Barash and Goertner [Ref. 6] (see Sect. 3 of these Proceedings). Since these equations are based on cube root scaling, they properly account for the finite amplitude effects on the peak pressure and decay constant. However, they have not been verified out to the 30 mi range at which we need P_1 and θ. So we use them to a range where they are known to be valid, and the peak pressure is low enough so that we may ignore finite amplitude effects beyond that range. The point at which we cease to account for finite amplitude effects is the range at which the peak pressure drops below 5 psi. From this point to the range of the caustic we assume acoustic spherical spreading to find P_1 and θ for our pulse.

We now have the shock wave in a frequency dependent form with the appropriate peak pressure and θ. The next step is to incorporate our amplification factor into the expression [Fig. 5].

The expression at the top of the figure is the Fourier series for the pressure history with refraction added. P_1 and θ are the pulse parameters we have just discussed. The function represented by the script f_p to the right of the summation sign is the refractive amplification factor. This along with the $\pi/4$ added to the arguments of the sine and cosine take into account the effect of refraction on the propagating pulse near the caustic. This new expression, if evaluated as it stands, would diverge. The physically unrealizable step discontinuity in the pulse would lead to an infinite spike when refraction was added. However, we have yet to take into account the attenuation of acoustic pressure disturbances that becomes important for long ranges and high frequencies. Not only is it an important effect over the long propagation path to the caustic, but it serves to force our series to converge and terminate at some finite frequency. The graph in the centre of this figure shows the relative strength as a function of wave number, k, of the refraction factor f_p and an absorption factor β. We can see that the ocean acts as a filter, damping the high frequency components

of the shock wave. Thus by adding absorption, we get the expression at the bottom of this figure for the pressure near a caustic. It is a Fourier series that now terminates at some finite frequency due to absorption. This limitation shows up as the summation now only extends to N rather than infinity. Once we find the range to the caustic for the depth of interest, and determine the absorption cut-off, N, the expression for the pressure may be thought of as being purely a function of Δr, the distance off the caustic. The next figures show pulses calculated for various Δr's, along with experimental pressure histories from the convergence zone experiment we treated [Fig. 6a]. The pulse on the right is a typical experimental record. Those on the left are calculated. For negative Δr, we are in the shadow zone. Here we see a broad, low amplitude pulse. This is a result of the action of the Airy function, which is monotonically decreasing with frequency in this region. In the caustic region [Fig. 6b], we observe a single arrival with a high amplitude and short decay time. As we move away from the caustic, the peak pressure at first grows and then starts to decrease. Also shown in the figure is the isovelocity pressure history. This is what the pressure history would look like at the range of the caustic if no refraction occurred. For larger distances off the caustic [Fig. 6c], there are two arrivals, the resultant of the two arrivals from various frequencies. The first has just been amplified and has approximately the same decay constant as the isovelocity pressure history. The second arrival has been amplified and further phase-shifted by 90°. This phase shift leads to a much shorter decay constant as seen in the figure. Thus, for a shock wave, the effect of the phase shift shows up clearly.

At this point, I have described the method for calculations near a caustic and shown qualitatively what to expect. Next, I will show the comparisons of calculated pressure histories and experimental results that have been made.

The first such comparison involves an oceanic experiment done by the Naval Ordnance Laboratory.

The purpose of this experiment was to record pressure histories in a convergence zone. Figure 1 showed an average sound velocity profile and associated ray diagram for the time period of the experiment. During the experiment, one ship set off charges of 8 lb and 900 lb of TNT in a region from near the surface to 1000 ft deep. Another ship some 30 mi away used a vertical array of more than 100 hydrophones to record pressure histories throughout the convergence zone. When the gauge array was placed so that it crossed the caustic for a given shot, pressure histories were then obtained for the shadow zone, caustic region, and double arrival region, simultaneously.

We selected five of these shots to test the method just described. We will show representative pressure histories from four of these shots.

In order to do the calculations, we must know the depth of the gauge string with respect to the caustic. For these shots, this was determined from an analysis of the experimental pressure histories. In Fig.7, the position of the gauge string for each shot is indicated on an enlarged view of the upper region of the convergence zone. We notice that there is a reflected branch of the caustic resulting from surface reflection, as well as the direct branch. Gauges at various positions will record different pressure histories due to their proximity to both branches of the caustic. For the first two shots considered, due to lack of complete data, we will only consider the contribution from the direct caustic.

We will first consider shot 151 [Fig. 8], an 8 lb shot where the gauge string was relatively deep. For shot 151, we first specify the gauge of interest, for example, the gauge near the top of the gauge string. Then we calculate the parameters needed for the amplification factor on the caustic at that depth using the given sound velocity profile and source depth. Then from this figure we determine Δr, the horizontal distance from the gauge to the caustic, and the final parameter needed.

Figure 8 contains this calculated pressure history, and the experimental record from this gauge in the shadow zone in the upper left-hand corner. Next to it is a comparison in the caustic region, and at the bottom of the slide are two comparisons in the double arrival region. In all cases the experimental record is a solid line, while the calculated record is a dashed line. In all three regions, the calculated pressure histories adequately match the experimental records. In the upper right-hand corner we have also plotted the isovelocity pressure history. This again is what the pressure history would look like at all four gauges at the range of the caustic if no refraction occurred.

Also of interest is the good agreement for relatively long times after the peak pressure. The caustic solution used in our pressure history retains some of the high frequency limitations of ray theory. This would suggest that for each arrival we could only make valid predictions near the peak pressure where high frequencies predominate. Yet these calculations yield good results beyond the point where the pressure history drops below zero and flattens out. This indicates a reasonably good description of the low frequency content of the pulse. This is probably due to the relatively small sound velocity gradients in the ocean which make the caustic solution valid for relatively low frequencies on the order of 100 Hz or less. This low frequency validity should extend to ray theory as well, despite the often made remark that ray theory is valid for high frequencies only.

The next shot we consider is shot 82 [Fig. 9], an 890 lb explosion at 1000 ft. The same general agreement between experimental records and calculated pressure histories is evident. In the records closest to the caustic, [Figs. 9b & 9c], gauge case ringing is very severe and interferes somewhat with the comparisons.

Now we will consider the two shots where both the direct and reflected arrivals were recorded. A gauge at the bottom of the gauge string for shot 120 is in the double arrival region of the direct branch caustic and in the shadow zone of the reflected branch caustic.

Hence, we would expect arrivals due to both branches. From ray geometry we can calculate the arrival time difference, or time delay, between these arrivals from different branches. We further assume that the surface acts as a perfect reflector for the reflected arrivals, causing only a phase reversal. We then combine the resulting pulses with the appropriate time delay to find the pressure history.

Figure 10 shows comparisons of these calculated pressure histories and experimental records from the top, middle, and bottom of the gauge string. In the bottom record, the pressure history starts with a direct double arrival, which is then followed by a negative shadow zone pulse from the reflected caustic. Again the general agreement of peak pressure and wave forms is good.

As the last of the oceanic comparisons, we calculated pressure histories for shot 119, an 8 lb shot [Fig. 11]. This differed from the previous shot in that it is a smaller charge weight, and so we are dealing with pulses with a much shorter decay time. This means there is proportionately more high frequency energy. By treating records with reflected arrivals in them, we are able to test the method for considerable distances off the caustic. in Fig. 11, the reflected arrival is approximately 1600 ft horizontally into the shadow zone, and the direct double arrival is approximately 2400 ft horizontally from the direct caustic. So with one record we gain information about a region 4000 ft wide.

In all four comparisons, the calculated pressures are in reasonable agreement with the experimental values from the oceanic test. Just as important, the entire waveforms are in good agreement. So for the oceanic convergence zone case, the method is a reasonable approximation for the various phenomena involved in propagation to a convergence zone.

We also tried matching pressure records from a test conducted by Woods Hole in a flooded quarry [Fig. 12]. As I have said, this type

of test models the thermocline related caustic that may occur at 2 mi to 5 mi. For the quarry case the solution to the wave equation is not clearly valid for the frequency domain of our pulse. Not only are the sound velocity gradients 1000 times larger in the quarry than in the ocean, but the caustic is much closer to the turning points of the rays. This could tend to restrict the validity to the higher frequencies in the pulse.

Also, we have to modify the pressure expression since absorption is no longer the high frequency cut-off mechanism as it was in the ocean. Here the gauge response restricts high frequencies more than absorption, so the gauge response as a function of frequency is used in the pressure expression instead of absorption.

Pressure histories were then calculated near the caustic and in the double arrival region for a 56 lb charge detonated at 50 ft [Fig. 13]. The dashed lines are the calculated pulses, the solid lines are the experimental pressure records. While the exact agreement of the peak pressures is no doubt fortuitous, good agreement between experimental and calculated peak pressures has been obtained for similar quarry data during the course of this analysis. However, it is also apparent from this figure that the decay from the peak pressure is much too steep.

If the solution to the wave equation is indeed valid only for high frequencies for this case, it may explain why our calculations only appear reasonable near the peak pressure where high frequencies predominate. Also, it is possible that a propagation mode other than the pure refracted one contributes to the pressure at a thermocline related caustic. For example, a lateral wave type of propagation could be occurring at the interface of the almost-isovelocity upper layer in the flooded quarry. This would be energy at relatively low frequencies which would affect most the decay from the peak. Or it is possible that the surface boundary is influencing the propagation of energy in a way not accounted for by ordinary ray theory. If this

were the case, a modified ray theory such as that described by Murphy and Davis in these Proceedings might be necessary for this type of situation. Whatever the reason, the calculation of the decay of the pulse for the quarry case remains the aspect of this work that requires the most improvement.

Finally, I would like to discuss the validity of ray theory near the caustic. Qualitatively we know that ray theory predicts an increasing intensity as one approaches the caustic from the double arrival region. This intensity, which is the same for all frequencies, reaches infinity on the caustic, a line of zero width. The caustic solution that we are using yields a different picture. For this solution, the caustic is a region of finite thickness in between the shadow zone and double arrival region. The lower the frequency of the source, or the larger the charge for the transient case, the wider the caustic region is. Inside the caustic region, the solution yields one arrival that slowly increases in amplitude as one moves away from the shadow zone boundary at $\Delta r = 0$. For large distances off the caustic, the expression yields two arrivals in the pressure history. This is the double arrival region as expected from ray theory. However, since the caustic solution was derived to be valid near the caustic, it is not obvious that it should yield reasonable results far from the caustic in the double arrival region. So really there are two questions to be answered: How different are ray theory and the caustic solution in the caustic region where ray theory is supposed to be breaking down? and How do ray theory and the caustic solution compare in the double arrival region, where the caustic solution was not originally intended for use?

Referring to Fig. 14, for reasons of simplicity, calculations were done for a harmonic source rather than the pulse sources we have been treating. For the figure we have assumed a 100 Hz harmonic source and the convergence zone sound velocity profile previously shown. In the caustic region, we have combined the two ray arrivals in order to compare the resultant to the caustic solution we have

been using. As expected, as we approach the caustic, the two solutions diverge as the ray solution increases rapidly. It should be remembered that this figure holds true for the particular convergence zone profile treated. We have examined others where the caustic region was narrower, and some where the caustic region was up to three times as wide as this one is. Also shown in the figure is the double arrival region. Here we can resolve two arrivals in the caustic solution. It turns out that each one has the same amplitude, which falls off as the fourth root of Δr. We have plotted this amplitude along with those of the two ray arrivals. If we combined the caustic solution arrivals at the caustic region boundary, the resultant would match the caustic region solution at the caustic region boundary. However, what is most striking is the agreement between ray theory and the caustic solution far into the double arrival region. This explains why our calculations of pulses in the double arrival region were in good agreement with the experimental pulses. While in the double arrival region, one would tend to trust ray theory more, this figure indicates that it is not a bad approximation to continue using the caustic solution that was used in the shadow zone and caustic region.

In order to put all of these results in their proper perspective, we must keep in mind the assumptions and approximations made. We assumed that the unrefracted shock wave could be approximated by an abrupt rise followed by an exponential decay. We then wrote the Fourier series for this pulse. In the oceanic case, we assumed that a superposition of finite amplitude effects, spherical spreading, and absorption on this series would adequately describe long distance propagation in the absence of refraction. Then we added refraction effects to find the pressure near a caustic. In the quarry, the gauge response was substituted for absorption. Our ability to apply these effects separately is no doubt due to the phenomena being treated. Finite amplitude effects occur relatively close in where pressures are high. Absorption for high frequencies takes effect only over long distances. While refraction effects occur throughout the path, the major effect is the significant amplification at the convergence zone. So while these effects no doubt interfere, their major influence is individual.

The main thrust of this work has been to describe the effect of refraction on the propagation of an underwater explosion shock wave. Particularly, we are interested in calculations near the caustic where the refractive amplification is greatest. We feel that in this method we have a reasonable means of calculating just such pressure histories for the oceanic convergence zone. What I also hope has been demonstrated by this paper, and the companion one by Barash and Goertner [Ref. 6], is that an underwater explosion can be more than just a source of energy at various frequencies for acousticians interested in harmonic sources. These transient sources can also lead to analyses and information about ray theory validity that would be otherwise difficult to obtain.

REFERENCES

1. I.M. Blatstein, "Calculations of Underwater Explosion Pulses at Caustics", J. Acoust. Soc. Am., Vol. 49, p. 1568, 1971.

2. I.M. Blatstein, "Refraction of Underwater Explosion Shock Waves: Calculations of Pressure Histories in a Convergence Zone", NOLTR 71-93, Naval Ordnance Laboratory, 1971.

3. L.M. Brekovskikh, "Waves in Layered Media", Academic, New York, Ch. 6, 1960.

4. I. Tolstoy and C.S. Clay, "Ocean Acoustics", McGraw-Hill, New York, Ch. 2, 1966.

5. D. Sachs and A. Silbiger, "The Focusing of Harmonic Sound and Transient Pulses in Stratified Media", J. Acoust. Soc. Am., Vol. 49, pp 824-840, 1971.

6. R.M. Barash and J.A. Goertner, "Experimental Data on the Refraction of Underwater Explosion Pulses". Paper presented at Conference on Geometrical Acoustics at SACLANT ASW Research Centre, La Spezia, Italy, 27-30 Sept 1971.

7 R.R. Brockhurst, J.G. Bruce and A.B. Arons, "Refraction of Underwater Explosion Shock Waves by a Strong Velocity Gradient", J. Acoust. Soc. Am., Vol. 33, No. 4, pp 452-456, 1961.

DISCUSSION

During the discussion the points were made that in a sense one was "saved by absorption", that taking more terms in the Fourier series expansion would not help, and that the use of a mix of linear and non-linear properties, although expedient, may not be valid at large distances.

SOUND VELOCITY PROFILE AND RAY DIAGRAM FOR A CONVERGENCE ZONE CAUSTIC

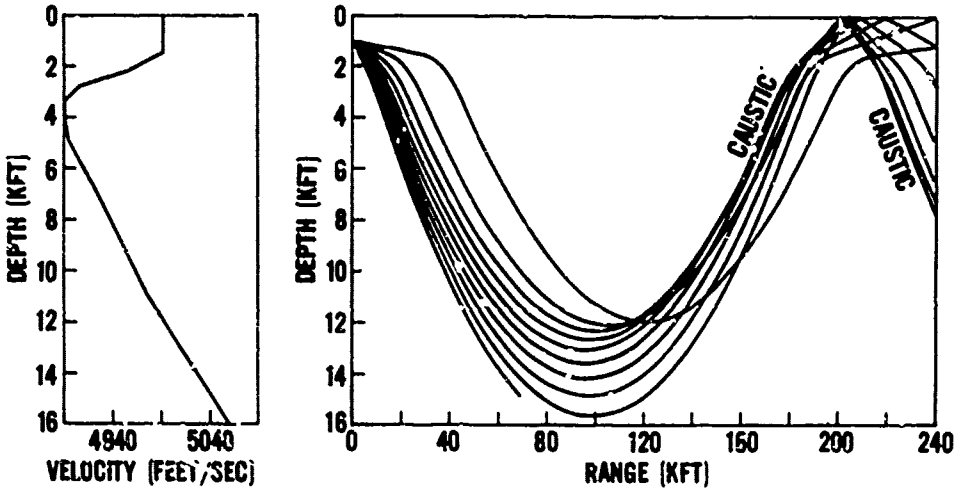

FIG. 1

SAMPLE VELOCITY PROFILE AND RAY DIAGRAM INDICATING WAVE EQUATION SOLUTION PARMETERS (AFTER SILBIGER)

FIG. 2

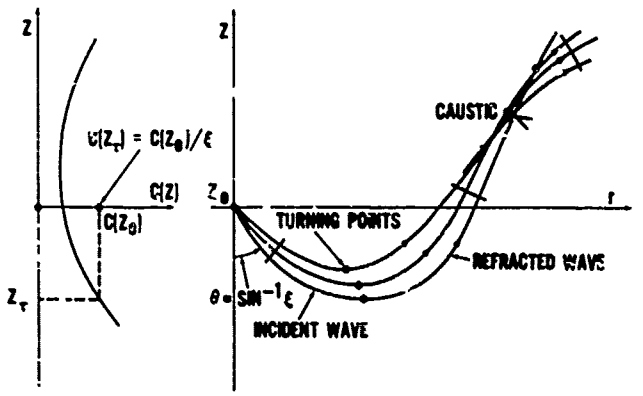

SOURCE: $P_S = P_0 \cos(\omega t)$

WAVE EQTN: $\nabla^2 P + K^2 n^2(Z) P = P_0 \delta(x)\delta(y)\delta(z)$

SOLUTION FOR PRESSURE IN THE CAUSTIC REGION:

$$P(r, Z_0) = \frac{P_0}{4\pi} K^{1/6} \zeta \left[\frac{2\pi\xi_c}{r_c (n^2(Z) - \xi_c^2)^{1/2} (1 - \xi_c^2)^{1/2}} \right]^{1/2} A_i(\pm K^{2/3} \zeta \Delta r) e^{iKW_c - i\pi/4}$$

AMPLIFICATION FACTOR

$$f_p(k,\tau) = Rk^{1/6}\zeta\left[\frac{2\pi\xi_c}{r_c(n^2-\xi_c^2)^{1/2}(1-\xi_c^2)^{1/2}}\right]^{1/2} Ai(\pm k^{2/3}\zeta,\tau)$$

where $Ai(\pm\rho)$ for $W'''_c \le 0$

FIG. 3

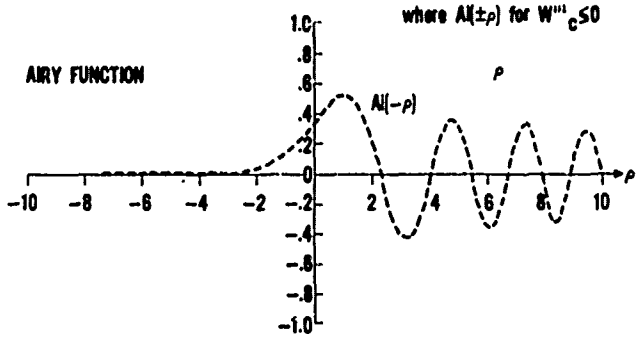

THE REGION OF DEFINITION FOR THE EXPONENTIAL DECAY REPRESENTED BY A FOURIER SERIES

SIMILITUDE EQUATIONS

$P_s(R,W) = 2.16 \times 10^4 (W^{1/3}/R)^{1.13}$ (PSI) $\quad P(t) = 0 \quad -C<t<0$

$\theta_s(R,W) = .096W^{1/3}(W^{1/3}/R)^{-.22}$ (MSEC) $\quad P(t) = e^{-t/\theta} \quad 0<t\le C$

R IS IN FEET, W IS IN LBS.

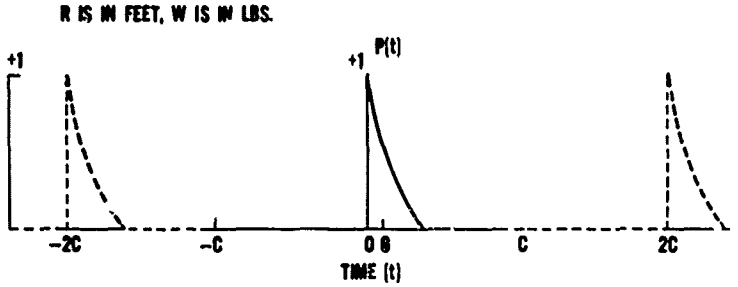

FIG. 4

PRESSURE HISTORY WITH REFRACTION

$$P_R(t) = P_1\left(B_0 + \sum_{q=1}^{\infty} f_p(k,\tau)B(q)\cdot\left[\frac{a}{\theta}\cos\left(\frac{q\pi t}{a}+\frac{\pi}{4}\right)+q\pi\sin\left(\frac{q\pi t}{a}+\frac{\pi}{4}\right)\right]\right).$$

WHERE $B(q) = \left[\frac{\theta^2}{a^2+(q\pi\theta)^2}\right]\left[1-(-1)^q e^{-\frac{a}{\theta}}\right]$

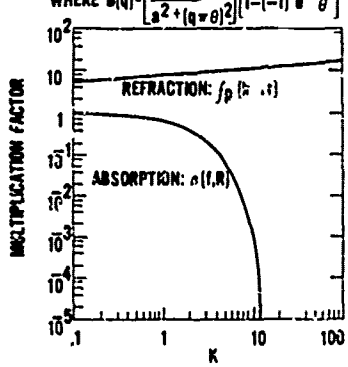

FIG. 5

PRESSURE HISTORY WITH REFRACTION AND ABSORPTION:

$$P_T(t) = P_1\left\{B_0 + \sum_{q=1}^{N} f_p(k,\tau)\sigma(f,R_1)B(q)\cdot\left[\frac{a}{\theta}\cos\left(\frac{q\pi t}{a}+\frac{\pi}{4}\right)+q\pi\sin\left(\frac{q\pi t}{a}+\frac{\pi}{4}\right)\right]\right\}.$$

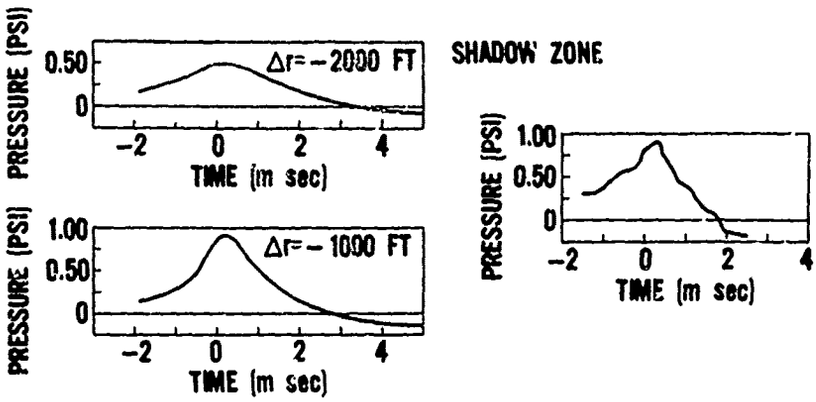

FIG. 6a

EXAMPLES OF PRESSURE-TIME HISTORIES FOR VARIOUS HORIZONTAL DISTANCES FROM A CONVERGENCE ZONE CAUSTIC

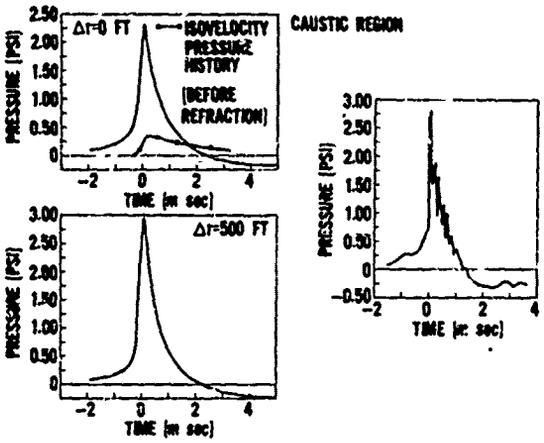

FIG. 6b

EXAMPLES OF PRESSURE-TIME HISTORIES FOR VARIOUS HORIZONTAL DISTANCES FROM A CONVERGENCE ZONE CAUSTIC

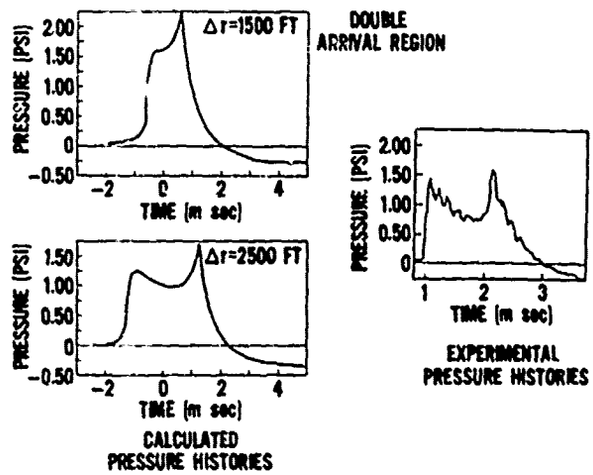

FIG. 6c

EXAMPLES OF PRESSURE-TIME HISTORIES FOR VARIOUS HORIZONTAL DISTANCES FROM A CONVERGENCE ZONE CAUSTIC

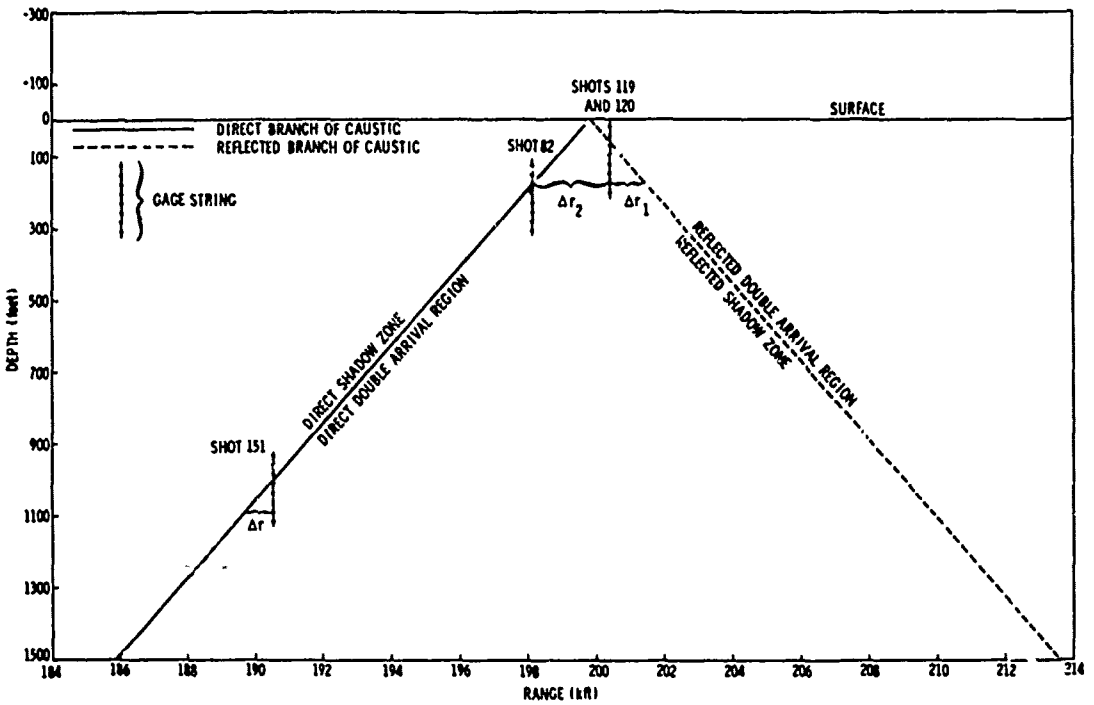

FIG. 7

THE POSITION OF THE GAGE STRING WITH RESPECT TO THE CAUSTIC FOR SAMPLE SHOTS

SHOT 151, W = 9LB., COMPARISON OF DATA AND CALCULATED PRESSURE HISTORIES.
(A) Z_g = 934 FT. (DEPTH OF GAGE), Δr = −934 FT.; (B) Z_g = 1029 FT., Δr = 379 FT
(C) Z_g = 1074 FT., Δr = 862 FT.; (D) Z_g = 1110 FT., Δr = 1152 FT.

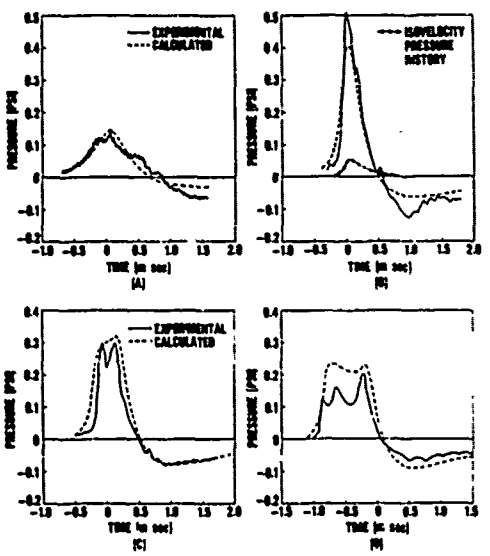

FIG. 8

SHOT 82, W = 800 LB. COMPARISON OF DATA AND CALCULATED PRESSURE HISTORIES.
(A) Z_g = 174 FT., Δr = 0 FT.; (B) Z_g = 221 FT., Δr = 303 FT.; (C) Z_g = 236 FT., Δr = 466 FT., (D) Z_g = 329 FT., Δr = 1191 FT.

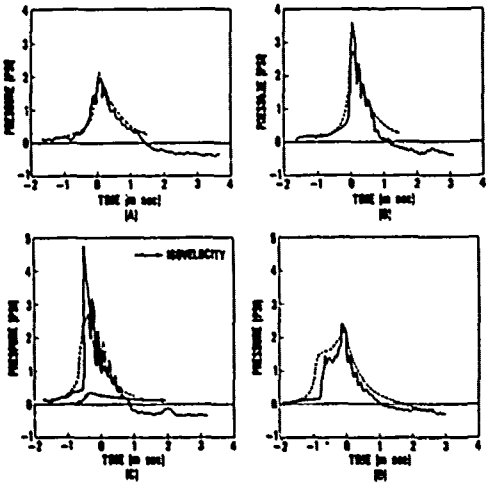

FIG. 9

SHOT 120, W=870 LB. COMPARISON OF DATA AND CALCULATED PRESSURE HISTORIES.
(A) Z_g = 44FT., Δr_2 = 604FT.; Δr_1 = −91FT.; (B) Z_g = 121FT., Δr_2 = 1219FT.
Δr_1 = −693FT.; (C) Z_g = 202FT., Δr_2 = 1861FT., Δr_1 = −1565FT.

FIG. 10

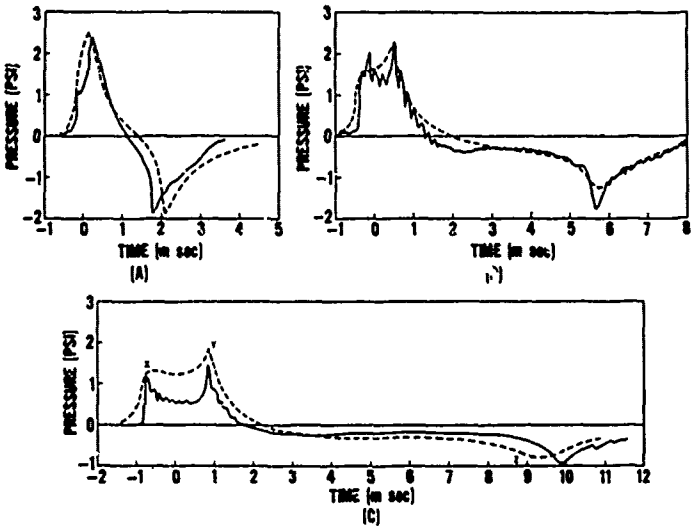

SHOT 119, W=8 LB. COMPARISON OF DATA AND CALCULATED PRESSURE HISTORIES.
(A) Z_g=2 FT., Δr_2=428 FT., Δr_1=390 FT.; (B) Z_g=59 FT., Δr_2=1062 FT.,
Δr_1=−254 FT.; (C) Z_g=202 FT., Δr_2=2365 FT., Δr_1=−1565 FT.

FIG. 11

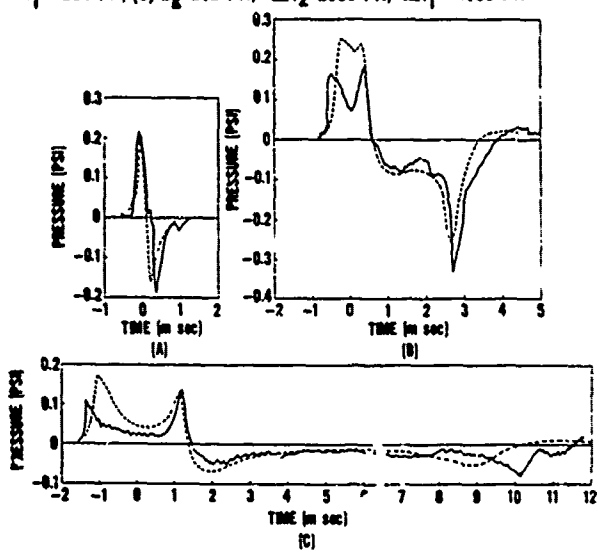

VELOCITY PROFILE AND RAY DIAGRAM FROM BLACKINGTON FARM QUARRY FOR DAY OF WHOI CASE #45

FIG. 12

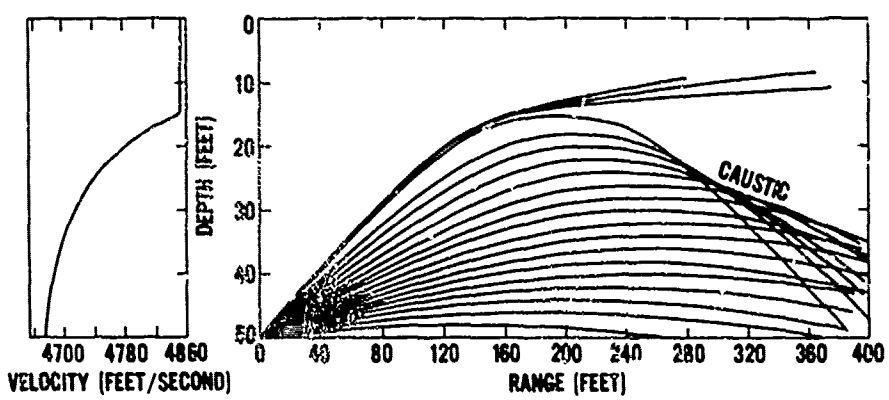

WHOI QUARRY CASE NO. 45, COMPARISON OF DATA AND CALCULATED PRESSURE HISTORIES

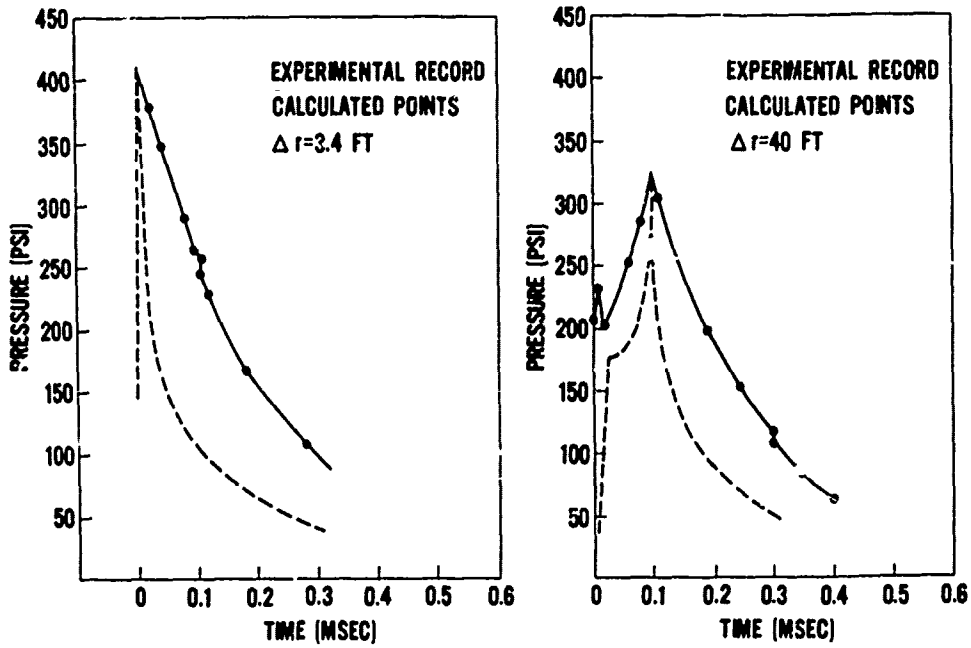

FIG. 13

COMPARISON OF RAY THEORY AND CAUSTIC SOLUTION FOR 100 Hz

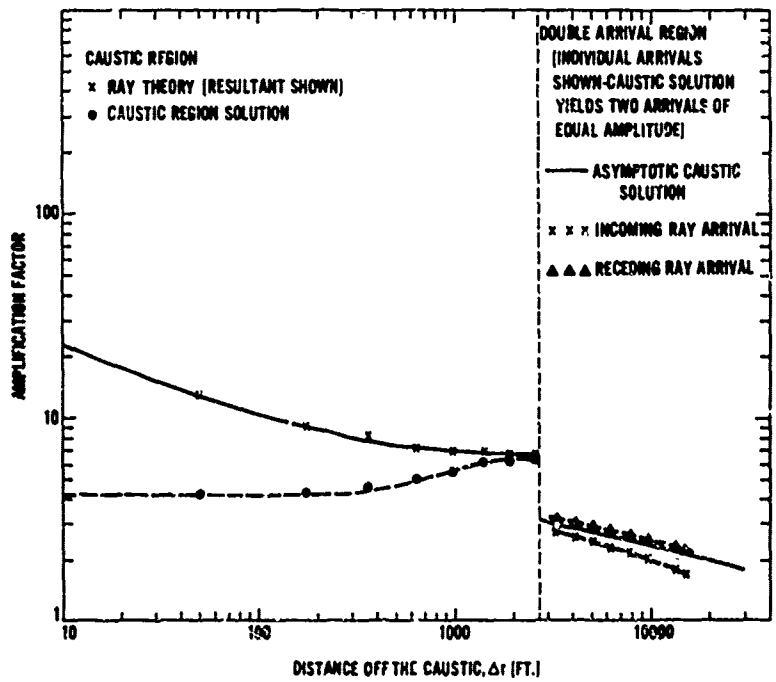

FIG. 14

INTENSITY AT CAUSTICS

by

C.W. Spofford
Bell Telephone Laboratories
Whippany, New Jersey, U.S.

The classical divergence expressions predict an infinite intensity at caustics. This infinite intensity is a fundamental limitation of geometrical acoustics (ray theory). The intensity at a caustic is of primary concern since the caustic is assumed to be the point of highest intensity within a convergence zone. Several approaches to estimating the field at a caustic have been made using stationary phase and more refined asymptotic methods.

The recent uniform asymptotics work of Ludwig and Kravtsov may be used to obtain both the intensity at the caustic and the transition from the caustic to the point where ray theory is applicable. Whereas in the context of uniform asymptotics, coherent ray theory* is the zeroth order solution (in wavenumber) to the wave equation, Ludwig shows that the first order solution is given (excluding a phase factor) by

$$\psi(\vec{r}) \sim \pi^{1/2} \{ (A_1 + A_2)\, x^{1/4}\, \mathrm{Ai}(-x) + i(A_2 - A_1)\, \bar{x}^{1/4}\, \mathrm{Ai}'(-x) \} \qquad \text{[Eq. 1]}$$

where

$$x = \left[\frac{3}{4}\, \omega(T_2 - T_1)\right]^{2/3} \qquad \text{[Eq. 2]}$$

---

* Coherent ray theory estimates intensity by adding all amplitudes on a phased basis.

and A_1, A_2, T_1, and T_2 are the amplitudes and travel times of the two rays intersecting the point of interest (R) on the illuminated side of the caustic. ω is the angular frequency, Ai and Ai' are the Airy function and its first derivative.

This result may be used to study the validity of coherent ray theory near a caustic. As one moves away from the caustic (on the illuminated side) ψ goes uniformly, with wavenumber, to the result obtained from coherent ray theory. In fact, if ψ is compared with the coherent sum of the paths (adding a $-\pi/2$ phase shift to Ray 2 after tangency to the caustic), one finds good agreement up to the last point (first point in range) of constructive interference. After this point, the coherent sum tends to infinity, whereas the uniform asymptotics result experiences an exponential decay into the shadow zone.

The intensity at the last peak is 3.5 dB greater than that at the caustic and the peak is frequently displaced from the caustic by many wavelengths. Also the position of this peak corresponds to the last point of constructive interference as given by ray theory, and the amplitude is given to within 0.5 dB by the in-phase sum of the geometric amplitudes.

The field at the caustic proper is given by

$$\psi_c \sim 2^{2/3}\,\pi^{1/2}\,\mathrm{Ai}(0)\left[\frac{c_R \cos\vartheta_S}{c_S \sin\theta_R R}\right]^{1/2}\frac{[\omega(T''' R'' - T'' R''')]^{1/6}}{(R'')^{2/3}} \qquad \text{[Eq. 3]}$$

where R'', R''', T'' and T''' are the second and third derivatives of range and travel time with respect to θ_S at fixed y_R, and θ_R is the angle at the receiver. These derivatives may be evaluated directly from the ray trace. In fact, for vertically stratified media, for which Snell's law holds, ψ_c may be written in terms of R''. The results of Fig. 1, however, suggest that it may not be necessary to evaluate Eq. 3 for the intensity at a caustic but merely calculate the coherent sum of the geometrical-acoustics amplitudes at the last point of constructive interference.

ACOUSTIC FIELD AT CAUSTICS

UNIFORM ASYMPTOTICS

$$\psi(\vec{r}) \sim \pi^{1/2} (A_1 + A_2) X^{1/4} Ai(-X) + \ldots$$

$$X = \left[\frac{3}{4} \omega (T_2 - T_1) \right]^{2/3}$$

$$\psi(R_C) = k(\theta_S, \theta_R, R_C) \frac{\left[\omega (T''' R'' - T'' R''')\right]^{1/6}}{(R'')^{2/3}}$$

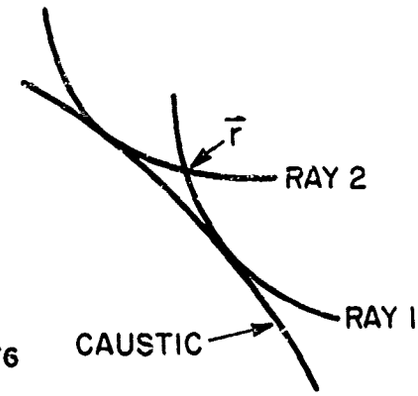

COHERENT RAY THEORY (---) VS UNIFORM ASYMPTOTICS (-)

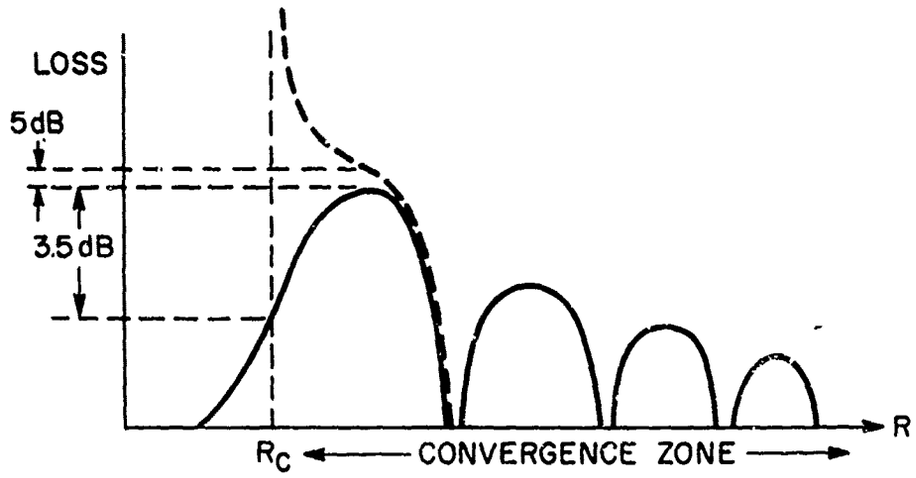

FIG. 1

SPECIAL FORMULATION OF MODIFIED RAY ANALYSIS FOR MACHINE COMPUTATION

by

E.L. Murphy
SACLANT ASW Research Centre
La Spezia, Italy

and

J.A. Davis
Woods Hole Oceanographic Institution
Woods Hole, Mass., U.S.

When the reflection coefficient for waves incident on a refracting or bounded region has a phase $\varkappa(\theta_0)$ that is a function of the angle of incidence θ_0 (measured at some reference level $Z = Z_0$), then in consequence, individual rays, or "beams" will be displaced from the location predicted by Snell's law. [See, for example, Ref.1, Ch. I). By $\varkappa(\theta_0)$ we mean phase changes other than those corresponding to the geometrical-optics phase integral along the ray path.

This phenomenon of beam displacement is the basis for modified ray analysis considered in this paper. The development of the theory is given in Refs. 2 to 5 (the nomenclature is somewhat altered for convenience from the symbols used in these references).

The problem in obtaining quantitative results lies in the determination of the reflection coefficient

$$R(\theta_0) = |R| \, e^{i\varkappa(\theta_0)} \qquad \text{[Eq. 1]}$$

for realistic sound speed profiles. In particular, the modifications of ray analysis are especially significant for rays with turning-points, or vertices, near boundaries, or near a local maximum in sound speed.

To determine $R(\theta_0)$ we use an extension of the geometrical-optics approximation in a form that can be made valid throughout regions near a vertex on a ray. This procedure does leave some freedom in the choice of the sound speed profile $c(z)$ other than those for which exact solutions are known.

The method is such that the phase, $\arg R(\theta_0) = \varkappa(\theta_0)$, and the amplitude $|R(\theta_0)|$, and many features of the modified ray analysis can be described entirely in terms of a parameter $E(\theta_0)$ determined by the integral,

$$E(\theta_0) = i\frac{2}{\pi}k_0 \int_{z_1(\theta_0)}^{z_2(\theta_0)} \sqrt{n^2(z) - \sin^2\theta_0}\, dz \qquad \text{[Eq. 2]}$$

where $n(z) = c_0/c(z)$ is the index of refraction referred to a reference sound speed $c_0 = c(z_0)$. The angle θ_0 is measured with respect to the vertical, or z-direction, at a point on the ray at reference depth $z = z_0$. The symbol k_0 is a reference wave number, $k_0 = 2\pi f/c_0$, where f is the frequency. (We are considering a formalism for a harmonic source, but we can extend the application of the results to other time functions by the use of Fourier analysis). The limits of the integral are zeros, z_1 and z_2, of the integrand for a given value of θ_0. The reason for the appearance of two zeros, z_1 and z_2, when a ray in reality has only one real vertex, say at $z = z_1$, is indicated in the sketch in Fig. 1. It turns out that modified ray results are most significant when $c(z)$, or $n(z)$, is such that there are at least two zeroes of the integrand in Eq. 2. Therefore in this paper we consider profiles with a local maximum in sound speed, or where a boundary at $z = z_b$,

as sketched above, gives rise to an "image" of the vertex at $z = z_1$. We confine our discussion to the three kinds of problems:

1) Zeros near a local maximum in sound speed (unbounded problem).

2) Zeros near a pressure release boundary.

3) Zeros near a rigid boundary.

The results for the phase $\varkappa(E)$ of the "plane wave" reflection coefficients for these three problems are as follows [see Ref. 4].

$$\varkappa(E) = -\chi(E) - \frac{\pi}{2} + \epsilon \arctan e^{\frac{\pi E}{2}} \qquad \text{[Eq. 3]}$$

ϵ = 0 unbounded
= -1 pressure release boundary
= +1 rigid boundary

where the spatial function $\chi(E)$ is given by the expression

$$\chi(E) = \frac{E}{2} - \frac{E}{2} \ln \frac{|E|}{2} + \mathrm{Im} \ln \Gamma \left(\frac{1 + iE}{2}\right) . \qquad \text{[Eq. 4]}$$

The symbol $\ln|E|$ refers to the natural logarithm of the absolute value of E. The last term is the imaginary part of the logarithm of the gamma function [see Ref. 6, Ch. 6].

In Fig. 2, these phases are plotted as a function of the parameter E. Large positive values of this ray parameter E correspond, for the bounded problems, to rays that hit the surface, and the phases approach the limits we usually associate with such boundaries when the bounded medium is homogeneous ($-\pi$ for pressure release, 0 for rigid boundary). On the other hand, large negative E-values correspond to rays with vertices far from the boundaries, and all curves for phase approach the value $-\pi/2$, the phase change for plane waves reflected in a smooth monotonic profile.

The curves are continuous and not the simple "patched-up" step function that would result if we assume $\varkappa = -\pi$ for all rays hitting the surface, or $-\pi/2$ for all rays with vertices.

The amplitude of the reflection coefficient is, of course, unity for the bounded problems, while for the unbounded problem it has the following relatively simple form,

$$|R(E)| = \frac{1}{(1+e^{\pi E})^{1/2}} \quad . \qquad \text{[Eq. 5]}$$

The formula for the displacement ΔR, of a ray that has transited a "two-turning-point" region is determined from the derivative of $\varkappa$ with respect to $\sin\theta_o$ [see Ref. 2],

$$\Delta R = -\frac{1}{k_o}\frac{d\varkappa}{d\sin\theta_o} = -\frac{1}{k_o}\frac{dE}{d\sin\theta_o}\frac{d\varkappa}{dE} \quad . \qquad \text{[Eq. 6]}$$

The derivative $d\varkappa/dE$ can be expressed as follows:

$$\frac{d\varkappa}{dE} = -\frac{d\chi}{dE} - \epsilon\frac{\pi}{4}\,\mathrm{sech}\,\frac{\pi E}{4} \qquad \text{[Eq. 7]}$$

where $d\chi/dE$ can be written in the form

$$\frac{d\chi}{dE} = -\frac{1}{2}\ell n\frac{|E|}{2} + \frac{1}{2}\,\mathrm{Re}\,\psi\left(\frac{1+iE}{2}\right) \quad . \qquad \text{[Eq. 8]}$$

The last term involves the real part of the digamma function ψ [see Ref. 6, p. 258].

Since $\varkappa(E)$, $d\varkappa/dE$, and $|R(E)|$ are functions of E only, then the preparation of computer programs for the contribution of these functions to modified ray analysis is relatively simple. We only need to program their evaluation as functions of E. When the actual sound speed profile is selected then $E(\theta_o)$ and the derivative $dE/d(\sin\theta_o)$ needed for ΔR can be evaluated separately.

In our current programs, which have been written for the Woods Hole Oceanographic Institution's SIGMA 7 computer, and Hewlett-Packard

computer, a composite linear/parabolic profile for $1/c^2$, or equivalently, for $n^2(z)$, is used. The function $n^2(z)$ and its first derivative are made continuous at some "matching" distance ρ, as sketched in Fig. 3.

In the sketch at the bottom of Fig. 3, for a more or less realistic profile, the regions in which "two-turning-point" phenomena may occur are shaded. Perhaps these programs may eventually be useful as simple subroutines added to already existing ray programs. When some "flag" tells a ray it has transited such a region, the subroutine supplies a displacement. The ordinary ray program in its usual way then continues the displaced ray until it again reaches a "diffraction" region. If the diffraction region is a region of local sound speed maximum the subroutine also supplies a change in amplitude due to leakage and splitting of rays.

The functions $\chi(E)$ and $d\chi/dE$ are the only terms in $\varkappa(E)$ and $d\varkappa/dE$ requiring special procedures for machine computation.

With series expansions for the gamma and diagamma functions [see Ref. 6, Ch. 6] inserted into Eqs. 4 and 8, $|\chi|$ and $d\chi/dE$ can be put into the form

$$|\chi| = \frac{1-\gamma}{2}|E| - 2|E|\ln 2|E| + \sum_{m=0}^{\infty}\left(\frac{|E|}{2m+1} - \arctan\frac{|E|}{2m+1}\right) \qquad \text{[Eq. 9]}$$

and

$$\frac{d\chi}{dE} = -\frac{1}{2}\ln 2|E| - \frac{\gamma}{2} + |E|^2 \sum_{m=1,3,5..}^{\infty} \frac{1}{m(m^2+|E|^2)} \qquad \text{[Eq. 10]}$$

where γ is Euler's constant,

$$\gamma = 0.57721 \ldots\ldots$$

The logarithmic terms in Eqs. 9 and 10 lead to computational difficulties since they become infinite for $E = 0$, that is for the grazing ray in the bounded case, or the split ray in the unbounded case. However, these infinities rather than being

troublesome are one of the most physically significant contributions of the modified ray analysis. The following illustration shows why. Consider a purely parabolic profile for $n^2(z)$, for example,

$$n^2(z) = a + bz^2 \ . \qquad \text{[Eq. 11]}$$

For a source and receiver at depths z_0 below the profile extremum, the ordinary ray theory result for the range R_{ray} of the ray emitted at angle θ_0 and connecting source and receiver, is given by the relation

$$R_{ray} = \frac{2 \sin \theta_0}{\sqrt{b}} \ln \frac{[z_0^2 - z_1^2]^{1/2} + z_0}{z_1} \qquad \text{[Eq. 12]}$$

where z_1 is the depth of the ray vertex below the extremum of the n^2-profile. Note the logarithmic infinity for the grazing or split-ray ($z_1 = 0$). However, for the profile of Eq. 11, the integral for E can be evaluated to give,

$$E = -k_0 \sqrt{b} \ z_1^2 \qquad \text{[Eq. 13]}$$

and, in turn,

$$-\frac{1}{k_0} \frac{dE}{d \sin \theta_0} = \frac{2 \sin \theta_0}{\sqrt{b}} \ . \qquad \text{[Eq. 14]}$$

In consequence, it follows that the logarithmic term in the displacement is of the form

$$\Delta R = \frac{2 \sin \theta_0}{\sqrt{b}} \ln (k_0^{1/2} \ b^{1/4} \ z_1) + \text{other terms} \ . \qquad \text{[Eq. 15]}$$

Therefore, in the modified range R_{MOD} defined by the relation

$$R_{MOD} = R_{ray} + \Delta R \qquad \text{[Eq. 16]}$$

the logarithmic singularities cancel leaving a finite, wavelength-dependent range. For machine computation, therefore, we remove

the logarithmic singularities from the displacement ΔR and R_{ray} before programming.

This feature of the modified ray theory that would arise for all smooth profiles (continuous derivatives in the region of the profile extremum), leads to the result that there is a split-beam shadow at finite range when modifications are included. Without the modifications every point is illuminated by a ray.

On the other hand, for a bilinear profile (discontinuous derivatives) ordinary ray theory does give a split-beam shadow at finite range, that is to say, there is no singularity in R_{ray}. For "non-smooth" profiles (discontinuous derivatives) we can also develop a modified ray analysis [see Ref. 4]. It turns out that in this case there is no singularity in the displacement ΔR. In fact, as we shall see, when the modified ray results are compared for a bilinear profile and a smooth profile where the smoothing compared with the bilinear case is only over a depth increment of a few wavelengths, the results are approximately the same. The modifications introduced by modified ray theory have removed some of the pathological sensitivity of ordinary ray analysis to small changes in the sound speed profile.

For the presentation of the results of the computer program, we currently use the format sketched in Fig. 4. The cycle range $R(\delta)$ for source and receiver at the same depth is plotted as a function of the grazing angle δ measured at the source point on a ray.

In Fig. 5 the solid curves represent examples for the three kinds of problems (1) unbounded, (2) pressure release boundary, and (3) rigid boundary. In the small figure in the upper left-hand corner, the shape of the R vs δ curve based on unmodified ray analysis is sketched; of course it is the same for all three problems, but different for the bilinear and composite profiles. Note the singularity in the ordinary ray theory results for a smooth profile. Note also that for the ordinary ray theory result for the bilinear profile the extremum in range would not be considered a caustic, in fact the

derivatives of the R vs δ curve are discontinuous for this extremum (grazing ray).

The following conclusions can be drawn from the results presented in Fig. 5:

1) The modifications have removed the singularity in the R vs δ curves for smooth sound speed profiles. The resulting R_{MOD} vs δ curves are smooth so that the extremum does represent a caustic.

2) The modifications also lead to smooth R_{MOD} vs δ curves for the bilinear profile, so again the extremum actually is a caustic.

3) The derivatives of the R_{MOD} vs δ curves can be found and used as parameters in quantitative descriptions (Airy integrals) for the field in the neighbourhood of this caustic. Pedersen [Ref. 7] has shown how false caustics can arise in ordinary ray analysis for linear-segmented profiles. It is rather interesting to see that with modified ray analysis, the modifications not only may act to remove some of this pathology, but also may result in real caustics at places not recognized as caustics in the ordinary ray analysis for bilinear, or bounded linear $n^2(z)$ profiles.

4) The caustics are displaced in range compared with the location we might anticipate on the basis of ordinary ray analysis. For rays with vertices near a pressure release boundary, displacements are toward the source; for a rigid boundary, displacements are mostly away from the source.

5) The modifications have made the results different for all three kinds of problems, even for rays whose vertex would lie below the region where the models differ.

6) For the bilinear profile, and for a bilinear profile "smoothed" over a depth increment of "half-width" $\rho = 2$ wavelengths, the results are approximately the same.

In the lower part of Fig. 5, the values of the magnitude of the reflection coefficient for the unbounded problem are plotted to give quantitative results for the splitting of the rays into reflected and transmitted branches. The diffraction regions can be sources of "leakage" rays and diffraction reflected rays (from rays that according to ordinary ray theory would be totally transmitted).

In some of the examples we have analysed, it appears that for frequencies of the order of a kiloHertz the displacements can be hundreds of feet; while at lower frequencies, of 100 Hz or so, displacements amount to thousands of feet.

Finally, we would like to point out that whereas here we have considered a harmonic source represented as an integral over ray parameter θ_o, it is also possible to consider signals of different time behaviour, Fourier-analysed so that the integral is over the variable ω. In that case, we can also show that there are time delays or advances Δt, in arrival times, that are related to derivatives of the phase with respect to ω. It can be shown that these time displacements can also be written in terms of the derivative $d\varkappa/dE$, as follows,

$$\Delta t = \frac{d\varkappa}{d\omega} = \frac{d\varkappa}{dE}\frac{dE}{d\omega} \qquad \text{[Eq. 17]}$$

$$= \frac{E}{\omega}\frac{d\varkappa}{dE} \quad .$$

Recently, a number of laboratories have been using machine programs for modal analysis where a sufficient number of modes (perhaps a thousand, if necessary) are summed to describe the sound field for comparison with ray computations. It should be borne in mind, when making such comparisons, that the modal analysis is a more complete and exact analysis for the field, and if there is any validity for the displacements or modifications we have described in this paper, the modal results should already include such effects.

REFERENCES

1. L.M. Brekhovskikh, "Waves in Layered Media". Academic Press Inc., New York, 1960. English translation.

2. E.L. Murphy, "Ray Representation of Diffraction Effects in the Split-beam Sound Field", J. Acoust. Soc. Am., Vol. 43, pp. 610-618, 1968.

3. E.L. Murphy, "Modified Ray Theory for Two-turning-point Problem", J. Acoust. Soc. Am., Vol. 47, pp. 899-908, 1970.

4. J.A. Davis and E.L. Murphy, "Modified Ray Analysis in the Presence of a Boundary". Paper presented at Eighty-first Meeting of the Acoustical Society of America, Washington, D.C., April 1971. Manuscript in preparation.

5. E.L. Murphy, J.A. Davis and J. Doutt, "Application of Modified Ray Theory to Underwater Sound Propagation". Paper presented at the Eighty-first Meeting of the Acoustical Society of A rica, Washington, D.C., April 1971. Manuscript in preparation.

6. "Handbook of Mathematical Functions", Nat. Bur. Stand. Appl. Math. Ser. 55, 1955.

7. M.A. Pedersen, "Acoustic Intensity Anomalies Introduced by Constant Velocity Gradients", J. Acoust. Soc. Am., Vol. 33, pp. 465-474, 1961.

DISCUSSION

In answer to questions the first author said that, broadly speaking, modifications to ray analysis were needed if the ray has a vertex within 4 or 5 acoustic wavelengths of a surface; and that the linear/parabolic model with "half-width" ρ was chosen for purposes of illustration.

The first author affirmed that amplitudes could be obtained straight-forwardly from modified ray analysis. In reply to a suggestion that this was equivalent to including higher order terms in an inverse-wavenumber expansion, the first author said that this may be so, but that the individual terms were not the same as in the traditional expansion.

Some discussion at this session, and in later private sessions, revealed that the techniques of modified ray analysis might be usefully applied to remove some of the pathological aspects of discontinuities when velocity profiles are approximated by constant-gradient segments.

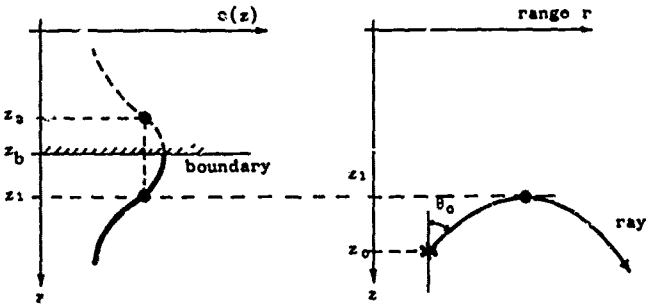

FIG. 1

FIG. 2

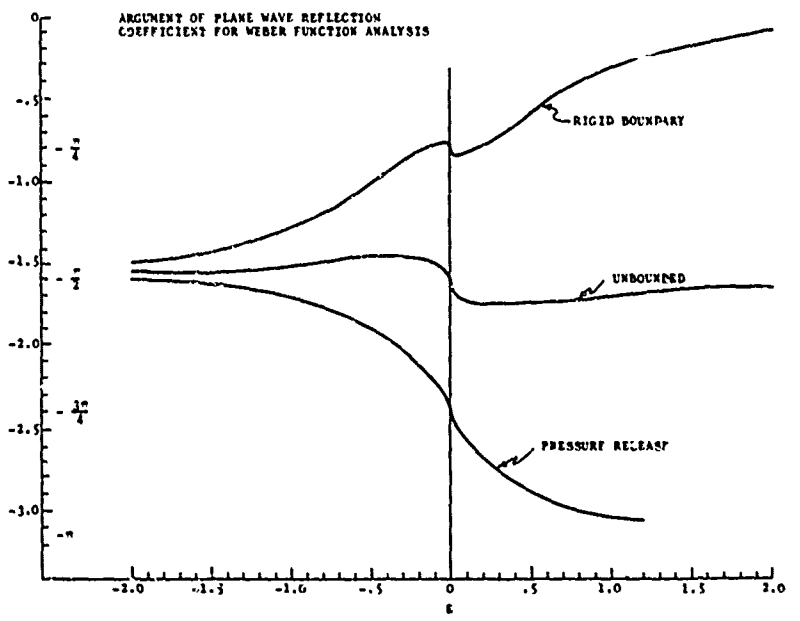

LINEAR + PARABOLIC $n^2(z)$ -
PROFILE FOR MODIFIED RAY ANALYSIS

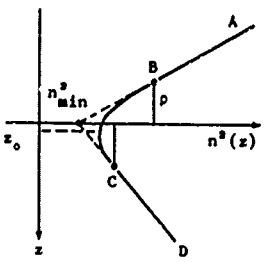

$n^2_{AB} = n^2_{min} - g_1 z$

$n^2_{CD} = n^2_{min} + g_2 z$

$n^2_{BC} = a + b(z - z_o)^2$

GIVEN: gradients g_1, g_2,
and matching distance ρ

FIND : z_o, a, b so that n^2 and $\frac{dn^2}{dz}$
are continuous

DIFFRACTION PHENOMENA
OCCUR IN SHADED AREAS

FIG. 3

WAVE EQUATION:

$\nabla^2 \Phi + k_o^2 n^2(z) \Phi = 0$

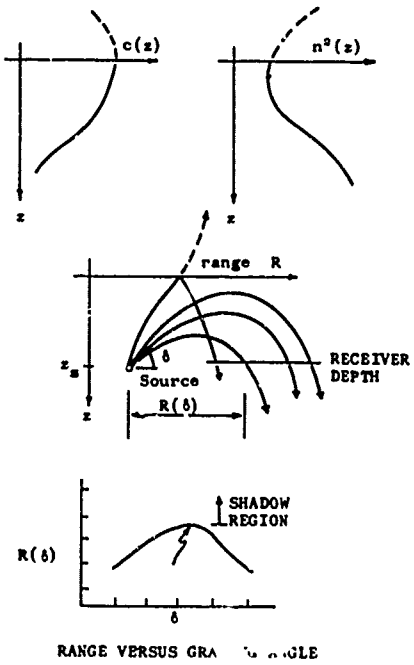

RANGE VERSUS GRAZING ANGLE

FIG. 4

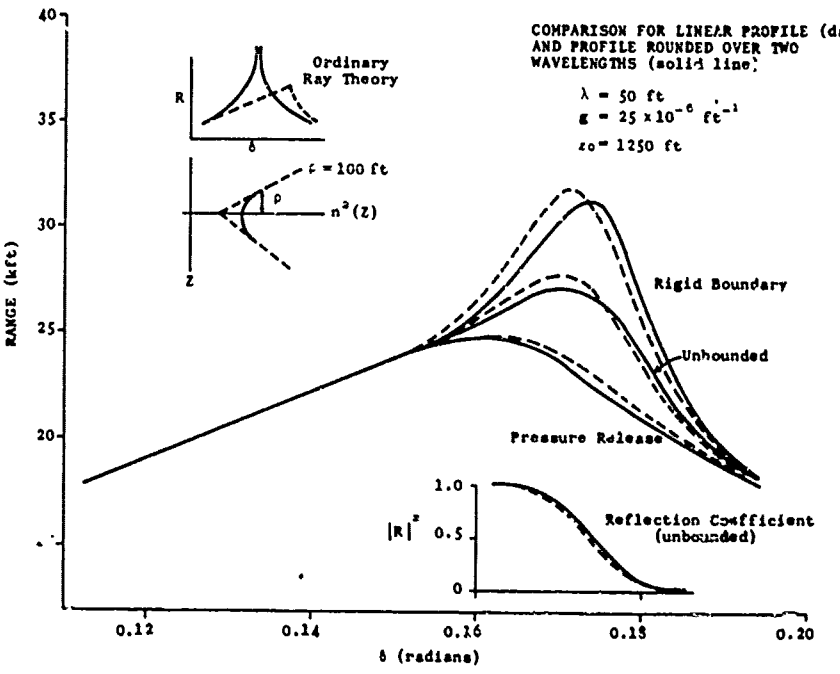

FIG. 5

THE EFFECT OF GRAVITY-FORCED OSCILLATIONS AT THE BASE OF THE DUCT ON ITS EFFECTIVE DEPTH AS A CHANNEL FOR ACOUSTIC RAYS

by

I. Roebuck
(read by G. Murdoch)
Admiralty Underwater Weapons Establishment
Portland, Dorset, U.K.

This talk must begin with a justification, since at first sigh (and possibly even after further glances) it is difficult to s what place a problem of classical applied mathematics (which was originally chosen as a companion to the author's earlier paper on below duct sound levels due to scattering from the sea surface) can rightfully claim to occupy in this gathering of ray tracers and computing enthusiasts. This is especially so when one realises that, as in the earlier paper, given here six months ago, the object is to formulate the problem in such a way as to obtain the maximum of predictive results with the minimum of computation.

Nevertheless, this account of the effect of gravity-forced internal waves at the base of an isothermal layer on its efficiency as a duct for acoustic energy is opposite to this particular convention; it has the laudable aims of saving effort for the sceptical perfectionists, and saving face for the lazy intuitionists, by demonstrating that it is not necessary to develop three-dimensional ray-tracing programs, nor to solve numerically the wave equation for a duct with one sinusoidal boundary, in order to take account of the horizontal stratification of sound velocity introduced by internal waves.

This is a very worthwhile simplification, but to achieve it it is necessary to have some background as to the generation and acoustic effects of internal waves; we start, as always, with the classical picture of acoustic propagation in the upper ocean, with the isothermal surface duct, and associated underlying shadow zone at long ranges [Fig. 1]. This is the ideal, on which computations of field intensities can be made with relative ease, as the stratification purely in horizontal planes makes a two-dimensional ray analysis valid.

Unfortunately, in the real world, things aren't that simple. Even if we retain the basic framework of ray theory, there are three major perturbing effects to be taken into account when considering the idealised situation as a predictive model for in-duct propagation. The first of these is diffraction which, as shown schematically in Fig. 2, can distribute energy into zones forbi by simple ray acoustics. This is obviously important as far as energy levels in the shadow zone are concerned; there is a school of thought that claims that, as far as in-duct propagation is concerned, the effect is negligible. The argument runs that the effect of diffraction is merely to alter the effective depth of the duct, and that the "below layer" field is an integral part of the trapped modes. Even so it is clear that there is a net energy leakage by this mechanism.

The second complication to be considered is scattering from the rough sea surface of energy which is seemingly entrapped within the duct, so that it is deflected into the thermocline region and escapes. This is shown schematically in Fig. 3; much work has been carried out on this, both numerical and analytic (the papers by van Ness, Schweitzer and the present author, to name but three), and it is fair to say that the effect of this mechanism is now quantifiably determined, or determinable, for most 'typical' duct conditions.

Finally, among these mechanisms, we come to anomalous refraction due to internal waves, the least well documented and most speculative of the three. Schematically, the way in which acoustic energy which has been trapped in the duct can be guided out of it by the action of internal waves is shown in Fig. 4; the dominant effect is the change from upward to downward curvature on crossing the internal-waves profile. It was on the basis of this type of diagram that Schulkin made his widely accepted estimate of the effect of internal waves, reducing the effective duct depth by the rms height of the typical internal wave; the argument running that any ray which vertexes at a greater distance than this from the surface will in time intersect such an internal wave and be refracted out of the duct.

Unfortunately, this conclusion is invalid, as this diagram is totally misleading — an inevitable consequence of the distortion of vertical and horizontal scales to get the figure on to a conventional slide. What in fact happens, because the curvature of the acoustic rays is so small and they are being propagated almost horizontally, is that the ray path, even taking account of refractive differences, occupies several periods of the internal wave in any transition from in-duct to below-duct propagation. The true schematic is more like the one shown in Fig. 5 — again noting that this is grossly distorted — the true grazing angle to the internal waves is less than 1°; this, however, at least indicates that a ray may penetrate into the internal-wave region and even so re-emerge into the surface duct.

Now we are getting to the core of the problem — if some rays can be refracted back into the surface duct while others are lost from it, how do we calculate what is the effect of the internal waves in quantitative terms? To do this obviously requires a more detailed knowledge of the mechanism of generation and propagation of internal waves and so I must ask you to lay down your acoustics and follow into the uncharted depths of oceanography. The forcing mechanism for internal waves is gravity (salinity can also cause

them, but for the purpose of this paper it will be neglected), and buoyancy forces are dominant.

We start with a water mass which was in equilibrium at a depth z below the surface, under a pressure p, its density at that time being ρ, and which by some mischance has been adiabatically displaced a small distance δz from this position. The general definition of the word 'adiabatic' in this context is beyond the scope of this paper; in this context it means that if the same supernatural agency that caused the change in the first place decides to put the water back in its original place, its density and pressure will also revert to their initial values. Even more confusingly, but more importantly, it means that although sea water is a viscous non-Newtonian fluid we can treat it as though it were a perfect gas and obeys the gas laws, $P \propto \rho T$ and $P \propto \rho^{\gamma}$. Anyway, in its new position, the density of this element is

$$\delta z \left\{ \frac{P(z+\delta z)}{P(z)} \right\}^{1/\gamma}$$

whereas the local equilibrium density is $\rho(z+\delta z)$. Thus this element has a density deficiency of

$$\rho(z)\ \delta z \left(\frac{1}{\rho}\frac{d\rho}{dz} - \frac{1}{\gamma p}\frac{d\rho}{dz}\right)$$

relative to its surroundings, and experiences a gravity-fed restoring force. The equation of motion is

$$\frac{d^2 s}{dz^2} + N^2(z)\ s = 0 \quad \text{(simple harmonic motion)}$$

with s the vertical displacement and N, the Brunt-Väisälä frequency, the frequency of the oscillations. There are various expressions for N, all equivalent, the most convenient of which is

$$N^2 = \frac{+g}{\theta}\frac{d\theta}{dz}\ .$$

That has introduced yet another variable, θ, so I had better explain what that is. It is the temperature the element would end up at if it adiabatically was transferred to a position where it was subject to a standard pressure of 1 atmosphere, and it is called the potential temperature.

N is a measure of the speed of reaction of the ocean to a perturbation — in other words of its stability. The bigger N^2 the more stable the ocean. Figure 6 shows the actual distribution of N^2 in the upper ocean in one typical case, together with the normal idealisation of it used by theorists. Normal in this case means

a. that it is the one normally used;
b. that it is a normal distribution;
c. that any ocean to which it is a valid approximation is completely abnormal.

So now we know what happens when a fluid element is displaced vertically; an internal wave, though, has a horizontal particle velocity component, so the full equation of motion must be used. We can simplify them by applying Boussinesq's Approximation, which says that, for slow enough motions (which internal waves are) we can treat the fluid as incompressible <u>except</u> that buoyancy must be taken into account. The equations are the top four in Fig. 7, which I do not intend to go into any detail over, except to say that you can eliminate all the other dependent variables and come up with this general equation for the vertical component of velocity, w

$$\frac{\partial^2}{\partial t^2}\left(\frac{\partial^2}{\partial x^2}+\frac{\partial^2}{\partial z^2}\right) w + N^2(z)\,\frac{\partial w^2}{\partial x^2} = 0$$

which holds no matter what kind of internal motion we are discussing.

However, we are after a propagating internal wave, so we take the most general disturbance which is sinusoidally periodic in time and travelling in the horizontal direction, writing [Fig. 8]

$$w = W(z)\ \exp\{i(kx - nt)\}$$

and find that W must obey the equation

$$\frac{d^2W}{dz^2} + \frac{N^2 - n^2}{n^2}\ k^2W = 0$$

which means immediately that the disturbance decays everywhere except inside the region where its time frequency is less than the local Brunt-Väisälä frequency. So, from Fig. 8 that shows the distribution of N^2 with depth, we can say that internal waves, except the very slow ones, are confined to the region of the thermocline. With that fact established, we can go further and derive a dispersion relation between the time frequency n and the horizontal space frequency k.

$$n^2 = \frac{\delta\rho}{\rho}\ \frac{kg}{1 + \coth kD} \qquad (kD >> 1)\ .$$

In this D is the depth at which the thermocline is situated and $\delta\rho$ is the change in density across it. Now in this, an increase in k causes an increase in n, but n cannot be greater than the Brunt-Väisälä frequency, so we can find a maximum value of k for each value of N. That defines the minimum wavelength for a wave of this frequency; the wave's amplitude is limited by the depth of the region in which the Brunt-Väisälä frequency is large enough to support it, so we have a relation between amplitude and wavelength.

More usefully, we can plot from Fig. 9, which you can read as either the maximum slope a wave of given amplitude can have, or the maximum amplitude for a wave of given slope on the mean thermocline plane.

These will be the ones which have the greatest effect on acoustic propagation, and Fig. 10 shows the model adopted for calculating this effect. Sinusoids make the calculation too difficult, so they have been replaced by truncated prisms of the same wavelength and maximum slope, cut off so that the area of "intrusion" is the same as that under the sine wave. The assumed velocity profiles are the same as the ones used for the undisturbed situation with the rays in the region of intrusion being straight lines, as the perturbation occurs without change of sound velocity. To calculate the ray path we just use Snell's Law so the calculation is straightforward but tedious.

Because it is so tedious, all that the author has considered are those rays which would be horizontal at the base of the undisturbed duct. He has not finished even these, but says that no matter what the internal wave, more than 90% of the time the ray ends up back in the duct. So it seems that everyone can go away happy in the knowledge that their previous neglect of internal waves, whether due to ignorance or indolence, was and still is justified.

FIG. 1

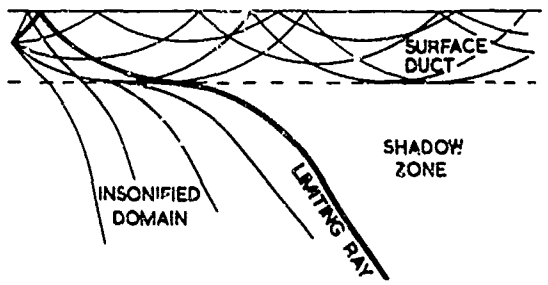

CLASSICAL UPPER OCEAN RAY PICTURE FOR VELOCITY STRUCTURE WITH SURFACE ISOTHERMAL LAYER

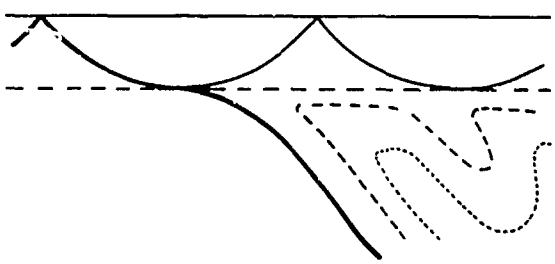

FIG. 2

INSONIFICATION OF SHADOW ZONES BY DIFFRACTIVE PROCESSES. EQUAL LOSS CONTOURS (SCHEMATIC)

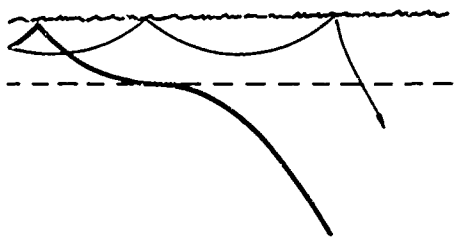

FIG. 3

INSONIFICATION OF THE SHADOW ZONE BY SCATTERING AT THE SEA SURFACE (SCHEMATIC)

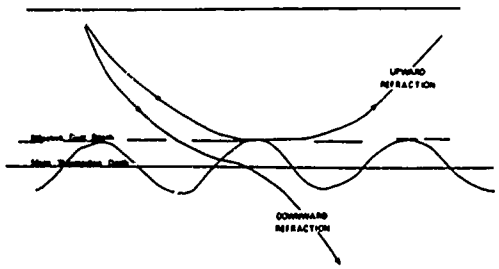

FIG. 4

INTERNAL WAVES AS A FACTOR IN ACOUSTIC DUCT THICKNESS
(after SCHULKIN)

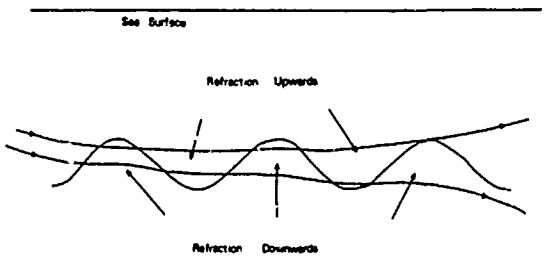

FIG. 5

EFFECT OF INTERNAL WAVES ON RAYS NEAR THE BASE OF THE DUCT (REVISED SCHEMATIC)

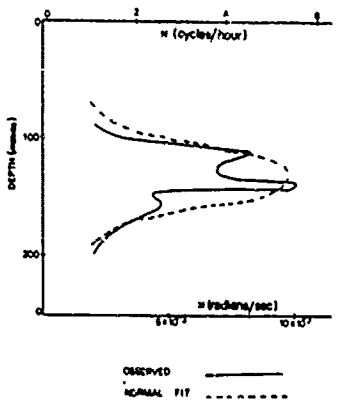

FIG. 6

DISTRIBUTION OF BRUNT - VAISSÄLÄ FREQUENCY ACROSS AN OCEAN THERMOCLINE

BOUSSINESQ's APPROXIMATE EQUATIONS

$$\frac{\partial \sigma}{\partial t} - N^2 w = 0 \qquad \frac{\partial u}{\partial x} + \frac{\partial w}{\partial z} = 0$$

$$\frac{\partial u}{\partial t} + \frac{\partial p'}{\partial x} = 0 \qquad \frac{\partial w}{\partial t} + \frac{\partial p'}{\partial z} + \sigma = 0$$

FIG. 7

GENERAL EQUATION FOR VERTICAL VELOCITY

$$\frac{\partial^2}{\partial t^2}\left(\frac{\partial^2}{\partial x^2} + \frac{\partial^2}{\partial z^2}\right) w + N^2(z) \frac{\partial^2 w}{\partial x^2} = 0$$

$$w = W(z) \exp\left\{i(kx - nt)\right\}$$

$$\frac{d^2W}{dz^2} + \frac{N^2 - n^2}{n^2} k^2 W = 0$$

$$n^2 = \frac{dp}{\rho} \frac{kg}{1 + \coth kD}$$

FIG. 8

GOVERNING EQUATIONS FOR INTERNAL WAVES

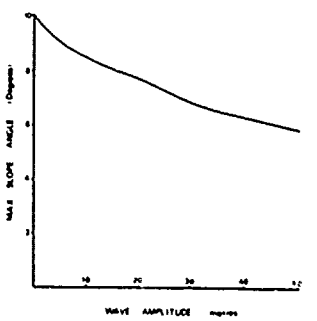

FIG. 9

RELATION BETWEEN INTERNAL WAVE AMPLITUDE AND SLOPE OF WAVE PROFILE

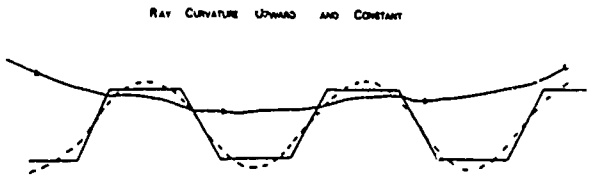

FIG. 10

MODEL ADOPTED FOR CALCULATION OF INTERNAL WAVE EFFECTS

SESSION 5

THEORY, STATISTICAL ASPECTS, AND RANGE DEPENDENT RAY TRACING

Session Chairman : B.W. Conolly

Session Secretary : H.R. Krol

5.1 Application of the Riesz Potential to the Cauchy Problem For Wave Propagation in an Inhomogeneous Medium

by L.A. Lopes

5.2 Hamiltonian Methods in Hydro-Acoustic Propagation

by B.C. Koopman

5.3 Rays and Statistical Diffraction Theory

by R.H. Clarke

5.4 Approximate Methods for Ray Tracing

by M.J. Daintith

5.5 Considerations on Numerical and Experimental Propagation Models for Two-Dimensional Variation of Medium Properties

by W. Sluyterman van Langeweyde

5.6 Application of Ray Tracing with Horizontal Gradient to Monostatic Boundary Reverberation

by L.B. Palmer

APPLICATION OF THE RIESZ POTENTIAL TO THE CAUCHY PROBLEM FOR WAVE PROPAGATION IN AN INHOMOGENEOUS MEDIUM

by

I.A. Lopes
Naval Undersea Research and Development Center
San Diego, California, U.S.

ABSTRACT

The method of Riesz [Ref. 1] for the solution of hyperbolic partial differential equations is applied to the Cauchy problem for the wave equation. It is shown that the first term in the Riesz potential function, which is represented in series form, yields the geometrical acoustics solution when applied to the problem of radiation from a point source.

THE WAVE EQUATION AND ITS RIEMANNIAN GEOMETRY

We seek a solution to the partial differential equation

$$Lu = \frac{1}{c^2} u_{tt} - \nabla^2 u = f \quad , \qquad \text{[Eq. 1]}$$

where f is a function of $(t,\bar{r}) \in R \times E^3$. For simplicity we shall assume vanishing initial conditions, $u(0,\bar{r}) = u_t(0,\bar{r}) = 0$. The local sound speed c is assumed to be a function of $\bar{r} = (x,y,z)$ only.

Construction of the Riesz potential for the operator L rests on the Riemannian geometry associated with the operator. The semi-Riemannian metric is given by the differential form

$$ds^2 = c^2\, dt^2 - (d\bar{r})^2 \quad . \qquad \text{[Eq. 2]}$$

A displacement for which $ds^2 > 0$ is called timelike; one for which $ds^2 < 0$ is called spacelike. Let $P:(t_0, \bar{r}_0)$ and $Q:(t_1, \bar{r}_1)$ be two points of space time. A geodesic joining P and Q is a curve $\gamma:\{[t(\sigma), r(\sigma)] : 0 \leq \sigma \leq \sigma_0\}$ such that $[t(0), \bar{r}(0)] = (t_0, \bar{r}_0)$, $[t(\sigma_0), \bar{r}(\sigma_0)] = (t_1, \bar{r}_1)$, and

$$s(P,Q) = \int_{\gamma} ds \qquad \text{[Eq. 3]}$$

is an extremum with respect to all curves joining P to Q. Let

$$\left(\frac{ds}{d\sigma}\right)^2 = c^2 \left(\frac{dt}{d\sigma}\right)^2 - \left(\frac{d\bar{r}}{d\sigma}\right)^2 = w \quad .$$

Then the geodesic curves are extremum curves of the integral

$$\int_0^{\sigma_0} w^{\frac{1}{2}} \, d\sigma \quad . \qquad \text{[Eq. 4]}$$

The geodesic curves then satisfy the Euler-Lagrange equations

$$\frac{d}{d\sigma}\left(\frac{\partial w^{\frac{1}{2}}}{\partial v^0}\right) - \frac{\partial w^{\frac{1}{2}}}{\partial t} = 0 \qquad \text{[Eq. 5]}$$

$$\frac{d}{d\sigma}\left(\frac{\partial w^{\frac{1}{2}}}{\partial \bar{v}}\right) - \nabla w^{\frac{1}{2}} = 0 \quad , \qquad \text{[Eq. 6]}$$

where

$$v^0 = \frac{\partial t}{\partial \sigma} \qquad \text{[Eq. 7]}$$

$$\bar{v} = \frac{\partial \bar{r}}{\partial \sigma} \quad . \qquad \text{[Eq. 8]}$$

If we now choose w to be constant along a geodesic (σ is then a linear function of s) the equations for the geodesics become

$$\frac{d}{d\sigma}\left(c^2 v^0\right) = v^{0^2} c \frac{\partial c}{\partial t} = 0 \qquad \text{[Eq. 9]}$$

$$\frac{d\bar{v}}{d\sigma} = -(v^0)^2 \, c \nabla c \qquad \text{[Eq.10]}$$

Let $w = 1 - \rho^2$. Then $\rho = 1$ is the equation of the characteristic cone through P. We have

$$\left(\frac{ds}{d\sigma}\right)^2 = c^2 v^{o^2} - \bar{v}^2 = 1 - \rho^2 \quad . \qquad \text{[Eq. 11]}$$

If $0 \leq \rho \leq 1$ $ds^2 > 0$ and the geodesics are timelike. Since w is constant along a geodesic

$$s = \sigma\sqrt{1 - \rho^2} \quad . \qquad \text{[Eq. 12]}$$

Using the notation introduced by Hadamard we set $\Gamma(P,Q) = s^2(P,Q)$. The region $\{Q: \Gamma(P,Q) \geq 0, \quad t \leq t_1\}$ is called the retrograde conoid with vertex P. We see from Eq. 12 that it is also defined by $0 \leq \rho \leq$; $t \leq t_1$. The region $\{Q: \Gamma(P,Q) \geq 0, \quad t \geq t_1\}$ is called the direct conoid with vertex P.

In the theory of the Riesz potential a particular coordinate system for the conoid with vertex P plays an important role. This is the Riemannian coordinate system with coordinates defined by

$$X^i = v^i(0)\sigma, \quad i = 0, 1, 2, 3 \qquad \text{[Eq. 13]} \quad .$$

In this coordinate system the geodesics emanating from the point P appear as straight lines. It is shown by Riesz [Ref. 1] that

$$\Delta\Gamma = 8 + 2\sigma \frac{d \ell n \sqrt{a}}{d\sigma} \qquad \text{[Eq. 14]}$$

where Δ represents the second order Beltrami operator, or space-time Laplacian, and a is the determinant of the metric tensor, expressed in Riemannian coordinates. We have

$$a = J^2 c^2 \qquad \text{[Eq. 15]}$$

where $J = D\begin{pmatrix} t & x & y & z \\ x^0 & x^1 & x^2 & x^3 \end{pmatrix}$, the Jacobian transformation from the original coordinate system to the Riemannian coordinate system. Expressed in our original coordinates, t, x, y, z, we have

$$\Delta\Gamma = \frac{1}{c}\left(\frac{1}{c}\,\Gamma_t\right)_t - \frac{1}{c}\,\nabla\cdot(c\,\nabla\Gamma)$$

$$= L\Gamma - \nabla \ell n\, c \cdot \nabla\Gamma \qquad \text{[Eq. 16]}$$

$$= L\Gamma + 2\sigma\,\frac{d\,\ell n\, c}{d\sigma}$$

since $\frac{\partial c}{\partial t} = 0$,

Hence, from Eqs. 14 and 16,

$$L\Gamma = 8 + 2\sigma\,\frac{d\ell n\, J}{d\sigma} \qquad \text{[Eq. 17]}$$

From Eq. 9 we see that $c^2 v^o$ is constant along a geodesic. Letting the constant be $-c_o = -c(P)$,

$$\frac{dt}{d\sigma} = -\frac{c_o}{c^2} \qquad \text{[Eq. 18]}$$

$$\frac{d\bar{r}}{d\sigma} = \bar{v} \qquad \text{[Eq. 19]}$$

$$\frac{d\bar{v}}{d\sigma} = -\frac{c_o^2}{c^3}\,\nabla C = \frac{1}{2}\,\nabla\left(\frac{c_o}{c}\right)^2 \qquad \text{[Eq. 20]}$$

Moreover, from Eq. 11,

$$[\bar{v}(0)]^2 = \rho^2 \qquad \text{[Eq. 21]}$$

THE RIESZ POTENTIAL

Following Duff [Ref. 2] we denote by D^p the interior of the retrograde conoid with vertex P. Let S be the intersection of D^p with the initial manifold, $t = 0$, and let D^p_s be the part of the conoid cut-off by the initial manifold, i.e. the intersection of D^p with the half-space $t > 0$. For twice

differentiable functions u, v, defined on D_s^p we have by Green's theorem

$$\int_{D_s^p} (u\,L\,v - v\,L\,u)\,dt\,dx\,dy\,dz \qquad \text{[Eq. 22]}$$
$$= \int_{SUC_s^p} \left\{ \frac{1}{c^2} (uv_t - vu_t)n_t + (v\nabla u - u\nabla v)\cdot \bar{n}\,dS \right.$$

where C_s^p is the part of the characteristic cone $(\Gamma = 0)$ cut off by the initial plane $t = 0$, and $(n_t, \bar{n})$ is the exterior normal to the boundary.

The Riesz potential $V^\alpha(P,Q)$ is defined as a function of points P,Q, in the Riemannian space of the wave equation and the complex variable α. It satisfies the relations

$$LV^{\alpha+2}(P,Q) = V^\alpha(P,Q) \qquad \text{[Eq. 23]}$$

and

$$\lim_{\alpha \to 0} \int_{D_s^p} f(Q)\, V^\alpha(P,Q)\, dt\,dx\,dy\,dz = f(P) \quad , \qquad \text{[Eq. 24]}$$

for any continuous function f. V^α is expressed in the form

$$V^\alpha(P,Q) = \sum_{k=0}^{\infty} \frac{s^{\alpha+2k-4} V_k(P,Q)}{H(\alpha,k)} \quad , \qquad \text{[Eq. 25]}$$

where $s = s(P,Q)$ is the geodesic distance between P and Q. The functions $V_k(P,Q)$ are to be determined from the conditions 23 and 24, while

$$H(\alpha,k) = \pi\, 2^{\alpha+k-1}\, \Gamma(\tfrac{1}{2}\alpha)\, \Gamma(\tfrac{1}{2}\alpha + k - 1) \qquad \text{[Eq. 26]}$$

For sufficiently large $\mathrm{Re}\,\alpha$, V^α is an analytic function of α and vanishes on C_s^p. Thus, for those values of α, and for functions u satisfying the vanishing initial conditions of the Cauchy problem [Eq. 1], we have from Eq. 22

$$\int_{D_s^p} u\, L V^{\alpha+2}\, dt\, dx\, dy\, dz = \int_{D_s^p} V^{\alpha+2}\, Lu\, dt\, dx\, dy\, dz \quad . \qquad [\text{Eq. } 27]$$

Equation 27 remains valid for all values α to which analytic continuation is possible. From Eqs. 23 and 24, then, letting α tend to zero, we obtain for a solution to Eq. 1

$$u(P) = \lim_{\alpha \to 0} \int_{D_s^p} V^{\alpha+2}\,(P,Q)\, f(Q)\, dt\, dx\, dy\, dz \quad . \qquad [\text{Eq. } 28]$$

Equation 28 provides a representation of the solution to the Cauchy problem. Determination of the coefficients $V_k(P,Q)$ remains.

From the definition given by Eq. 26 and the properties of the Gamma function we obtain the relations.

$$H(\beta,k) = 2(\tfrac{1}{2}\beta + k - 2)\, H(\beta,\, k-1) \qquad [\text{Eq. } 29]$$

$$H(\beta+2,\, k) = 2\beta\,(\tfrac{1}{2}\beta + k - 1)\, H(\beta,k) \quad . \qquad [\text{Eq. } 30]$$

Now

$$L(\Gamma^\beta \psi) = \Gamma^\beta L\psi + \psi L\Gamma^\beta + 4\beta\, \Gamma^{\beta-1}\, \sigma \frac{d\psi}{d\sigma} \quad . \qquad [\text{Eq. } 31]$$

[Here we have used Eq.4.5.19 of Duff (Ref. 2).] Using Eq. 17 this becomes

$$L(\Gamma^\beta \psi) = \Gamma^\beta L\psi + 4\beta\Gamma^{\beta-1} \{\sigma \frac{d\psi}{d\sigma} + (\beta + 1 + \tfrac{1}{2}\sigma \frac{d\, \ell n\, J}{d\sigma})\, \psi\}. \qquad [\text{Eq. } 32]$$

Operating with L on $V^{\beta+2}(P,Q)$, given by Eq. 25, and using Eq. 32, we have

$$LV^{\alpha+2} = \sum_{k=0}^{\infty} \frac{1}{H(\alpha+2,\, k)} \{4(\tfrac{\alpha}{2} + k - 1)\, \Gamma^{\frac{\alpha}{2}+k-2} \qquad [\text{Eq. } 33]$$

$$[(\tfrac{\alpha}{2} + k + \tfrac{1}{2}\sigma \frac{d\, \ell n\, J}{d\sigma})\, V_k + \sigma \frac{dV_k}{d\sigma}] + \Gamma^{\frac{\alpha}{2}+k-1} LV_k \}$$

Using Eq. 29 this becomes

$$LV^{\alpha+2} = \sum_{k=0}^{\infty} \frac{1}{H(\alpha+2,\,k-1)} \left\{ \left(\alpha + 2k + \sigma \frac{d\ell n J}{d\sigma}\right) V_k + 2\sigma \frac{dV_k}{d\sigma} + LV_{k-1} \right\} \Gamma^{\frac{\alpha}{2}+k-2} \qquad \text{[Eq. 34]}$$

where we have introduced $V_{-1}(P,Q) = 0$. Now choose $V_k(P,Q)$ so that for $k = 0,1,2,$

$$\left(2k + \sigma \frac{d\ell n J}{d\sigma}\right) V_k + 2\sigma \frac{dV_k}{d\sigma} + L V_{k-1} = 0 \qquad \text{[Eq. 35]}$$

Then, using Eqs. 29 and 30, we have

$$LV^{\alpha+2} = \sum_{k=0}^{\infty} \frac{\alpha}{H(\alpha+2,\,k-1)} V_k \Gamma^{\frac{\alpha}{2}+k-2} \qquad \text{[Eq. 36]}$$

$$= \sum_{k=0}^{\infty} \frac{1}{H(\alpha,k)} V_k \Gamma^{\frac{\alpha}{2}+k-2} = V_\alpha$$

Thus requiring V_k to satisfy Eq. 35 results in V^α satisfying Eq. 23. We may rewrite Eq. 35 in the form

$$\frac{d}{d\sigma}\left(\sigma^k J^{\frac{1}{2}} V_k\right) = -\tfrac{1}{2}\sigma^{k-1} J^{\frac{1}{2}} LV_{k-1} \qquad \text{[Eq. 37]}$$

Choosing $V_0(0) = c_0$, so that V^α will satisfy Eq. 24 [Ref. 1], we have

$$V_0(P,Q) = c_0 J^{-\frac{1}{2}} \qquad \text{[Eq. 38]}$$

since $J = 1$ at P. For $k \geq 1$ we set $V_k(0) = 0$. Then

$$V_k = -\tfrac{1}{2} J^{-\frac{1}{2}} \sigma^{-k} \int_0^\sigma \sigma^{k-1} J^{\frac{1}{2}} LV_{k-1}\, d\sigma \qquad \text{[Eq. 39]}$$

APPROXIMATE SOLUTION TO THE CAUCHY PROBLEM

Let us now replace $V^{\alpha+2}(P,Q)$ by the first term in the series [Eq. 25] in computing the integral [Eq. 28]. Define

$$\tilde{u}_\alpha(P) = \int_{D_s^P} f(Q) \frac{V_o \Gamma^{\frac{\alpha}{2}-1}}{H(\alpha+2,0)} \, dt\, dx\, dy\, dz \quad . \qquad \text{[Eq. 40]}$$

We consider $\lim_{\alpha \to 0} \tilde{u}_\alpha(P)$ to be a first approximation to the solution to the Cauchy problem. In order to carry out the integration indicated in Eq. 40 we introduce a coordinate system for D_s^P based on the geodesics defined by Eqs. 18, 19, and 20. With $\vec{v} = (v^1, v^2, v^3)$ we set

$$\begin{aligned} v^1(0) &= \rho \cos\theta \cos\varphi \\ v^2(0) &= \rho \cos\theta \sin\varphi \\ v^3(0) &= \rho \sin\theta \end{aligned} \qquad \text{[Eq. 41]}$$

Then Eq. 21 is satisfied. The geodesic equations provide a correspondence between points $(t,x,y,z) \in D_s^P$ and $(\sigma,\rho,\varphi,\theta)$. This correspondence will not be one-to-one in general. If multi-paths occur a point (t,x,y,z) may correspond to many points $(\sigma,\rho,\varphi,\theta)$. However, except at exceptional points (t,x,y,z), each of the points $(\sigma,\rho,\varphi,\theta)$ will have a neighbourhood that is in one-to-one correspondence with a neighbourhood of (t,x,y,z). At the exceptional points, called caustic or focal points, this local one-to-one property will not hold. As a consequence the Jacobian determinant $D\binom{t\ x\ y\ z}{\sigma\ \rho\ \varphi\ \theta}$ will vanish at such points.

The geodesic Eqs. 18, 19 and 20 uniquely define (t,x,y,z) as functions of $(\sigma,\rho,\varphi,\theta)$. Transforming coordinates in Eq. 40 we have

$$\tilde{u}_\alpha(P) = \int_0^{2\pi} d\varphi \int_{-\frac{\pi}{2}}^{\pi/2} d\theta \int_0^1 d\rho \int_0^{\sigma_{t_o}} d\sigma \; f(t,x,y,z)\, V_o \left[\sigma^2(1-\rho^2)\right]^{\frac{\alpha}{2}-1} D\binom{t\,x\,\cdot}{\sigma\,\rho\,\varphi\,\theta}$$

[Eq. 42]

where $\sigma t_o = \sigma t_o(\rho,\varphi\ \theta)$ is the value of σ for which the geodesic curve reaches the initial manifold. This will happen at a finite value since we assume c is bounded. It is well known that if $F(\rho,\epsilon)$ is a continuous function for $0 \le \rho \le 1$, $\epsilon \ge 0$, that

$$\lim_{\epsilon \to 0} \epsilon \int_0^1 F(\rho,\epsilon)\ (1-\rho)^{\epsilon - 1}\ d\rho \ = \ F(1,0) \qquad \text{[Eq. 43]}$$

We will write, for continous $g(\rho)$,

$$\int_0^1 g(\rho)\ \delta(1-\rho)\ d\rho \ = \ g(1) \quad . \qquad \text{[Eq. 44]}$$

Equation 44 is the definition of the generalized function $\delta(1-\rho)$. Since $H(\alpha+2,\,0) \sim 4\pi/\alpha$ as $\alpha \to 0$ we can apply Eq. 43 to Eq. 42 to obtain

$$\tilde{u}(p) \ = \ \lim_{\alpha \to 0} \tilde{u}_{\alpha}(p) \qquad \text{[Eq. 45]}$$

$$= \frac{1}{4\pi} \int_0^{2\pi} d\varphi \int_{-\frac{\pi}{2}}^{\pi/2} d\theta \int_0^1 d\rho \int_0^{\sigma t_o} d\sigma\ f\, V_o\, \sigma^{-2}\ \delta(1-\rho)\ D\begin{pmatrix} t & x & y & z \\ \sigma & \rho & \varphi & \theta \end{pmatrix}$$

Note that in the latter equation we have assumed $f\, V_o\, D\begin{pmatrix} t & x & y & z \\ \sigma & \rho & \varphi & \theta \end{pmatrix}$ to be a continuous function of ρ in a neighbourhood of $\rho = 1$. The solution to the Cauchy problem is represented approximately by Eq. 45. Multipaths cause no problem in this representation, since they are sorted out by the $(\sigma,\rho,\varphi,\theta)$ coordinates.

Letting f represent a point source we set

$$f(t,x,y,z) \ = \ S(t)\ \delta(x,y,z) \qquad \text{[Eq. 46]}$$

where $\delta(x,y,z)$ is the 3-dimensional delta function and $S(t)$ is the transmitted waveform. Although we cannot, strictly speaking, use Eq. 46 in Eq. 45 directly because it is not a continuous function, we could replace the delta function by an approximating sequence of continuous functions. However, the formal manipulations are perhaps more clear if we are less rigorous. Thus we introduce

the generalized function defined by Eq. 46 in Eq. 45. In order to carry out the integration over the delta functions in Eq. 45 it is necessary to revert to (ρ,x,y,z) as variables of integration. Since we do not in general have a one-to-one correspondence between (t,x,y,z) and $(\sigma,\rho,\varphi,\theta)$ a point $(\tau,0,0,0)$ may be covered by many points $(\sigma,\rho,\varphi,\theta)$. We assume there are finitely many. In addition we assume that the origin is isolated from caustics of C_s^p. Each of the points $(\sigma,\rho,\varphi,\theta)$ covering $(\tau,0,0,0)$ then has a neighbourhood U_n that has a one-to-one mapping onto a neighbourhood V_n of $(\tau,0,0,0)$. Then

$$\tilde{u}(P) = \sum_n \int\int_{U_n}\int\int S(t)\,\delta(x,y,z)\,V_0\,\sigma^{-2}\,\delta(1-\rho)\,D\begin{pmatrix} t & x & y & z \\ \sigma & \rho & \varphi & \theta \end{pmatrix} d\sigma\,d\rho\,d\varphi\,d\theta \qquad \text{[Eq. 47]}$$

$$= \frac{1}{4\pi}\int\int_{V_n}\int\int S(t)\,\delta(x,y,z)\,V_0\,\sigma^{-2}\,\delta(1-\rho)\,dt\,dx\,dy\,dz$$

Now, considering t to be a function of (ρ,x,y,z) we write

$$t = t_0 - T(\rho,x,y,z) \qquad \text{[Eq. 48]}$$

where T may be interpreted as the travel time along the geodesic emanating from the point P. Then

$$\tilde{u}(P) = -\frac{1}{4\pi}\sum_n \int\int_{V_n}\int\int S(t_0-T)\,\delta(x,y,z)\,V_0\,\sigma^{-2}\,\delta(1-\rho)\,T_\rho\,d\rho\,dx\,dy\,dz$$

$$= -\frac{1}{4\pi}\sum_n S(t_0-\tau_n)\,V_0\,\sigma_n^{-2}\,T_\rho\,(1,0,0,0) \qquad \text{[Eq. 49]}$$

where τ_n is the travel time along the n-th ray from (x_0,y_0,z_0) to the origin, and σ_n is the corresponding value of σ.

From Eqs. 18, 19 and 20 t and $\bar{r}$ are determined as functions of $(\sigma,\rho,\varphi,\theta)$. We write

$$t = t(\sigma,\rho,\varphi,\theta) \qquad \text{[Eq. 50]}$$

$$\bar{r} = \bar{r}(\sigma,\rho,\varphi,\theta) \qquad \text{[Eq. 51]}$$

Then

$$\frac{\partial t}{\partial \rho} = -\frac{\partial T}{\partial \rho} - \nabla T \cdot \frac{\partial \bar{r}}{\partial \rho} \quad . \qquad \text{[Eq. 52]}$$

Now $\psi = t + T(\rho,x,y,z)$ is, for fixed ρ, an integral surface of the linear partial differential equation

$$\frac{1}{c^2}\,\psi_t^2 - (\nabla\psi)^2 = \text{constant} \qquad \text{[Eq. 53]}$$

whose characteristic strips are generated by the geodesic Eqs. 18, 19 and 20. Comparison with Eq. 11 shows that the constant on the right-hand side of Eq. 53 must be $(1-\rho^2)/c_o^2$ and $\nabla\psi = \bar{v}/c_o$. Hence

$$c_o \nabla T = \frac{\partial \bar{r}}{\partial \sigma} \quad . \qquad \text{[Eq. 54]}$$

Thus, from Eq. 52

$$\begin{aligned} -c_o \frac{\partial T}{\partial \rho} &= c_o \frac{\partial t}{\partial \rho} + \frac{\partial \bar{r}}{\partial \rho} \cdot \frac{\partial \bar{r}}{\partial \sigma} \\ &= c_o \frac{\partial t}{\partial \rho} + \frac{\partial \bar{r}}{\partial \rho} \cdot \bar{v} \quad . \end{aligned} \qquad \text{[Eq. 55]}$$

Now, differentiating Eq. 55 with respect to σ we have

$$\frac{\partial}{\partial \sigma}\left(-c_o \frac{\partial T}{\partial \rho}\right) = c_o \frac{\partial^2 t}{\partial \rho\, \partial \sigma} + \frac{\partial^2 \bar{r}}{\partial \rho\, \partial \sigma} \cdot \bar{v} + \frac{\partial \bar{r}}{\partial \sigma} \cdot \frac{\partial \bar{v}}{\partial \sigma} \quad . \qquad \text{[Eq. 56]}$$

Let us temporarily write $(c_o/c)^2 = \beta(x,y,z)$. Then the geodesic Eqs. 18, 19 and 20, become

$$c_o \frac{\partial t}{\partial \sigma} = \beta \qquad \text{[Eq. 57]}$$

$$\frac{\partial \bar{v}}{\partial \sigma} = \frac{1}{2} \nabla\beta \quad . \qquad \text{[Eq. 58]}$$

From Eq. 11 we obtain

$$\beta - \bar{v}^2 = 1 - \rho^2$$

or

$$\bar{v}^2 = \beta + \rho^2 - 1 \quad . \qquad \text{[Eq. 59]}$$

Referring again to Eq. 56 we then have

$$\frac{\partial}{\partial\sigma}\left(-c_o \frac{\partial T}{\partial\rho}\right) = -\frac{\partial\beta}{\partial\rho} + \frac{1}{2}\frac{\partial}{\partial\rho}(\bar{v}^2) + \frac{\partial\bar{r}}{\partial\rho}\cdot\left(\frac{1}{2}\nabla\beta\right) = 0 \qquad \text{[Eq. 60]}$$

Hence

$$-c_o \frac{\partial T}{\partial\rho} = \rho\sigma \qquad \text{[Eq. 61]}$$

since the relation clearly is valid for small σ. Thus Eq. 49 becomes

$$\tilde{u}(P) = -\frac{1}{4\pi}\sum_n S(t_o - \tau_n)\, V_o/(C_o\,\sigma_n) \qquad \text{[Eq. 62]}$$

where V_o is given by Eq. 38.

The Riemann coordinates involved in the definition of J [Eq. 15] are given in terms of $(\sigma,\rho,\varphi,\theta)$ by

$$x^0 = -\sigma/c_o \qquad \text{[Eq. 63]}$$

$$x^1 = \rho\sigma\cos\theta\cos\varphi \qquad \text{[Eq. 64]}$$

$$x^2 = \rho\sigma\cos\theta\sin\varphi \qquad \text{[Eq. 65]}$$

$$x^3 = \rho\sigma\sin\theta \qquad \text{[Eq. 66]}$$

Then

$$J = D\begin{pmatrix} t & x & y & z \\ x^0 & x^1 & x^2 & x^3 \end{pmatrix}$$

$$= D\begin{pmatrix} t & x & y & z \\ \sigma & \rho & \varphi & \theta \end{pmatrix} / D\begin{pmatrix} x^0 & x^1 & x^2 & x^3 \\ \sigma & \rho & \varphi & \theta \end{pmatrix} \qquad \text{[Eq. 67]}$$

$$= -D\begin{pmatrix} t & x & y & z \\ \sigma & \rho & \varphi & \theta \end{pmatrix} \cdot c_o/(\rho^2 \sigma^3 \cos\theta)$$

$$= -c_o T_\rho D\begin{pmatrix} x & y & z \\ \sigma & \varphi & \theta \end{pmatrix} /(\rho^2 \sigma^3 \cos\theta) = D\begin{pmatrix} x & y & z \\ \sigma & \varphi & \theta \end{pmatrix} / (\rho \sigma^2 \cos\theta)$$

Hence, setting $\rho = 1$,

$$V_o = c_o \sigma \left[\cos\theta / D\begin{pmatrix} x & y & z \\ \sigma & \varphi & \theta \end{pmatrix}\right]^{\frac{1}{2}} \qquad \text{[Eq. 68]}$$

and Eq. 62 becomes

$$\tilde{u}(P) = \frac{1}{4\pi} \sum_n S(t_o - \tau_n) \left[\cos\theta / D\begin{pmatrix} x & y & z \\ \sigma & \varphi & \theta \end{pmatrix}\right]^{\frac{1}{2}} \qquad \text{[Eq. 69]}$$

This is the geometrical acoustics solution in its generalized form.

REFERENCES

1. M. Riesz, "L'intégrale de Riemann-Liouville et le problème de Cauchy", Acta Math, Vol. 81, 1949, pp. -223.

2. G.F.D. Duff, "Partial Differential Equations", University of Toronto Press, 1956.

DISCUSSION

The author confirmed that the signal distortion can be obtained directly if the source function is bounded.

HAMILTONIAN METHODS IN HYDRO-ACOUSTIC PROPAGATION

by

B.O. Koopman
Arthur D. Little, Inc.
Cambridge, Mass., U.S.

The investigation that I wish to outline here originated in the military need of forecasting detection probabilities of underwater acoustic emitters, in cases in which only a somewhat general idea of the sound speed profile is available, based, for example, on a known geographical location and average sound speed behaviour at a given time of year. Since detection of a distant object is the objective, only very faint signals enter — certainly nothing that could produce the non-linear effects, shock-waves, etc., that have been discussed in many of the papers reported here. Evidently the object of present interest is not this or that result of meticulously accurate computations based on exact knowledge of the sound speed c as a function of position, but more general facts that are relatively stable — i.e., are not radically altered by slight changes in the function c. Moreover, it is not only necessary that the stable evaluations be rather rough approximations (since we cannot know values of c in an area of future enemy operations except roughly) — but this is sufficient for military applications.

These requirements lead us in two directions: quantitative generalities: mathematically this means theorems rather than detailed computations; and a statistical attribute of the results. Our situation suggests a similar one in the quantitative study of those other complex physical systems, composed of the molecules of

* The investigation reported here grew out of an earlier phase, supported by the U.S. Naval Ordnance System Command. The author is uniquely responsible for all views expressed herein.

a gas; and just as statistical mechanics bases its methods on Hamiltonian theory, phase-space and its integral invariants, so we shall find, rather surprisingly, that similar branches of classical mathematics will play an essential part in our investigations.

It is not too surprising that the methodology of classical Hamiltonian dynamics should enter our problems of hydro-acoustic propagation: mathematics does not know the difference between Fermat's principle of least time and Maupertuis' principle of least action, which led immediately to the Hamiltonian theory. But let us start from the beginning.

Our starting point is D'Alembert's wave equation in the velocity potential ψ

$$\nabla^2\psi - \psi_{tt}/c^2 = 0$$

(with possible slight modification in derivatives of lower order) together with the energy density expression

$$E = \frac{\rho_o}{2}\left[|\nabla\psi|^2 + |\psi_t|^2/c^2\right]$$

and the energy flux vector

$$\vec{F} = -\rho|\bar{\psi}_t\ \nabla\psi| \ .$$

Note that we are using the absolute values, to allow for complex wave functions ψ. We recall that for every c which is a function of geometrical position and is <u>independent of time t</u>, the wave equation has a consequence that an equation of continuity is satisfied; i.e., that

$$\partial E/\partial t + \nabla\cdot\vec{F} = 0 \ .$$

Geometrical acoustics is a valid approximation at sufficiently high frequencies: $\omega >> c/\text{depth}$, where $\omega = 2\pi \times$ frequency. The element which transports hydro-acoustic energy is the <u>travelling</u>

wave, that is, a solution of the wave equation of the form

$$\psi = uf[\omega(t - S)], \qquad S = S(x,y,z) \ .$$

Here the function $f = f(x)$ must be defined for all x. For monochromatic steady state propagation, we take $f(x) = e^{ix}$, while for an infinite pulse, $f(x) = \delta(x)$, the Dirac delta function, etc. The coefficient u depends on x, y, z, t, and even ω; but it is thought of as varying "slowly" with these quantities. When the above ψ is inserted in the wave equation and only terms in ω^2 retained, the eikonal equation is obtained,

$$|\nabla S|^2 - 1/c^2 = 0 \ .$$

A solution $S = S(x,y,z)$ of this, when set equal to a constant has for locus a wave front; and the family of such loci: $S(x,y,z) = t$ is a moving surface as the time t increases — the wave front of the travelling wave. In space-time it is a characteristic hypersurface of the wave equation.

The eikonal equation has, in its turn, characteristic manifolds, the bicharacteristics of the wave equation or rays. The classical theory of all these relations — known for well over a century — gives us the rule for writing the differential equations of the latter. We replace $\partial S/\partial x$, etc., in the eikonal equation by p_x, etc., and set

$$H = \tfrac{1}{2}(p_x^2 + p_y^2 + p_z^2 - \frac{1}{c^2}) \ ,$$

so that the eikonal equation could be written as $H = 0$. Then we write the system of six differential equations

$$d\tau = \frac{dx}{H_{p_x}} = \frac{dy}{H_{p_y}} = \frac{dz}{H_{p_z}} = \frac{dp_x}{-H_x} = \frac{dp_y}{-H_y} = \frac{dp_z}{-H_z}$$

where the denominators are the partial derivatives of H with respect to the six independent variables (x,y,z,p_x,p_y,p_z), and τ is a parameter.

Clearly the equations for the bicharacteristics are in Hamilton's canonical form:

$$\frac{dx}{d\tau} = \frac{\partial H}{\partial p_x} = p_x, \text{ etc.}, \quad \frac{dp_x}{d\tau} = -\frac{\partial H}{\partial x} = \frac{\partial}{\partial x}\frac{1}{2c^2}, \text{ etc}.$$

They are the equations of the motion of a particle of unit mass, solicited by a force derived from the potential $-1/2c^2$, referred to a "time" parameter τ. We shall call it the pseudo-particle and τ the pseudo-time.

If in these equations the three "momentum" variables p_x,p_y,p_z are eliminated, we find a system of three differential equations of the second order. If, finally, we replace the independent variable $d\tau$ by the physical time t by means of the relation $d\tau = c^2 dt$, our equations become identical with the differential equations of the rays, as obtained by minimizing the time $\int ds/c$ in Fermat's principle.

Further relationships now become clear: We have $p_x = dx/d\tau = dx/cds = \cos\alpha/c$, $\cos\alpha$ being the first direction cosine, etc. Thus the "momenta" are directional quantities along the rays. The pseudo-velocity is seen to be $ds/d\tau = 1/c = \nu$, the refractive index. This is all part of the wave-particle complementarity, which worried physicists as far back as the Newton-Huygens arguments about light.

What is the relationship between the rays and the hydro-acoustic energy? The answer is given by going back to the expressions for the density of energy E and its flux vector density $\vec{F}$, and replacing ψ by its travelling wave expression. On discarding lower powers of ω and then using the eikonal equation, we find simple expressions for these quantities in terms of the intensity $|u|^2$; the fact that

the energy flux vector $\vec{F}$ is in the direction of the momentum (p_x, p_y, p_z), that is, of the tangent to the rays, becomes evident from this substitution. Finally, the equation of continuity obeyed by $E, \vec{F}$ leads to the following one in the present picture: If the pseudo-time τ is used instead of t, and if p_x, p_y, p_z are regarded as the components of a fluid velocity field (based on the function S we are using), then the energy (in these units) obeys the classical equation of continuity.

We may forecast one of our results in the following terms: If in the above picture of a spatial flow, the fluid were incompressible, then the energy density would be a "first integral" of the ray equations; i.e., it would remain constant along each ray, so that, by tracing it to its source (the emitter) where its value is regarded as known, we would have its value at the point in space of interest (the detector). This would enormously simplify our problem. But since the above flow in $x\,y\,z$-space is very far from incompressible, the above method is totally inapplicable[1]. However, by using, not a single travelling wave, but a statistical ensemble of such waves, randomly out of phase, we can easily establish an equation of continuity in the 5-dimensional "space" of values of the six variables (x, y, z, p_x, p_y, p_z) which satisfy the equation $H = 0$. Now the Hamiltonian theory comes to our aid, showing that this flow in 5-dimensions is incompressible. This is the consequence of Liouville's theorem, of fundamental importance in classical statistical mechanics. Therefore the energy density is constant along each bi-characteristic, or ray in the 5-dimension representation.

The "model" of the action of the ocean in transmitting acoustic energy over long ranges from an emitter of naval interest to a receiver, experiencing all the random viscissitudes of the environment as well as of these two objects, is a statistical ensemble $\{\psi_n\}$ of travelling waves ψ_n, and only approaches a single one (a point source, plane wave, etc.) in the limit. It happens that for the present purpose it is easier to deal with the ensemble (however near to its limit) than the limit itself.

There is a two-fold situation that may appear paradoxical: First, the sum of two travelling waves is not in general a travelling wave and does not have a wave front in the usual sense. This fact, which should be evident from the analytical expressions, has too frequently been overlooked and has led to errors in some standard text books in acoustics. Second, in spite of the inapplicability of the wave front picture, the ray picture and the Hamiltonian form of the equations continue to be valid. Moreover, the additivity of energies transmitted along several intersecting rays is an immediate consequence of their corresponding to travelling waves that are randomly out of phase. If they were in phase their amplitudes would add vectorially: there would be interference. This is not observed under the physical conditions of our military situation, with its multi-path reception, etc., lending support to the validity of our model.

From the ensemble $\{\psi_n\}$ we are led to the replacement of the E and $\vec{F}$, which were functions of position only, to corresponding quantities which depend on ray direction (momentum) as well. Let (dV) be an element of volume in the $x\,y\,z$-space and let $\vec{D}$ be a direction (a point on the unit sphere). If (dD) is an elementary cone of directions (elementary area on the sphere) containing $\vec{D}$, we shall select the sub-ensemble of $\{\psi_n\}'$ consisting of those waves whose individual wave fronts at (dV) have a direction in (dD). To be precise, this has to be required at some chosen reference point in (dV); but the results depend only infinitesimally on its exact choice. Consider the sum of energies in (dV) contributed by all the members of the sub-ensemble $\{\psi_n\}'$: to quantities of higher order, it is proportional to the volume dV and the rea dD, and may be written as

$$E\,dV\,dD = E(x, y, z, p_x, p_y, p_z)\,dV\,dD ,$$

where, of course, p_x, p_y, p_z, are the components of the vector $\vec{D}/c$. The coefficient E in this expression is the energy density per unit 5-volume in the phase-space M_5. When integrated over the whole unit sphere it gives the energy density of the radiation field in ordinary 3-space.

A corresponding definition is given for the energy flux density in M_5. Then by an additive process, starting with the ordinary equations of continuity for the individual elements ψ_n in our ensemble, and making obvious assumptions about the latter, an equation of continuity in the phase space M_5 is obtained. We give only one result at this point: Let dS be an element of surface in ordinary 3-space and dD an element of directions. If θ is the angle between the normal to dS and the direction $\vec{D}$ in dD, the rate of flow of energy across dS due to the waves of ray directions in dD is given by

$$E \cos\theta \, dS \, dD \quad ,$$

where E is the value calculated at a reference point in dS and the direction $\vec{D}$. [Note that any change in $\vec{D}$ and dD during the elementary time $d\tau$ considered has only a higher order effect on the flux.] This result corresponds to the following:

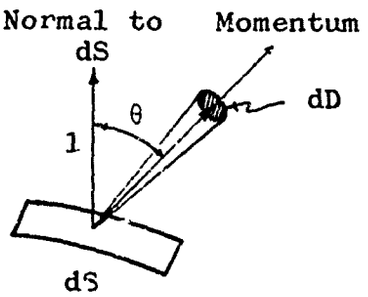

$$[d\Omega^2]/2 = \frac{1}{c^2} \cos\theta \, dS \, dD$$

We shall find an invariantive expression for the $\cos\theta \, dS \, dD/c^2$, which will lead to the desired conclusion of the behaviour of E along each ray.

We return to our Hamiltonian equations. The six first-order differential equations determine one and only one integral curve through each point of the six dimensional phase space of the variables x, y, z, p_x, p_y, p_z. Furthermore, as the independent variable τ increases, each point moves continuously along its integral curve (the ray). This gives rise to a continuous one-parameter group of transformations — a "flow". Liouville's theorem declares that this flow is incompressible.

The only part of the six-dimensional phase space is the sub-space M_5 of five dimensions defined by the equation

$$M : H(x,y,z, p_x, p_y, p_z) = 0 \quad .$$

Since the Hamiltonian H is a first integral it remains constant along each integral curve. Therefore the locus M_5 is invariant in the flow, and contains the whole of every integral curve containing a point in common with it. Thus there is produced a flow in the sub-phase-space M_5. As a corollary of Liouville's theorem it too is conservative.

The concept of integral invariant was developed at the end of the last century by H. Poincaré [2] in connection with dynamical systems, and greatly extended and given wide applications by E. Cartan [3] in the early decades of this century. In its simplest forms it is a familiar notion: the density ρ of a fluid, when integrated over any given volume of the latter, remains invariant during the flow, since the mass it represents is conserved. In a perfect fluid, the integral, around a closed curve drawn in the fluid, of the tangential component of the velocity, is invariant during the flow: this is Lagrange's theorem of the constancy of "circulation", which is basic to his theory, as well as to Helmholtz's theory of vortices. In this case, for invariance, the integral has to be taken about a <u>closed</u> curve: it is called a "relative" integral invariant. When this condition is unnecessary, the invariance is called "absolute". An example of an absolute integral invariant is obtained by applying Stokes' theorem to the circulation, thus expressing the circulation as a surface integral of the normal component of the curl of the velocity -- the <u>vorticity</u> (tourbillon).

The Hamiltonian theory gives us a set of integral invariants, starting with the basic relative one. Setting

$$\Omega = p_c \, \delta x + p_y \, \delta y + p_z \, \delta z$$

and using the notation $d\Omega$ for the curl, and bracketed product for "outer" or Grassmann product (actually a determinant operation) we have the series

$$\oint \Omega\,, \quad \int_2 d\Omega\,, \quad \int_4 [d\Omega\, d\Omega] = \int_4 [d\Omega^2]\,,$$

$$\int_6 [d\Omega^6]\,, \quad \int_5 u\, dS_5 \quad .$$

The existence of the six-dimensional one is simply the statement of Liouville's theorem, and the five-dimensional one is a direct consequence. The "density" u in the latter case can be computed as a simple single-valued expression in terms of the 6-gradient of H.

For our purposes the integrand of the four-dimensional integral invariant is of particular importance because of its simple geometrical interpretation. We have, in fact, when the 4-dimensional element in M_5 is taken as the pair (dS, dD) used before, that

$$[d\Omega^2] = \frac{2}{c^2} \cos\theta\ dS\, dD \quad .$$

This is derived from the expression for the quantity

$$\tfrac{1}{2}[d\Omega^2] = [dp_x\, dx\, dp_y\, dy] + [dp_x\, dx\, dp_z\, dz] + [dp_y\, dy\, dp_z\, dz]$$

where each bracket is the Jacobian determinant of the indicated quantities with respect to the four parameters in the representation of the surface element in question.

Since, as we have seen, the flux of energy across the above element is given by

$$E\, \frac{c^2}{2}\, [d\Omega^2] \quad ,$$

and since as stated before, this flux is the integrand of an integral invariant — by the conservation of energy — it follows by the general theory (actually by Cartan's theorem) that the ratio, namely E, is a scalar invariant, constant along each ray. By referring it back to its point of contact with the emitter, its value can be determined. By doing this for each ray through the receiver, the total energy received can be found by integration. Since one usually assumes the initial values of E at the receiver constant, the above process reduces to that of finding the solid angle subtended at the receiver by the directions of those rays which connect it with the emitter.

The most limited view of the above results is that we have established the validity of a ray tracing process in the case of a general sound speed function $c = c(x,y,z)$ [4]. Actually we have done more, we have laid the basis for a statistical treatment of perturbations of the system. But this cannot profitably be discussed in its general terms in this Conference, so we shall sample it in a simple special case below. Before leaving this subject, it is noted that when our equations are written in general curvilinear coordinates, our densities become multiplied by the factor $\sqrt{g}$, where g is the determinant of the matrix of coefficients in the general expression for the length squared, ds^2. With coordinates appropriate to cylindrical spreading, $\sqrt{g} = r$; for spherical spreading, $\sqrt{g} = r^2 \sin\theta$, etc. This in combination with the invariance of the energy density automatically introduces the appropriate spreading factors, $1/r$, $1/r^2$, etc.

Finally, we note that in our use of integral invariants, they are understood in Cartan's sense — "sliding invariants", remaining constant when all points are slid an arbitrary amount along the integral curves, without requiring to be moved to synchronous points, as required by the Poincaré conception.

We turn now, to illustrate the ideas graphically, to the special case (to which so much of present ray-tracing is confined!) in which we have a "fixed profile", with c depending on depth alone, $c = c(z)$. Then, as is generally known, the equations can be integrated explicitly, requiring, however, a set of numerical integrations of numerically given functions. For purposes of

illustration, we shall exhibit the phenomena graphically, after the easy reductions have been made.

The first reduction in this case replaces the geometrical 3-space by a vertical plane, the (x,z) plane or, more appropriately to cylindrical spreading, the (r,z) plane. The two momenta (p_r, p_z) and equation $H = 0$ show that the phase-space becomes a 3-dimensional one, M_3 instead of M_5. This makes it possible to draw diagrams of it on paper.

The next simplification when $c = c(z)$ is the validity of Snell's law in the large, which states that p_r is constant along each ray. This constant, which we denote by w, is called the Snell constant. The set of all rays in M_3 having a given Snell constant are on the locus of the equation

$$p_z^2 + w^2 = 1/c^2 \quad .$$

This makes it convenient to use, for specifying points in M_3, the three coordinates (r,z,p_z). This M_3 is shown in Fig. 1 drawn with these three coordinates as rectangular.

This is not a tank of water — the ocean is represented as the (r,z) plane — but, if a tank of anything, a tank of phase space. But the flow in M_3 is <u>incompressible</u>.

Since the above equation, given the fixed Snell constant value w, does not contain r, its locus is a horizontal cylindrical surface whose elements are parallel to the axis of r. Each ray with this value of w winds around the cylinder in helix-like fashion.

Let a plane be drawn perpendicular to the r-axis. It cuts all the rays in one and only one point. As the value of r at its intersection increases, i.e., as the plane is moved along the r axis and always perpendicular to it, the points of intersection of a given ray move in this plane; such a plane is called the <u>surface of section</u>, and was introduced in the study of dynamical systems by H Poincaré, and later by G.D. Birkhoff and the author [5]. The transformation induced by the rays when r is

changed, as described above, can be pictured as a flow in the lane. During this flow, the representative point of each ray moves about its curve of given Snell constant. Finally, the flow is incompressible. This is a consequence of the sliding integral invariant $\int_{\Omega} d\Omega$, which, when evaluated on a region of the surface of section, is equal to its area.

Since, as in the more general case, energy flux is a constant along the rays, the application of the relations just outlined can serve as a basis for the study of propagation, showing shadow zones, etc. It may be noted that caustics have disappeared in this representation; they re-appear only when we project sets of rays of M_3 onto the (r,z) plane.

A case of great practical importance is that in which the ranges are very large — quite a number of ray periods. Then the practical uncertainty of the exact lengths of periods leads to the replacement of the energy flux density by its average over a period. Either on this basis, or by reasoning based on "ergodic mixing", we are led to consider an energy flux density, which depends on the Snell constant w only, and therefore has the path curves on the surface of section as its level lines. With a slightly higher degree of perturbing influences, this flux becomes essentially constant over those parts of the surface of section where long-range propagation is not intercepted (by underwater obstructions, etc.) — and zero over the latter parts. Then the acoustic power born by a bundle of rays is proportional to the (invariant) area in which it is cut by the surface of section. On reducing the picture back into geographical space the spreading factor comes out of the equations automatically.

NOTES AND REFERENCES

1. It would be sufficient if, instead of being incompressible, the flow in the x y z-space were conservative, i.e., had a density function whose integral over any piece of this space remains constant: then the ratio of the energy flux density to the latter would be the required first integral. Such a density exists -- and is put in evidence by convential ray-tracing -- as long as we stay sufficiently close to the emitter. This provides the justification of the standard methods; but only under this proviso. Further away, in fact at distances of particular interest, the densities become increasingly multiple-valued (indeed, singular at the branch-loci, the caustics); therefore the justification breaks down. It is for this reason that the present approach is not submitted merely as an alternative to a more conventional one, but as a method of salvaging the latter when it ceases to be applicable.

2. H. Poincaré, "Méthodes Nouvelles de la Mécanique Céleste", Vol.III (Gauthier-Villard, Paris, 1899).

3. E. Cartan, "Leçons sur les Invariants Intégraux" (Hermann, Paris, 1922).

4. Thus justifying the conventional ray-tracing method in the neighourhood of the emitter, and replacing it by a method that is valid at greater distances. See Ref. 1 above.

5. H. Poincaré, l.c.; G.D. Birkhoff, "The Restricted Problem of Three Bodies" (Rendiconti del Circolo Matematico di Palermo, 23 August 1914); B.O. Koopman, "On Rejection to Infinity and Exterior Motion in the Restricted Problem of Three Bodies", (Trans. Amer. Math Soc., 1927).

6. The simplified picture (given in so many treatments) of the "limiting critical ray" composed of two tangent circles, one above and one below the horizontal ray, is derived from the two-line "approximation" to the acoustic profile. Unfortunately,

for this picture, the differential equations determining the rays involve the derivative of the profile as coefficients. Since the two-line "approximation" has no derivative at the point at which this critical ray is constructed, it is difficult to understand the logic of the construction.

Instances of the surface of section are shown in Fig. 2 (one duct) and Fig 3 (two ducts). These show the lines of the 2-dimensional flow, along each of which the Snell constant w has a fixed value. They enclose the ducts. In the two duct case, they intersect at the point of maximum sound speed, corresponding to the unstable horizontal ray, approached asymptotically by its neighbours (with increasing or with decreasing range. In Fig. 2 we have heavily shaded the region at which the emitter injects its energy. Since the vertical dimensions of the emitter are small in comparison with the depth, the region is a slender band. Its horizontal extent is wide since this corresponds to the directions (or momentum values) at which it emits power. For a point source, the band would shrink up to a horizontal line segment.

Figure 4 shows the effect of an underwater obstruction, with a key to the calculation on the left, which refers back to the surface of section. Time does not permit us to go into details here; we merely note that the fraction intercepted by the obstruction is the horizontal interval through which the ray (in rz-space) can be moved and still cut the obstruction, divided by the ray period.

Figure 5 shows a graphical method of exhibiting the source-to-duct coupling. The case shown is that of a single duct under an inversion layer, and assumes perfect specular reflection (plus phase randomization) at the water's surface. One may think of the whole diagram as reflection in the latter surface (method of images, or "Lloyd's mirror"), whereupon it resembles the case of three ducts separated by two unstable horizontal rays. Again the thin horizontal band shows the

energy injected by the emitter, its heavily shaded part being that portion that survives bottom absorption and can undergo long range propagation. Their ratio might be called the "source-to-duct coupling factor". At the receiver is drawn a horizontal band representing what it can receive (or, by reversal of path, emit). The dotted part of the receiver band shows the part of the emitted energy that reaches the receiver. Clearly the fraction of emitted power reaching the receiver is not even approximately equal to the product of an emitter coupling factor (determined by its depth) times a receiver coupling factor (determined by its depth): given the acoustic profile, the fraction in question is a function of two variables (the two depths); but not a product of two functions of one variable each.

DISCUSSION

The author stated that the theory would have to be reworked for the 5-dimensional case when applied to a range-dependent sound-speed profile. Also, since a flat bottom was assumed in the theory, it would have to be modified if that were not the case.

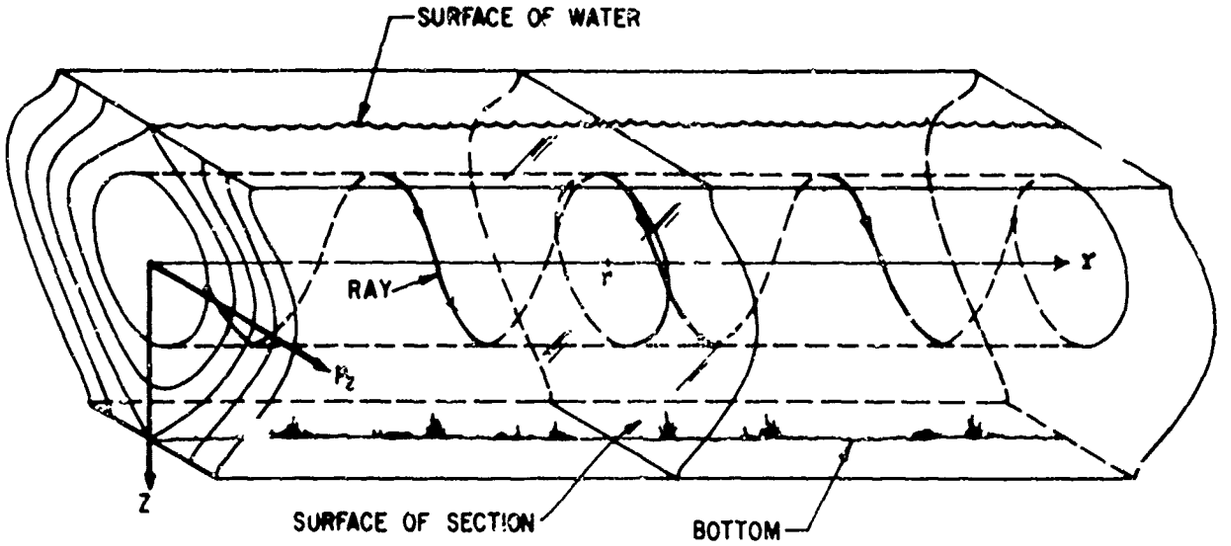
SURFACE OF WATER
RAY
r
r
P_z
Z
SURFACE OF SECTION
BOTTOM

FIG. 1

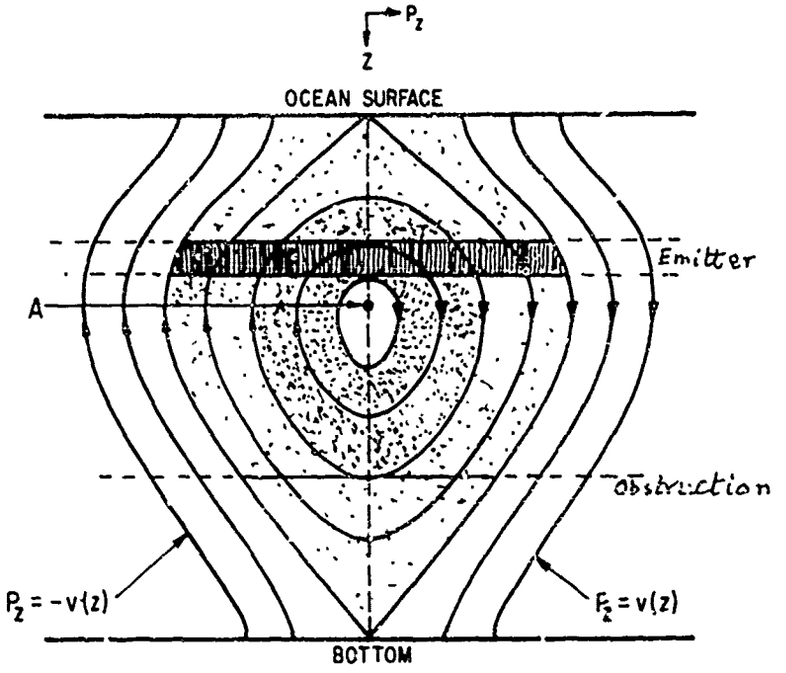
P_z
Z
OCEAN SURFACE
Emitter
A
obstruction
$P_z = -v(z)$
$P_z = v(z)$
BOTTOM

FIG. 2

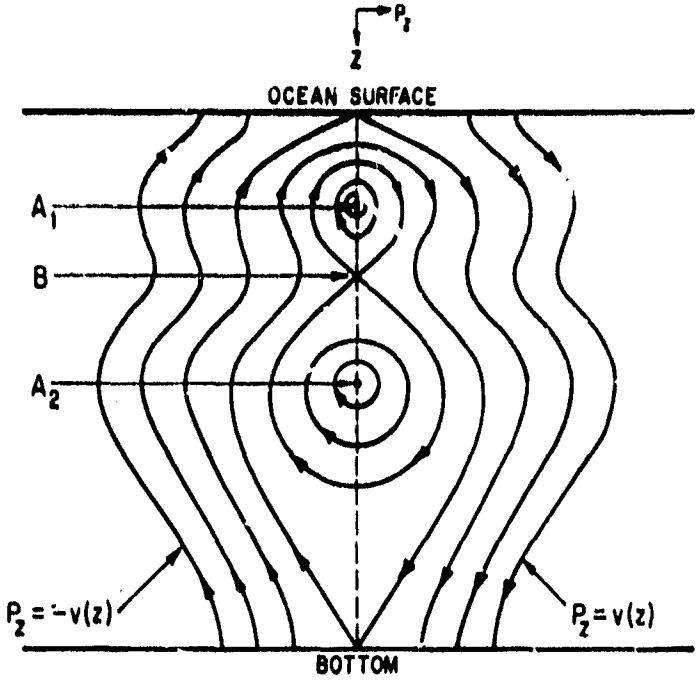

FIG. 3

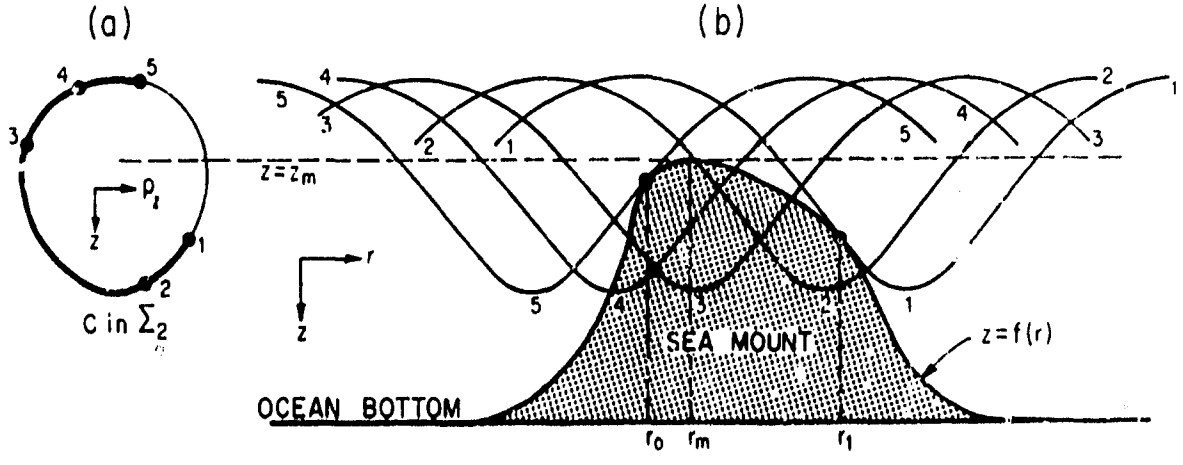

FIG. 4

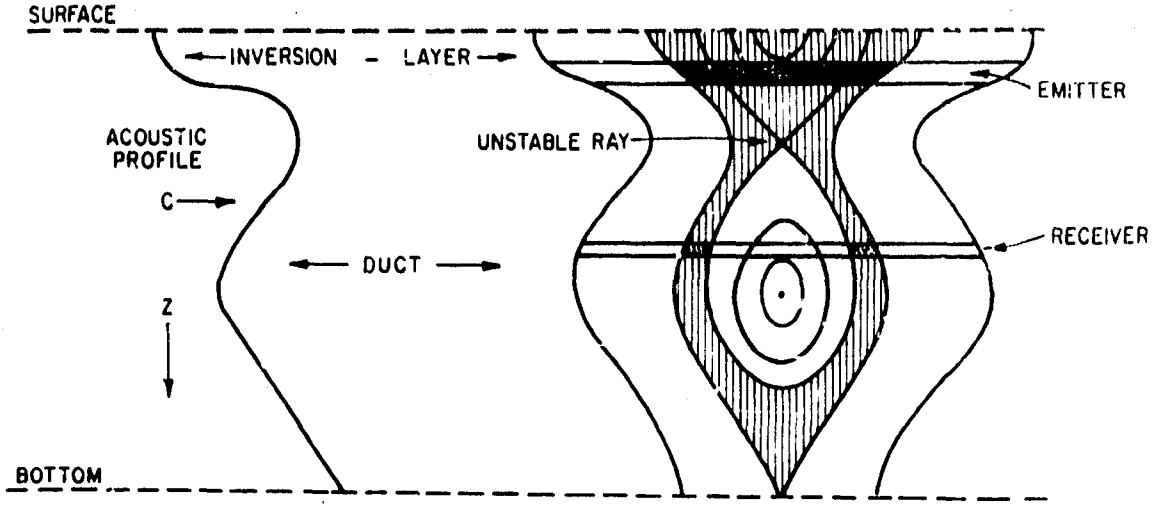

FIG. 5

RAYS AND STATISTICAL DIFFRACTION THEORY

by

R.H. Clarke
SACLANT ASW Research Centre
La Spezia, Italy

ABSTRACT

A method of extending ray tracing is proposed, such that medium-scale irregularities of a statistical nature are taken into account along with large-scale irregularities in refractive index of the medium.

INTRODUCTION

Ray tracing is a relatively simple and very practical method of obtaining solutions to the fundamentally very difficult problem of wave propagation in an inhomogeneous medium. These solutions are admittedly approximate, but give perfectly satisfactory "engineering" answers, provided the scale size of the inhomogeneities is large compared to the propagating wavelength, and provided one does not require answers in regions of focusing or shadowing.

I want to address myself to the problem of dealing with irregularities, both in the medium and on the boundaries, whose scale size is not large compared to the propagating wavelength. In particular, I am interested in scale sizes of the same order or somewhat larger than the propagating wavelength. I shall exclude from consideration those irregularities whose scale size is smaller than the propagating wavelength, since in a sense these will be invisible to the propagating wave and are likely to have only a collective effect.

(For example, bubbles will have the effect of changing the acoustic properties of the water when encountered by metre wavelengths, and so the problem reverts to that of the effect of conglomerates of such bubbles of scale sizes of a wavelength or larger.)

One can state the problem in a somewhat more restricted fashion by asking how one can retain the advantages of using ray tracing to deal with large-scale irregularities when medium-scale irregularities are also present. I eventually want to discuss the effect of medium-scale irregularities on the sea surface, in the depth of the thermocline and in the medium everywhere. But it is useful to start with the rough surface.

EXAMPLE OF SURFACE ROUGHNESS

After a more-or-less tortuous path, some of the rays leaving the source will strike the surface [Fig. 1]. A straightforward extension of the ray tracing concept would be to say that each ray is reflected in the local specular direction. But there are two objections to this course: (1) this idea is only valid for large-scale irregularities and (2) a hideously large number of ray tracings would have to be made in order to obtain a satisfactory statistical ensemble.

An alternative approach, and the one I shall advocate, is to use ray tracing to just below the surface; then to employ statistical diffraction theory to account for the effect of the statistically rough surface; and then to employ ray tracing again to describe the subsequent progress of the field. This gets over the two disadvantages I mentioned in connection with the first approach: (1) since diffraction is taken into account the validity of the method is not restricted to large-scale irregularities, and (2) the ensemble averaging is performed <u>at</u> the surface and so a single ray tracing suffices to describe the subsequent reflected field.

I shall give more details of this in a moment. But first, I must describe more clearly how one can make the transition from rays to fields and back again.

RAYS AND PLANE WAVES

Dating from Rayleigh's treatment of the problem of reflection from a corrugated surface [Ref. 1], the expansion of acoustic fields in terms of plane waves travelling in different directions has become increasingly popular. Intuitively, one expects there to be an equivalence between such plane waves and the purely geometrical concept of rays; that equivalence will now be demonstrated.

Uniform Medium

The pressure field $p(x,y,z)$ in the half space $z \geq 0$ can be represented [Ref. 2] by the plane-wave spectrum $F(\alpha, \beta)$, such that

$$p(x,y,z) = \int_{-\infty}^{\infty}\int F(\alpha,\beta) \exp\{-jk_o(\alpha x + \beta y + \gamma z)\}\, d\alpha\, d\beta \qquad \text{[Eq. 1]}$$

where (α, β, γ) are the cosines of the angles formed between the direction of a single plane-wave component and the three rectangular coordinate axes (x,y,z), and k_o is the phase constant (wave-number) of the medium.

Assuming the acoustic source to be at the origin, at a large distance r from the source, such that $k_o r >> 1$, it can be shown by applying stationary phase methods that the pressure field is asymptotically

$$p \sim j\frac{\lambda\gamma}{r} F(\alpha,\beta)\, e^{-jkr} . \qquad \text{[Eq. 2]}$$

Thus the angular plane-wave spectrum $F(\alpha, \beta)$ is proportional to the directivity pattern of the source.

The associated intensity is

$$I = \frac{|p|^2}{2Z_0} = \frac{\lambda^2 r^2 |F(\alpha, \beta)|^2}{2Z_0 r^2}$$

where Z_0 is the characteristic impedance of the medium. It will be useful later to refer intensities to the "intensity at unit distance", which is

$$\mathcal{I}_0 = \frac{\lambda^2 r^2 |F(\alpha, \beta)|^2}{2Z_0} \quad . \qquad \text{[Eq. 3]}$$

Layered-Inhomogeneous Medium

When the acoustic properties of the medium change with z, then the angular spectrum $F(\alpha, \beta)$, which describes the field at the source level $z = 0$, no longer describes the field for any other z. However, by writing the angular spectrum as a function of z, namely $F(\alpha, \beta, z)$, it can be supposed that all plane waves emanating from the source follow the ray paths prescribed by geometrical acoustics, provided the irregularities in the medium are of scale-size very large compared to the acoustic wavelength. Hence [Ref. 3],

$$p(x,y,z) = \int_{-\infty}^{\infty}\int F(\alpha, \beta, z) \exp\left\{-jk_0\left(\alpha x + \beta y + \int_0^z q\, dz\right)\right\} d\alpha\, d\beta \qquad \text{[Eq. 4]}$$

where $q = n \cos\theta$, the refractive index $n = n(z) = c(0)/c(z)$ is the ratio of the sound speeds, and θ is the local angle to the vertical of the ray path [Fig. 2]. From Snell's law it is obvious that

$$q^2 = n^2 - \alpha^2 - \beta^2 \quad . \qquad \text{[Eq. 5]}$$

The W.K.B. solution [Ref. 4] for a plane wave travelling in a layered-inhomogeneous medium yields

$$F(\alpha,\beta,z) = \left(\frac{\rho c \cos\theta_o}{\rho_o c_o \cos\theta}\right)^{1/2} F(\alpha,\beta) \qquad \text{[Eq. 6]}$$

where $\rho = \rho(z)$ is the density, and the subscript 0 refers to the source level. (Note that $Z = \rho c$ is the characteristic impedance at the level z).

Integrating Eq. 4 by stationary phase methods, asymptotically

$$p\ j\ \frac{\lambda}{\Delta^{1/2}} F(\alpha_o,\beta_o,z)\ \exp\{-jk_o(\alpha_o x + \beta_o y + \int_o^z q\,dz)\} \qquad \text{[Eq. 7]}$$

where (α_o,β_o) are the direction cosines at the source which satisfy the stationary-phase conditions. These conditions are that

$$x = -\int_o^z \frac{\partial q}{\partial \alpha}\,dz \qquad \text{[Eq. 8a]}$$

and that

$$y = -\int_o^z \frac{\partial q}{\partial \beta}\,dz \qquad \text{[Eq. 8b]}$$

which are just the equations of the ray path. The quantity Δ is a determinant in the general case [Ref. 3], but in the x-z plane reduces to

$$\Delta = \left(\int_o^z \frac{\partial^2 q}{\partial \alpha^2}\,dz\right)\left(\int_o^z \frac{\partial^2 q}{\partial \beta^2}\,dz\right). \qquad \text{[Eq. 9]}$$

The intensity corresponding to the pressure of Eq. 7 is

$$I = \frac{|p|^2}{2Z} = \frac{\lambda^2 |F(\alpha,\beta,z)|^2}{2Z\Delta} \qquad \text{[Eq. 10]}$$

where, as can be shown by applying Eq. 9 to Eq. 5,

$$\Delta = \frac{x}{\sin^2 \theta_o} \int_o^z \frac{\sin \theta}{\cos^3 \theta} \, dz \ . \qquad \text{[Eq. 11]}$$

Then, the final intensity formula is

$$I = \mathfrak{I}_o \frac{\sin^2 \theta_o}{x \cos \theta \cos \theta_o \int_o^z \frac{\sin \theta}{\cos^3 \theta} \, dz} \qquad \text{[Eq. 12]}$$

and is equivalent to the formula developed by Krol [see Session 2 of these Proceedings] using purely geometrical arguments.

Thus an equivalence between a ray description and a plane-wave description of acoustic fields in a layered inhomogeneous medium has been established, which takes care of the effect of large-scale irregularities.

The next step in the argument is to consider how each of these plane-wave components, which go to make up the total field, are affected by medium-scale statistical irregularities encountered either in the medium or at its boundaries.

STATISTICAL DIFFRACTION THEORY

Consider the simplest case, shown in Fig. 3, of a plane wave incident normally on a "random phase screen". Such a screen alters the phase of a wave propagating through it in a random manner, but leaves its amplitude unchanged. (The physical mechanisms in the ocean which produce such random phase screens will be discussed in the next section.)

If the random phase induced by the screen is a zero-mean, gaussian random process of variance σ_ϕ^2, then the transmitted field will

consist of a coherent part and an incoherent part. (Coherence is used here in the sense of the phase having a deterministic relation to the incident phase.) It can be shown [Ref. 5] that the coherent part of the transmitted field is a plane wave, in all respects the same as the incident field, except that its amplitude is reduced by $\exp\{-\frac{1}{2}\sigma_\Phi^2\}$. This can be expressed by saying there is a "coherence loss" of intensity of

$$\exp\{-\sigma_\Phi^2\} \quad \text{or} \quad 4.34\,\sigma_\Phi^2 \ \text{dB} \ .$$

But this is not a real, absorptive loss, and the remaining transmitted energy is incoherently scattered in a pattern which is determined by the second-order (i.e., lateral correlation) statistics of the phase across the screen.

In terms of rays: the incident ray suffers a "loss", but apart from that continues as though the screen were not there. The lost energy is converted at the screen into new, incoherent sources of energy whose angular pattern can be determined. Ray tracing can be applied to follow the subsequent behaviour of this new source of acoustic energy.

RANDOM MECHANISMS IN THE SEA

Rough Sea Surface

For a plane wave incident obliquely on a randomly rough sea surface, [Fig. 4], the simplest (and most common) approach is to ignore amplitude effects and to consider only the random phase induced in the incident wave arising from the local excess path travelled by the wave to and from the surface, compared with reflection from the mean surface. Thus the surface is replaced by a random phase screen. If the surface profile is a zero-mean, gaussian random process of variance σ_h^2 the random phase variance is

$$\sigma_\Phi^2 = (2k\cos\theta)^2\,\sigma_h^2 \ .$$

Thus the incident ray is specularly reflected with a coherence loss of $4.34\,\sigma_\Phi^2$, and the remaining energy is scattered incoherently with an intensity pattern determined by the spatial correlation function of the surface roughness.

Internal Waves

Figure 5 shows an idealized model of an abrupt thermocline boundary separating two regions of the ocean in which the sound velocities, and hence the phase constants, k_1 and k_2, are slightly different. If the boundary profile is a zero-mean, gaussian random process of variance σ_h^2, then the same sort of arguments used for the rough surface establish the first-order effect on an obliquely incident plane wave of such a boundary as a random phase screen with phase variance

$$\sigma_\Phi^2 = (k_2 - k_1)^2 \sec^2\theta\, \sigma_h^2 .$$

(A similar expression has been used to examine the effect of irregularities in dielectric holograms [Ref. 6].)

Volume Irregularities

If a plane wave travels a distance ℓ [see Fig. 6] through a slab of tenuous irregularities in refractive index, then it is physically plausible to suppose that the emerging field is randomly modulated in phase but unaltered in amplitude. (For a more rigorous validation of this approach, see the résumé of the work of Fejer and Bramley in Ref. 5.) Hence the slab of irregularities behaves as a random phase screen. If ℓ is many times a typical scale size, ζ_0, of the irregularities, then a crude application of the Central Limit Theorem establishes that the emerging phase is approximately gaussian, with variance

$$\sigma_\Phi^2 = k^2 \zeta_0 \ell\, \sigma_n^2$$

where σ_n^2 is the variance of the refractive index fluctuations. Hence as a ray traverses such irregularities it will suffer a loss of

$$4.34\, k^2\, \zeta_0 \sigma_n^2 \quad \text{dB/unit length}$$

of its energy to incoherent scatter, the angular spread of which will be determined — as in the other examples — by the lateral scale size of the irregularities.

REFERENCES

1. Lord Rayleigh, "The Theory of Sound", Vol. 2, 2nd ed., 1896, Dover Publications Reprint, 1945, p.89.

2. R.H. Clarke, "Coherent Reflection by the Rough Sea Surface of the Acoustic Field from a Source of Arbitrary Directivity", SACLANTCEN Technical Memorandum No. 152, April 1970. (Also available as AD 870 497 and N70 28947, and to be published in J. Acoust. Soc. of America, January 1972.)

3. K.G. Budden and P.D. Terry, "Radio Ray Tracing in Complex Space", Proc. Roy. Soc. London, Series A, Vol. 321, February 1971, pp. 275-301.

4. L.M. Brekhovskikh, "Waves in Layered Media", Academic Press, 1960, p.198.

5. J.A. Ratcliffe, "Some Aspects of Diffraction Theory and their Application to the Ionosphere", Rep. Progr. Phys., Vol. 19, 1956, pp. 188-267.

6. J. Upatnieks and C.D. Leonard, "Characteristics of Dielectric Holograms", IBM J. Res. Develop., Vol. 14, No. 5, September 1970, pp. 527-532.

DISCUSSION

The author confirmed that these ideas could be applied to a surface sinusoid with roughness superimposed, and also to a rough and randomly layered bottom - although the latter is more difficult.

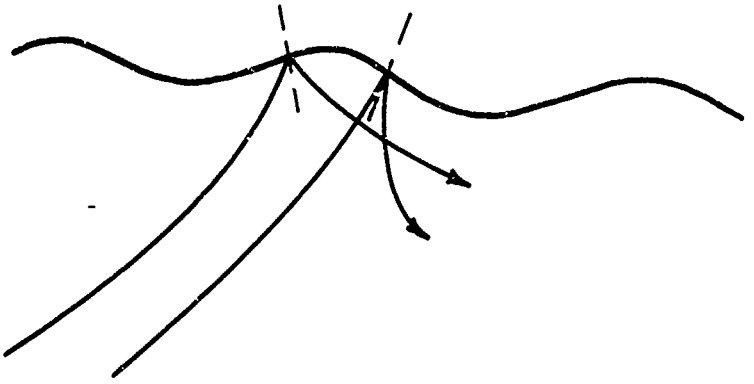

FIG. 1

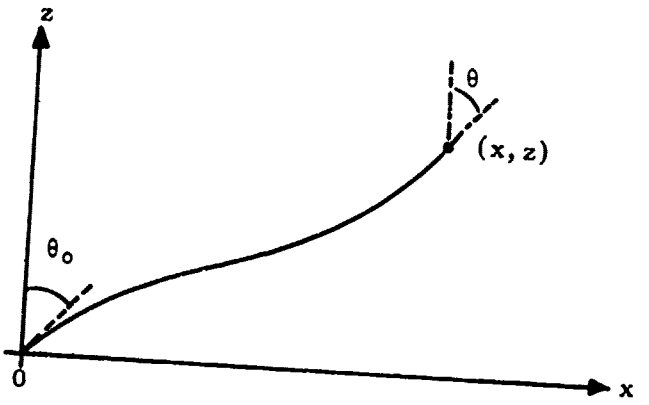

FIG. 2

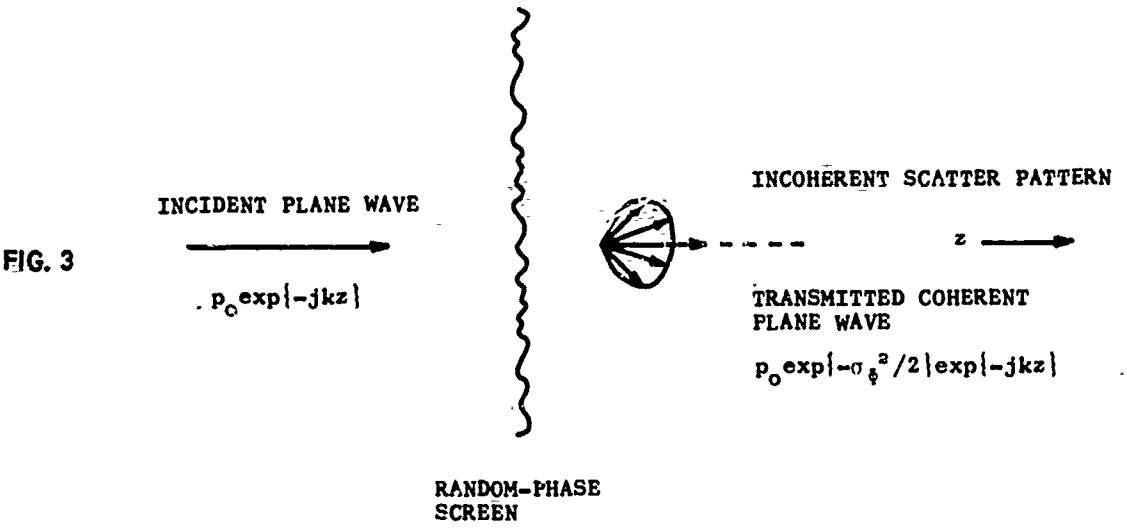

FIG. 3

ROUGH SURFACE

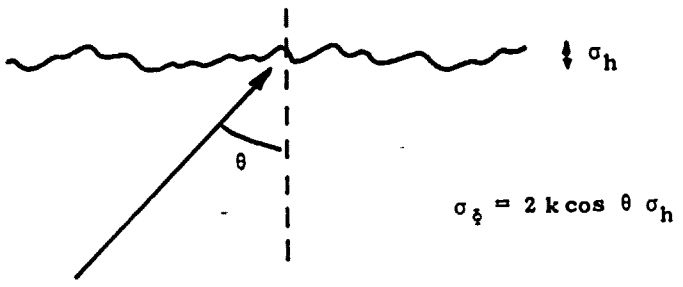

FIG. 4

INTERNAL WAVES

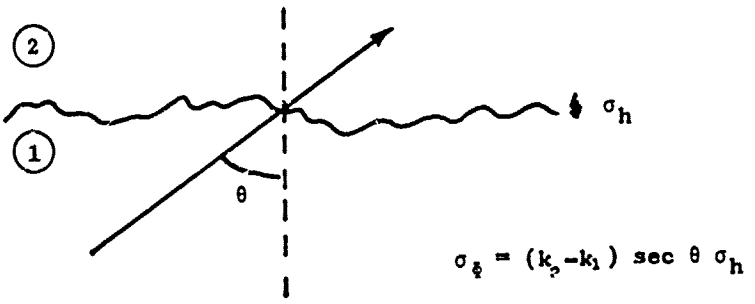

FIG. 5

VOLUME IRREGULARITIES (MEDIUM SCALE)

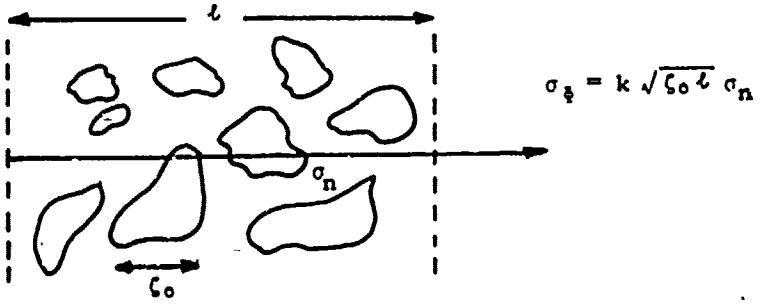

FIG. 6

APPROXIMATE METHODS FOR RAY TRACING

by

M.J. Daintith
Admiralty Underwater Weapons Establishment
Portland, Dorset, U.K.

INTRODUCTION

The conventional approach to ray tracing is to follow one ray, usually specified by its initial direction, by standard techniques of numerical integration along the ray path, building up a set of values of horizontal displacement, direction, and travel time, as a function of vertical displacement (horizontal stratification of the sound speed profile in the medium is assumed). This process demands computer time and storage. By this means a family of ray plots may be built up [e.g. Fig. 1]

In many applications, however, this forward computation is inconvenient, in that an inverse problem requires solution. Examples are:

a. Given the terminal points of the ray, what is the grazing angle at one point on it (this frequently occurs in experimental determinations of bottom reflectivity).

b. Given the measured travel time from surface to bottom, what is the true slant range (e.g. the use of bottom transponders in some navigational systems).

c. Given the known slant range, what is the true travel time (the converse of (a), also often encountered in bottom studies).

A common feature of these problems is that they do not involve rays having turning points (i.e., the slope is always of the same sign), and basically the theory to be described is restricted to this special, but important, situation. It is possible to extend the treatment to

rays having a turning point, but the advantages of the approach are not as marked, and this extension will not be discussed here.

THEORY

Figure 2 shows the geometry of the situation. Horizontal range is denoted by x, vertical depth by z, and the grazing angle at any point on the ray by θ. The terminal points of the ray will be denoted by $(0,0)$ and (X,Z). The sound speed profile (horizontally stratified) is assumed known, the sound speed at depth z being c. The slope of the slant range line θ_0, and the slant range is D.

The basic ray-tracing equations are that along the ray:

$$\tan\theta = dz/dx \quad . \qquad \text{[Eq. 1]}$$

$$\cos\theta/c = p = \text{constant} \quad \text{(Snell's Law)} \quad . \qquad \text{[Eq. 2]}$$

$$dz/dt = c \sin\theta, \text{ where } t = \text{travel time} \quad . \qquad \text{[Eq. 3]}$$

On integrating along the whole path, we obtain

$$X = \int_0^Z \cot\theta \; dz \quad . \qquad \text{[Eq. 4]}$$

$$t = \int_0^Z (\operatorname{cosec}\theta/c) \, dz \quad . \qquad \text{[Eq. 5]}$$

If we use Eq. 2 to express Eq. 4 in terms of c and p, we note that, if given X and Z, Eq. 4 becomes essentially an integral equation for determining p. The method to be described is based on noting that integration is an averaging process, and that this suggests that we are in effect computing some rather complex weighted average of c.

As far as Eq. 5 is concerned, we may note that another average value of c is defined by travel along the straight line path; since by Fermat's principle the true travel time represents a stationary value, the change due to moving to the displaced straight line path can differ only be second order quantities.

We therefore express c in terms of its deviation from the mean value over depth $\bar{c}$, where $\bar{c} = \frac{1}{Z}\int_0^Z c\,dz$, and write $c = \bar{c}[1+\varepsilon(z)]$, where for real profiles

$$\varepsilon(z) \ll 1 \quad . \qquad \text{[Eq. 6]}$$

It is also convenient to replace the Snell's law constant p by an angle $\bar{\theta}$, defined by the equation

$$\cos\bar{\theta}/\bar{c} = p \quad . \qquad \text{[Eq. 7]}$$

Since $\bar{c}$ is a value which actually occurs on the sound speed profile, $\bar{\theta}$ is a real angle for any real ray.

The mean of ε over z is clearly zero, and we may define higher moments by such equations as

$$\overline{\varepsilon^2} = \frac{1}{Z}\int_0^Z \varepsilon^2\,dz \quad . \qquad \text{[Eq. 8]}$$

On making the appropriate substitutions in Eqs. 4 and 5, we obtain

$$X/Z = \cot\theta_0 = \frac{\cot\bar{\theta}}{Z}\int_0^Z (1+\varepsilon)\,[1-\cot^2\bar{\theta}\,(2\varepsilon+\varepsilon^2)]^{-\frac{1}{2}}\,dz \quad . \qquad \text{[Eq. 9]}$$

$$t = (\operatorname{cosec}\bar{\theta}/\bar{c})\int_0^Z (1+\varepsilon)^{-1}\,[1-\cot^2\bar{\theta}\,(2\varepsilon+\varepsilon^2)]^{-\frac{1}{2}}\,dz \quad . \qquad \text{[Eq.10]}$$

Equations 9 and 10 may now be expanded as binomial series in ε, the results being

$$\cot\theta_0 = \cot\bar{\theta}\,[1+{}^3/_2\,\overline{\varepsilon^2}\operatorname{cosec}^2\bar{\theta}\cot^2\bar{\theta}+O(\overline{\varepsilon^3})] \qquad \text{[Eq.11]}$$

$$\bar{c}t/Z = \operatorname{cosec}\bar{\theta}\,[1+\overline{\varepsilon^2}\,(1-\tfrac{1}{2}\cot^2\bar{\theta}+{}^3/_2\cot^4\bar{\theta})+O(\overline{\varepsilon^3})] \qquad \text{[Eq.12]}$$

the first-order terms vanishing identically.

If we retain only terms to the second order, Eqs. 11 and 12 are very easy to invert or otherwise manipulate, with the following results (noting that $D = Z\operatorname{cosec}\theta_0$) :

$$\cos\bar{\theta} = \cos\theta_0 \,(1 - {}^3\!/_2\, \overline{\varepsilon^2}\, \cot^2\theta_0) \qquad \text{[Eq. 13]}$$

$$D = \bar{c}t\,[1 + \tfrac{1}{2}\,\overline{\varepsilon^2}\,\{(\bar{c}^2\,t^2/z^2) - 3\}] \quad , \qquad \text{[Eq. 14]}$$

and the inverse of Eq. 14

$$\bar{c}t = D[1 - \tfrac{1}{2}\,\overline{\varepsilon^2}\{(D^2/Z^2) - 3\}] \quad . \qquad \text{[Eq. 15]}$$

These equations clearly give a very simple answer to the problems cited in the introduction. They are easy to compute, and require computer storage for only two environmental parameters, $\bar{c}$ and $\overline{\varepsilon^2}$, both of which are easily computed once for all for any given sound speed profile.

ACCURACY

Equations 13 to 15 are approximations in which terms in $\overline{\varepsilon^3}$ and higher moments have been ignored, and it is obviously necessary to determine the errors introduced (and indeed even to decide if the series is convergent).

This problem has been solved as follows. Considering all possible sound speed profiles for which $\bar{c}$ and $\overline{\varepsilon^2}$ are specified, and for given values of X and Z, for which of these profiles will the values of p or of t given by Eqs. 2, 4 and 5 have extremal values? This is a variational problem, which can be handled by the technique of using Lagrangian multipliers for the equations of condition. The result, for both p and t, is that extremal values will be attained when $c(z)$ is a function of (z) which can take only two discrete values, i.e., when the sound speed profile is that of a two-layered environment.

This, however, is not sufficient to determine a true maximum, since the two-layer profile is specified by only two conditions, but has three degrees of freedom. It is necessary to find a third constraint, and an obvious one is given by the observation that any real profile has bounded values of c, that is, that it has a maximum and a minimum value for sound speed. It can now be shown that the extremal values in this situation will be given when one of the layers is allocated either the greatest or the least value of c, denoted by c_{max} and c_{min} [Fig. 3].

From these extreme profiles it can be shown that the series expansion is absolutely convergent, and that the values of $\cos\bar{\theta}$ and D lie within the bounds given by the following expression:

$$\cos\bar{\theta} = \cos\theta_0 \left[1 - \tfrac{3}{2}\,\overline{\epsilon^2}\,\cot^2\theta_0\,(1+\gamma_1)\right]$$

$$D = \bar{c}t\left[1 + \tfrac{1}{2}\,\overline{\epsilon^2}\,\{(\bar{c}^2 t^2/z^2) - 3\}\,(1+\gamma_2)\right]$$

$$\left(\frac{\overline{\epsilon^2} - b^2}{3b}\right)(5\cot^2\theta_0 - 1) \leq \gamma_1 \leq \frac{a^2 - \overline{\epsilon^2}}{3a}\,(5\cot^2\theta_0 - 1)$$

$$\left(\frac{\overline{\epsilon^2} - b^2}{b}\right)\cot^2\theta_0 \leq \gamma_2 \leq \left(\frac{a^2 - \overline{\epsilon^2}}{a}\right)\cot^2\theta_0$$

$$c_{max} = \bar{c}(1+a) \qquad c_{min} = \bar{c}(1-b)$$

It is clear from these expression that the error is greatest at the maximum range, and falls off roughly as the fourth power of range.

If we make some simplifying assumptions (basically that gradients are never very large, so that the sound speed profile moves relatively smoothly between its extremes), it can be shown that, to a reasonable degree of accuracy, the error at maximum range is approximately equal to the correction introduced by adding the term in $\overline{\epsilon^2}$ for the Snell's law constant $\cos\bar{\theta}$, and is half the corresponding correction for the slant range determination.

ILLUSTRATIONS

To demonstrate the sort of accuracy that the approximations can give, a comparison has been made between the results of an exact computation, using a digital computer, and the approximations given above, for two profiles (chosen basically to ease the digital computer's task).

Figure 4 outlines the profiles used. That marked 'typical' has parameters not unlike those found in the real ocean; the 'extreme' profile was designed to have wide limits (a 10% variation in sound speed) and incorporates a marked inversion layer.

Figures 5 and 6 illustrate the results for travel time. The computed slant range errors are shown for

a. the very simple formula $D = \bar{c}t$ and

b. the second-order expression [Eq. 15]. The computer upper and lower bounds are also shown. It will be seen that, with one second order correction terms the error is at most 9 m in 28.9 km for the 'typical profile, and is only 23 m in 19.3 km for the 'extreme' profile.

A similar analysis was carried out to compute the error in initial grazing angle as deduced from the Snell's law parameter $\cos\bar{\theta}$. A summary of the results is given in the following table.

TABLE 1

ERRORS IN GRAZING ANGLE

Profile	Range (km)	True Grazing Angle (deg)	Error in Angle (deg)	Maximum Error Bounds (deg)
'Typical'	15	15	0.01	±0.05
	20	8	0.1	±0.17
	24.5	4	0.27	±0.4
	29.3	0	0.74	±0.87
'Extreme'	10	17.5	0.01	±0.15
	15	7	0.1	±0.8
	16.5	4	0.17	±1.2
	18.7	0	0.29	±1.9

It will be noted that the errors in grazing angle are larger for the 'typical' profile than for the 'extreme'; this is because the horizontal ranges with the 'typical' profile are much greater than for the 'extreme', and the strong range dependence outweighs the smaller variation in the sound speed. Even so, the errors are remarkably small over most of the range, and the accuracy everywhere is probably greater than is warranted by the reliability of the input data.

DISCUSSION OF RESULTS

It is apparent that for most purposes the errors introduced by the use of this approach are far smaller than the quality of the input data would justify, and the saving in computer size required is considerable. Furthermore it is clear that, because the sound speed enters only in the form of statistical averages it is easy to assess the precision to which individual measurements should be made. Again, from this analysis, it is evident that the effect of irregularities in the profile will not in general be of great importance; this is a deduction that would be difficult to make by conventional ray-tracing methods.

At first sight the high accuracy of this very simple approximation seems surprising. The following argument gives an explanation for this result. In the integration over z for X and t (Eqs. 4 and 5), the order in which successive increments are added is immaterial, and the profile can be redrawn so that c is a monotonically increasing function of z (this is the same as forming a Lebesgue integral). The approximation then consists, in effect, of replacing this 'regularised' profile by the constant gradient profile of best fit by least squares. The shape of the ray-path will be quite different, but the Snell's law constant and the travel time will be nearly unchanged. This argument also shows immediately why the two-layer profile gives the extreme bounds, since this is the one which is least well fitted by a single straight line.

The method is clearly capable of extension. For example, if in say, a side-scan sonar the launching grazing angle and the travel time are simultaneously recorded it is possible to estimate the height of a projection above the sea-bed (since in effect $\bar{\theta}$ and t are given) by suitable inversion of the equations. Such applications will be reported separately.

FIG. 1

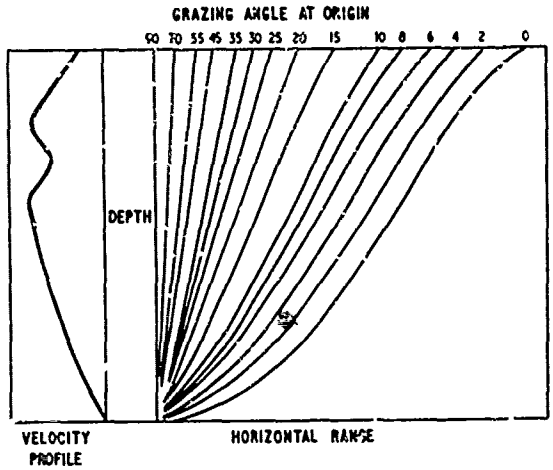

RAY TRACE FAMILY

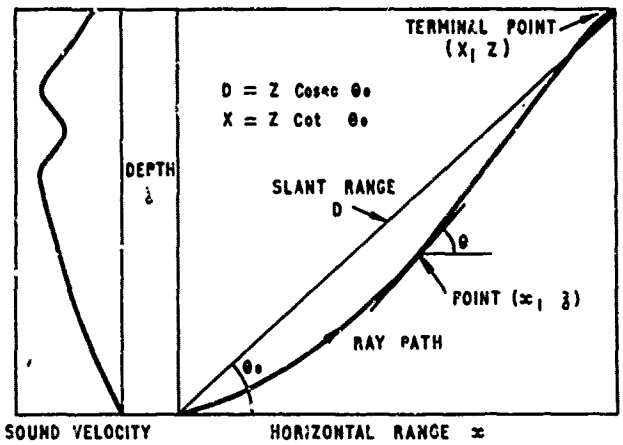

FIG. 2

RAY PATH GEOMETRY

FIG. 3

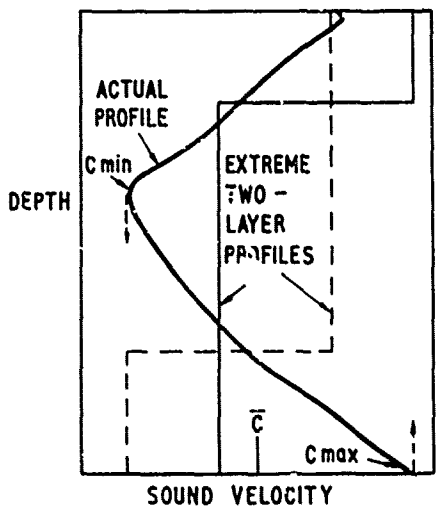

BOUNDING PROFILES

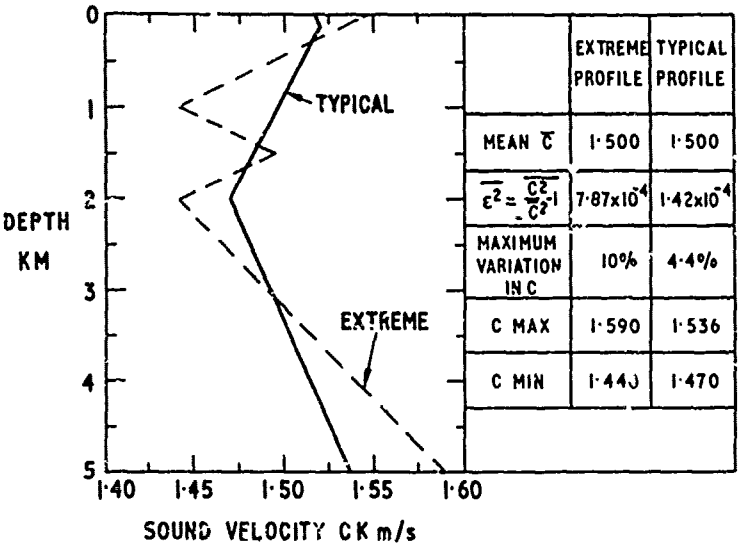

	EXTREME PROFILE	TYPICAL PROFILE
MEAN $\bar{C}$	1·500	1·500
$\overline{\varepsilon^2} = \overline{\frac{C^2}{\bar{C}^2}} - 1$	$7{\cdot}87 \times 10^{-4}$	$1{\cdot}42 \times 10^{-4}$
MAXIMUM VARIATION IN C	10%	4·4%
C MAX	1·590	1·536
C MIN	1·440	1·470

FIG. 4

SOUND VELOCITY PROFILES

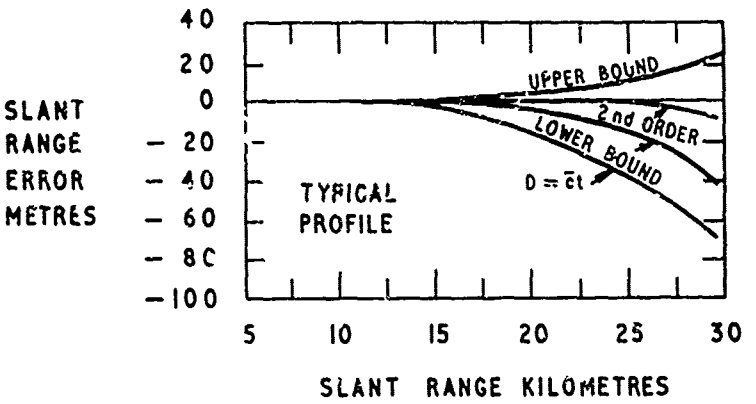

FIG. 5

ERROR IN SLANT RANGE DETERMINATION

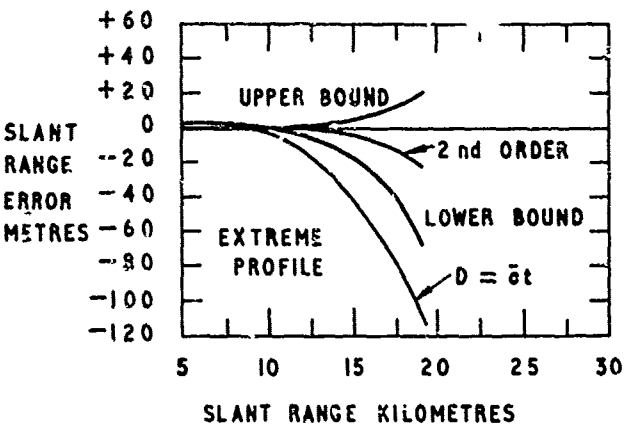

FIG. 6

ERROR IN SLANT RANGE DETERMINATION

CONSIDERATIONS ON NUMERICAL AND EXPERIMENTAL PROPAGATION MODELS FOR TWO-DIMENSIONAL VARIATION OF MEDIUM PROPERTIES

by

W. Sluyterman van Langeweyde
Forschungsanstalt der Bundeswehr für Wasserschall und Geophysik
Kiel, Germany

ABSTRACT

One of the problems the FWG is dealing with is the prediction of sound propagation loss in shallow water. A part of this problem is being treated by bringing measurements and numerical computation into relationship.

First a formal description was given of the general problem and then the concept of a partial problem. Some sets and a function were defined:

C : the set of oceanographic conditions.

E : the set of acoustical excitations under water.

$p = C \times E$: the carcesian product of C and E, so that $p = (c, e) \in P$ with $c \in C$ and $e \in E$ called the set of channel conditions.

A : the set of acoustical fields under water

$f : P \to A$: A function of the set P into the set A, so that $a = f(p)$ for $a \in A$, $p \in P$

The main problem, the prediction of $a \in A$ was divided into two subproblems:

(1) Subproblem: Prediction of $p \in P$

(2) Subproblem: To find f for all $p \in P$

The paper was confined to the treatment of subproblem two.

The methods used to approach the problem, relevant to propagation loss in shallow water, are:

(1) Simultaneous measurements of oceanographic and acoustical data in special areas of the North Sea and the Baltic.

(2) Acoustical measurement in a model basin with definite physical conditions as far as possible.

(3) Numerical model computations on a digital computer.

These three methods have to be related to each other. The corresponding sets and functions are written C', E', P', A' and f' for method two and C'', E'', P'', A'' and f'' for method three.

Taking measurements according to method one, finite subsets of C,E,A are found, which are marked by a bar.

$$\bar{C} = \{C_i \mid i \in I\} \subset C$$

$$\bar{E} = \{e_j \mid j \in J\} \subset E$$

$$\bar{P} = \{p_k \mid k \in K\} \subset \bar{C} \times \bar{E} = \{(C_i, e_j) \mid i \in I, j \in J\} \subset P$$

$$\bar{A} = \{a_k \mid k \in K\} \subset A$$

I,J,K : sets of Subscripts

The function thus found, $\bar{f}: \bar{P} \to \bar{A}$ is a restriction of f, so that $\bar{f} = f$ for $p \in \bar{P}$.

The next aim is to define a numerical model with an input set $\bar{P}''$ equivalent to $\bar{P}$, an algorithm f'' so that the output set $\bar{A}''$ is equivalent and comparable to A.

The numerical model $(\bar{P}'', \bar{f}'', \bar{A}'')$ will be called an <u>isomorph image</u> onto the triple $(\bar{P}, \bar{f}, \bar{A})$ with the <u>isomorphism (h_1, h_2)</u>, so that

$h_1 : \bar{P} \xrightarrow{bij} \bar{P}''$ is a bijective function $\bar{P}$ onto $\bar{P}''$

$h_2 : \bar{A} \xrightarrow{bij} \bar{A}''$ is a bijective function $\bar{A}$ onto $\bar{A}''$ and

[Remark: $g : X \xrightarrow{bij} Y \iff$
$Y = g(x)$ for all $y \in Y$, $x \in X$ and
$g(x_1) = g(x_2) \Rightarrow x_1 = x_2$]

$h_2[\bar{f}(\bar{p})] = f''[h_1(\bar{p})]$ for all $\bar{p} \in \bar{P}$

$$\begin{array}{ccc} \bar{P} & \xrightarrow{h_1} & \bar{P}'' \\ \bar{f} \downarrow & & \downarrow \bar{f}'' \\ \bar{A} & \xrightarrow{h_2} & \bar{A}'' \end{array}$$

The final goal is to extend this isomorphism onto whole sets P and A to come from P to A, without knowing f, via h_1, f'' and h_2^{-1} (reverse function h_2); however, in order to keep the problem tractable, the sets have to be decomposed into further cartesian factors, and these factor sets have to be reduced by classifications and by means of statistical descriptions.

By a simple concrete example of 6 series of model basin measurements the decomposition of the set $\bar{P}'$ was demonstrated to the point that the internal structure of the first function $\bar{h}_1'$ of the aspired isomorphism could be seen and the channel conditions described.

In a few words, the ray tracing program used and the representation of the function $\bar{f}''$ was described. The program traces rays in a plane, which is given the range-depth coordinates. A variability of sound velocity in both directions is taken into account in a manner that this plane is divided into triangles with constant sound velocity gradients with vertical and horizontal components. This causes the rays to be triangle-wise parts of circle arcs.

The equation

$$v(x,z) = \frac{\partial v}{\partial x}(x - x_c) + \frac{\partial v}{\partial z}(z - z_c)$$

with x_c, z_c as centre coordinates of the ray curvatures, is generally valid for two dimensional variability sound velocity. For $v = \alpha x + \beta z + \gamma$, x_c and z_c are constant, which leads to circles.

For the surface and bottom reflections exits for subroutines are provided which compute for instance random variable reflection angles at surface or reflection factors for stratified bottoms, subroutines which are being developed at this time.

Several subroutines compute coordinates, travel time and distance of rays. Calcomp ray plots can be drawn. The intensity is computed such that each ray is given a starting intensity according tc the directional diagram of the source. This intensity is being reduced stepwise by medium and bottom bounces. A number of rays, of the order of 2000, are being traced in that manner and their intensity parts are accumulated at given distances and depth classes incoherently.

After having decomposed the input set $\bar{P}''$ in an analogous manner as $\bar{P}'$ the internal structure of the first function $\bar{h}'_1$ was demonstrated. The second function $\bar{h}'_2$ was defined after describing the sets $\bar{A}'$ and $\bar{A}''$ averaging the intensities to sound level distributions with depth and total propagation losses.

The results of the four series which differed most were demonstrated by slides.

The influence of the internal waves present at condition 4 brought in the experiment a double value of total propagation loss in dB compared with the loss at the stationary profile, whereas for the computed propagation loss a rise of 10% occurred. The stationary profile was of nearly constant gradient with a sound velocity of 1487 m/s at the surface and of 1606 m/s at the bottom. Probably the still unknown directional diagram of the source and reflection

behaviour of the bottom in the experiment is responsible for this disagreement. These properties will be measured soon and put into the program.

With this simple example the formal concept was just demonstrated. But a concept of that kind will really be helpful in explaining, handling and controlling the problem, when large numbers of oceanographic parameters are to be taken into account.

APPLICATION OF RAY TRACING WITH HORIZONTAL GRADIENT TO MONOSTATIC BOUNDARY REVERBERATION

by

L.B. Palmer
Naval Research Laboratory
Washington, D.C., U.S.

ABSTRACT

Presented is the current work being done at the Naval Research Laboratory (NRL) on the development of a series of computer programs to predict long range, low frequency, monostatic boundary reverberation. The emphasis is on the ray tracing technique and its application to the special problems of estimating the transmission loss of rays that hit the boundaries of the medium. The ray tracing technique is to increment a ray from point to point along its ray path by evaluating Taylor series expansions in arc length of various ray parameters such as range, depth, travel time, and range angle, which are based on the ray equation. Possible horizontal variations in sound speed are accounted for by allowing multiple input profiles. Also, a linearly segmented ocean bottom and a flat surface are assumed. Monostatic boundary reverberation is estimated by means of a range dependent formulation developed at NRL. An underlying assumption of this formulation is that when a ray encounters a boundary, it continues to propagate in the direction of specular reflection, while a small amount of the incident radiation is scattered in all directions. By reciprocity, scattered energy will return to the source-receiver back along those ray paths emitting from the source and passing through the boundary point at which the hit occurred.

INTRODUCTION

The purpose of this talk is to present the current work being done at the NRL on the development of a series of computer programs to predict long range, low-frequency monostatic boundary reverberation. The emphasis will be on the ray tracing technique and its application to the special problems of estimating the transmission loss of rays that hit the boundaries of the medium, especially the bottom.

The tracing of rays utilizes an iterative technique first described in Hudson Laboratory Report 150 by W.A. Hardy et al in 1968. This ray tracing model accounts for the possibility of a horizontal sound speed gradient by allowing for multiple input profiles, and assumes a linearly segmented ocean bottom. This model has been programmed in FORTRAN by J.J. Cornyn of NRL as part of a series of ray tracing and transmission loss programs. The ray tracing model has since been extracted from this series of programs, modified, and then adapted to the purpose of calculating monostatic boundary reverberation. Also, computer programs have been written which organize the ray tracing results and estimate reverberation by means of a formulation developed by J.T. Warfield of NRL.

I. ORGANIZATION OF PROGRAMS

The operation of the series of programs proceeds in four basic stages [Fig. 1]. First, since the modelling of the velocity field is a problem unto itself because of the possible presence of horizontal variations in sound speeds, it is tackled separately. Therefore, first a magnetic tape is generated on which is written the multiple profiles located at discrete ranges along the track of interest. Each profile consists of the sound speed and its first two derivatives with respect to depth, specified at discrete depths and the ocean bottom as discrete depth versus range points.

This tape serves as input to the ray tracing program. This program employs the iterative ray tracing technique to determine all boundary hits for the rays of interest. These points as well as the associated travel times, ray angles at the boundary, and transmission losses are written onto an output tape. An initial ray trace may not furnish enough information to adequately describe where the boundary hits occur. If this is the case, additional rays will be traced and additional ray tracing output tapes created.

The next computer program uses as input the output tapes from one or more ray traces and reorganizes this information onto another magnetic tape. By reorganizing is meant the creation of "order contours", which will be discussed in a moment. This reorganizing procedure is done separately, due to computer storage requirements and for the convenience of handling multiple ray traces.

Finally, the reorganized tape of ray tracing information is the input to reverberation calculating program, which computes the boundary reverberation function at discrete times.

II. REVERBERATION FORMULA

Before proceeding to a description of the ray tracing model, I would like to briefly outline the model used for predicting monostatic boundary reverberation.

Equation 1 is the formula used for determining the reverberation from a boundary which is detected at the source-receiver at time t.

$$R(t) = I_1 \Phi \int_0^{\infty} \left[\sum_{p \in m(x)} \sum_{r \in m(x)} C_{pr}^{x}(t) \cdot I(p,r,x,z) \right] x\,dx \qquad \text{[Eq. 1]}$$

I_1 is the source level relative to 1 yd and the remaining expression represents an integration over the three-dimensional

boundary, assuming separable source-receiver beam patterns and an azimuthal symmetry of the boundary.

An underlying assumption in the development of the reverberation formula, is that when a ray encounters a boundary, it continues to propagate in the direction of specular reflection, while a small amount of the incident radiation is scattered in all directions. By reciprocity, scattered energy will return to the source-receiver back along those ray paths emitting from the source and passing through the boundary point at which the hit occurred.

Consider now, the expression within the brackets, which is evaluated at each range x. The set $m(x)$ is a set indexing all possible ray paths from the source-receiver which pass through the boundary at range x. A single term of the double sum represents the contribution to reverberation from energy travelling from the source to the boundary point (x, z) along path p and returning along path r [see Fig. 2].

C is a characteristic function which is equal to one if the reverberation contribution I, attributed to the ordered ray pair, (p,r), will be detected at the source-receiver at time t, and zero otherwise. The times of detection will be those times t satisfying the inequality of Eq. 2.

$$t-D \leq T_p(x,z) + T_r(x,z) \leq t \ . \qquad \text{[Eq. 2]}$$

D is the signal duration and T is the one-way travel time for a signal travelling to the boundary at range x, along the path denoted in the subscript.

The contribution, if detected, is given by Eq. 3.

$$I(p,r,x,z) = \frac{B(\theta_p)\ \overline{B}(\theta_r)}{L_p(x,z)\ L_r(x,z)}\ \sigma(\overline{\theta}_p, \overline{\theta}_r) \ . \qquad \text{[Eq. 3]}$$

B and $\overline{B}$ are the transmitting and receiving beam patterns respectively, and the L's are the transmission losses suffered by travelling along the respective paths and σ is the boundary scattering strength.

III. ORDER CONTOURS

In order to get a visual picture as to how the possible paths between the source-receiver and the boundary at range x are found, an explanation of order contours is necessary. For a fixed ray R such as shown in Fig. 3, each boundary hit and turning point (both of which are called occurrences) is assigned a positive integer order. Surface hits and down turning points (called crests) are defined to be of odd order, while bottom hits and up turning points (called valleys) are of even order. The first bottom hit, or valley, for the fixed ray R is assigned an order of 2. Subsequent bottom hits and valleys are assigned 4, 6, 8 and so on. Surface hits and crests are assigned orders of 1, 3, 5, etc., in such a manner that the orders of the occurrences of the ray R increase with range.

Now consider the contours of curves determined by the boundary hits of identical order, plotted on an initial source angle versus range coordinate system, as shown in Fig. 4. Incidentally, a given contour need not necessarily be a continuous curve, but rather several continuous and disjoint segments.

For the reverberation from a given boundary, only those contours corresponding to that boundary are pertinent. For the purpose of illustration, let us assume that bottom reverberation is being sought. To determine all ray paths between the source-receiver and the bottom at range x, consider a horizontal slice at range x, as shown in Fig. 5. Denote the three paths having initial angles of θ_1, θ_2, θ_3 by 1, 2, 3 respectively. Then the set m(x) consists of the integers 1, 2, and 3, and hence there are 3^3, or 9 possible routes from the source-receiver to the bottom at range x and back again.

In reality, the computer ray tracing program will produce only a finite number of bottom hits, or, in other words, a finite number of points on the order contours. Figure 6 illustrates two order contours of the type produced by the computer program. Here the BT's represent the bottom hits and the V's the valleys determined by tracing rays with initial source angles of θ_a, θ_b, θ_c, etc. The true order contours are approximated by linearly connecting the known bottom hits of the same order. Travel time, transmission loss, and ray hit angle values between computed hits are found in interpolating linearly with respect to range. The valley type turning points are displayed to indicate the end points of the contours.

IV. RAY TRACING PROGRAM

The purpose of the ray tracing then, is to determine the boundary hits and the transmission loss, travel time, and ray hit angle for each hit. The rays traced should be those rays which hit the boundary and are not masked out by the source beam pattern. Also, the resulting boundary hits should approximate the true order contours as accurately as possible. In the search for a ray tracing model, it was felt that such a model should allow for multiple nontrivial sound speed profiles and an irregular bottom contour. Such a model was developed at the Hudson Laboratories at Columbia University of New York. This ray tracing technique is an iterative one in which a ray is incremented from point to point along its ray path. This is accomplished by means of evaluating Taylor series expansions in arc length of various ray parameters such as range, depth, travel time, and ray angle. These expansions are derived from the ray equation shown as Eq. 4.

$$\frac{d}{ds}\left[\frac{1}{v(x,z)}\cdot\frac{d\vec{P}}{ds}\right] = \text{grad}\left[\frac{1}{v(x,z)}\right] . \qquad \text{[Eq. 4]}$$

The sound speed, $v(x,z)$, is assumed to be known at every range x, and depth z, throughout the two-dimensional medium, and ds is a differential increment along the ray path, $\vec{P}$.

The present version of this ray tracing model has the following features:

1. Accommodates multiple profiles for possible horizontal variations in sound speed.
2. Each profile is defined at discrete depths with weighted parabolic interpolation used between specified depths.
3. Assumes a linearly segmented ocean bottom and flat surface, with specular reflection applied to both.
4. Uses incremental finite Taylor series approximations to ray paths.
5. Transmission loss, ray angle, and travel time computed at boundary hits as opposed to predetermined ranges.
6. Each ray assigned two subliminal companion rays for computing the amount of geometric spreading.
7. Multiple bottom loss tables are applied to various range intervals.
8. Individual rays are terminated upon exceeding input maximum allowable travel time or bottom loss ceilings.
9. Up to 500 rays may be traced, not including companion rays.

Operationally, rays are selected whose initial source angles are from that part of the source beam pattern which will experience bottom hits. To each of these "primary" rays, is assigned two "companion" rays whose initial source angles tightly bracket that of the primary ray. The rays are then traced through the medium which is described by the multiple profiles, linearly segmented bottom and flat surface. They are traced on an individual basis

between predetermined "rectification" ranges. After all the rays are traced to one of these ranges, which necessarily include the ranges at which the profiles are specified, the accumulated boundary hit and turning point information is written onto a magnetic tape. A computer storage area is then reinitialized and the ray tracing continued to the next rectification range or until some predetermined maximum range is reached. However, individual primary rays will be terminated prematurely if they exceed input travel time or bottom loss ceilings. For each boundary hit by a primary ray, six statistics are recorded.

1. Initial angle of ray.
2. Order of hit.
3. Range of hit.
4. Travel time.
5. Ray angle relative to the boundary.
6. Transmission loss.

For the problem to which the present model is applied, transmission loss is assumed to be made up entirely of bottom loss and geometric spreading loss. Bottom loss is input to the ray tracing program as several bottom loss versus incident angle tables which are applied to different range intervals, and geometric spreading loss is assumed to be given by Eq. 5.

$$\frac{1}{L} = \left| \frac{a^2 \cos\theta_o}{x \cos\theta_x} \frac{d\theta_o}{dz} \right| = \left| \frac{a^2 d(\sin\theta_o)}{x \cos\theta_x} \cdot \frac{1}{dz} \right| \qquad \text{[Eq. 5]}$$

where

a = unit distance
x = range of boundary hit
z = depth of boundary hit
θ_o = initial source angle of ray
θ_x = ray angle at boundary hit

The companion rays [sec Fig. 7] are used to calculate the factor dz, by determining their respective depths and directions at the range where the primary ray hits the boundary. The companion ray which has not yet hit the boundary in this region and is still being directed towards it, is used to determine dz. After a primary ray has been specularly reflected off the bottom, the amount of bottom loss will be added to the ray's accumulated bottom loss.

V. RAY TRACING TECHNIQUE

Now let us look at the ray tracing technique itself. When a ray's location, as well as its ray angle and travel time to that point, are known, the sound speed and its spatial derivatives at that position are used to determine the ray's location and associated parameters at a point further along the ray path. A single profile could be employed throughout the track, but often, actually encountered velocity fields require the specification of different profiles along the track of interest. Each sound speed profile is specified at discrete depths and the first two derivatives of sound speed with respect to depth are approximated at the given depths by means of weighted difference equations. Weighted parabolic interpolation is applied vertically and linear interpolation horizontally to make sound speed and its first two depth derivatives functions of both range and depth. Therefore, the first derivative of sound speed with respect to range can be approximated at any range and depth by a linear first difference with respect to range. With the use of this horizontal gradient in the Taylor series expansions, it is hoped to reckon with the effects on ray paths due to horizontal variations in sound speed.

Once the sound speed, its first two derivatives with respect to depth, and its first derivative with respect to range are determined for a known location on the ray path, various convergence tests are performed to determine how far to increment the ray path location, and associated parameters, by evaluating the Taylor series expansions. Normally, an input incremental step size, Δ_{max},

will be used in evaluating the Taylor series expansions. However, if certain convergence tests fail, the step size will be appropriately reduced. One of these tests require that the ray path does not experience more than some predetermined maximum amount of bending between computed ray locations. By "bending" is meant the change in the trigonometric sine of the ray angle. Another test requires that the chosen step size be used to predict the sound speed at the new ray location within a predetermined accuracy of the "true" sound speed at that point. By the "true" sound speed at a point is meant that value found by interpolating between input profiles. Regardless of these tests, the step size is never allowed to become smaller than some predetermined minimum allowable step size. This is done to expedite the incrementing of the ray path. Therefore, first the initial maximum step size, Δ_{max}, is used to determine a trial sine, given in Eq. 6.

$$\sin \theta_t = \sin \theta_0 + \alpha(\Delta_{max}, x_0, z_0, Z_0, D_0, G_0) \quad \text{[Eq. 6]}$$

The sound speed derivatives Z, D and G,

$$Z = \partial v/\partial z$$

$$D = \partial^2 v/\partial z^2$$

$$G = \partial v/\partial x$$

are all evaluated at the known ray path location, (x_0, z_0). A new step size, Δ', is then determined from Eq. 7.

$$\Delta' = \min \begin{cases} \delta = \sqrt{\dfrac{S}{|\sin \theta_t - \sin \theta_0|}} \cdot \Delta_{max} \\ \sqrt{\dfrac{S\, v_0}{\cos \theta_0\, z_0\, \delta}} \\ \Delta_{max} \end{cases} \quad \text{[Eq. 7]}$$

where S is an input maximum allowable change in sine, say 0.02. Next, using the new step Δ', a new location (x_t, z_t), is found further along the ray path by evaluating their Taylor series expansions.

By interpolation between two known profiles, a sound speed v_t is determined for this location. Then a computed sound speed, v_c, is found for this location using the Taylor series expansion of Eq. 8.

$$v_c(x_t, z_t) = v_0(x_0, z_0) + Z_0(z_t - z_0) + \frac{D_0}{2}(z_t - z_0)^2 + G_0(x_t - x_0) \qquad \text{[Eq. 8]}$$

If the computed and interpolation sound speeds differ by more than an input accuracy criterion, ϵ, then a new step size is found from Eq. 9.

$$\Delta'' = \min \begin{cases} \dfrac{\epsilon}{|v_t - v_0|} \cdot \Delta' \\ \Delta' \end{cases} \qquad \text{[Eq. 9]}$$

The step size will be further reduced to a predetermined minimum allowable step size Δ_{min} if the cosine of the predicted ray angle θ_t is greater than one, where the cosine is found from Eq. 10.

$$\cos \theta_t = c_t v_t \qquad \text{[Eq. 10]}$$

and where c is found by evaluating a Taylor series in arc length.

The final step size is never allowed to be less than Δ_{min}, except in such cases as approaching a boundary or a known profile location. Once the final step size is determined, a new ray path location and corresponding ray parameters are found by evaluating the different series for this step size. The process is then repeated with the new location being taken as the known ray path location.

Although Δ_{max} and Δ_{min} are inputs to the program, they may be redefined as a ray is traced. If an increase results, Δ_{min} will be taken to be the vertical distance between the known ray depth and the nearest depth, in the direction the ray is headed, at which a sound speed is specified in the input profiles. Δ_{max} will be reduced appropriately, if a straight line projection of the ray direction, of length Δ_{max}, passes outside the medium. Also, when a ray location is determined which is within about 100 m of a boundary, the input Δ_{min} will be used as the iterative step size, without the various tests being conducted.

The boundaries, themselves, are assigned tolerance gates of some vertical distance, such as a half a meter, within which a ray is considered as having struck that boundary. In some cases, interpolation will be employed between computed ray path locations within and without the medium in order to determine the step size necessary to increment the ray to the boundary.

The described ray tracing technique represents an adaptation of the original version to the computation of transmission loss at boundary hits as opposed to predetermined receiver ranges.

CONCLUSIONS

After the reverberation and ray tracing models were programmed, two test cases were run to check the validity of the programs. Both test cases involved the use of a single profile, one case being a constant sound speed profile, the other a constant gradient profile. The computer results for these two test cases compared quite well with the corresponding analytic solutions. The ray tracing technique itself, has been verified for a multitude of cases.

Next, the programs were run on a case for which measured reverberation data existed. This case entailed a track of fairly long range over a relatively rough, upward sloping bottom. The low-frequency signal duration was about 30 s, with the source beam pattern dominated

by the main lobe. Input boundary scattering strength tables were based on data appearing in the literature, as were the bottom depth and bottom loss tables.

A comparison of the predicted bottom reverberation versus the total measured reverberation is shown in Fig. 8. For this low frequency study, surface reverberation is assumed to be doppler shifted. The vertical, or reverberation, axis has a scaling of 10 dB between the indicated tick marks. The relative level of the two curves do not agree as well as had been hoped, but the appearance of the peaks at the recorded times seem to correspond fairly well. The peaks of the predicted curve correspond to the main beam of the source striking the bottom. However, the relative level of these peaks are largely determined by a small angular span of rays whose initial source angles usually vary by less than 1°. These so-called "crucial" rays are those rays which experience both valley type turning points and bottom hits with very low grazing angles as they propagate down range. Some of these rays will be completely RSR until an initial bottom hit occurs far down range, at which point the intensity of the given ray will dominate those of other rays hitting the bottom nearby which will have accumulated bottom loss by that range. These "crucial" rays will also tend to encounter the bottom at very low grazing angles where the bottom loss tables are the most questionable. Another problem is the occasional focusing of the "crucial" rays near the bottom. That is, they are sometimes in near-caustic regions as they approach the ocean bottom. Because of the so-called "crucial" rays, the predicted bottom reverberation curve is sensitive to slight changes in bottom depth definition, as was discovered when different approximations to the ocean bottom were used.

The linear segmentation of the bottom is also a problem area. The abrupt changes in slope between linear segments tend to artificially break up the wavefronts. This shows up as radically jagged sections in the order contours, which tends to weaken one's belief in the computer approximation of the contours and the validity of the

interpolation performed between computed bottom hits. Finally, averaging over reverberation estimates for several different headings did not significantly improve the results.

Despite these apparent problem areas the main difficulty seems to be in predicting the level of the reverberation curves. Work is continuing on this problem and the extension to the bistatic case. Investigation is underway at NRL to approximate ray intensities in near caustic regions and to more efficiently model the ocean bottom. Also, the ray tracing program is being modified to improve the iterative procedure and the spreading loss estimation.

DISCUSSION

The author said that the rough-surface reflection coefficient was an empirical function of the angles of incidence and reflection.

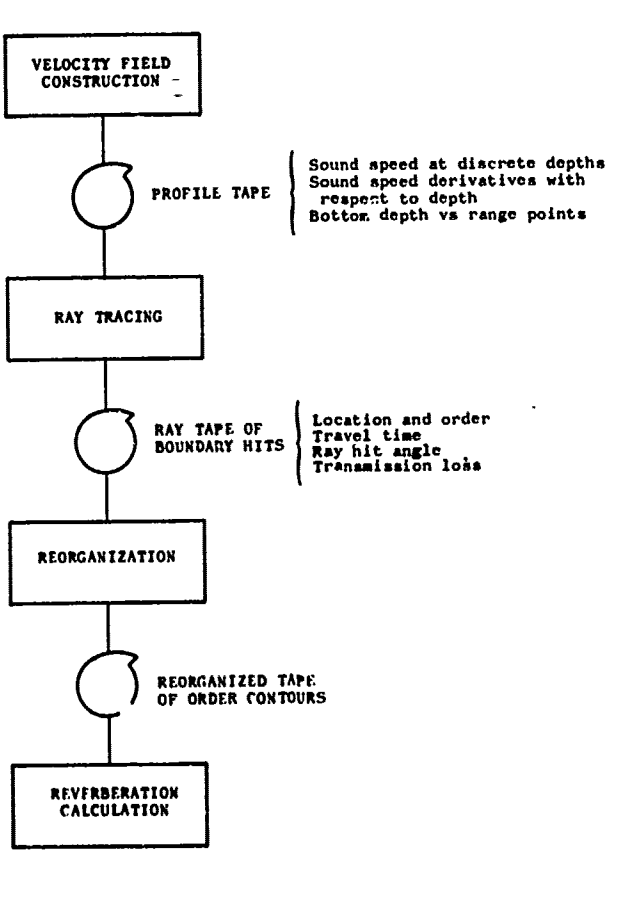

FIG. 1

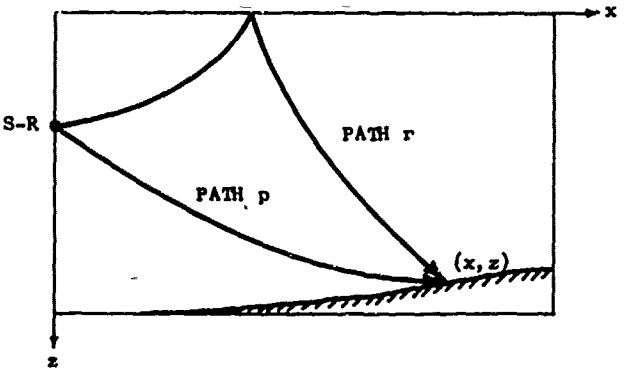

FIG. 2

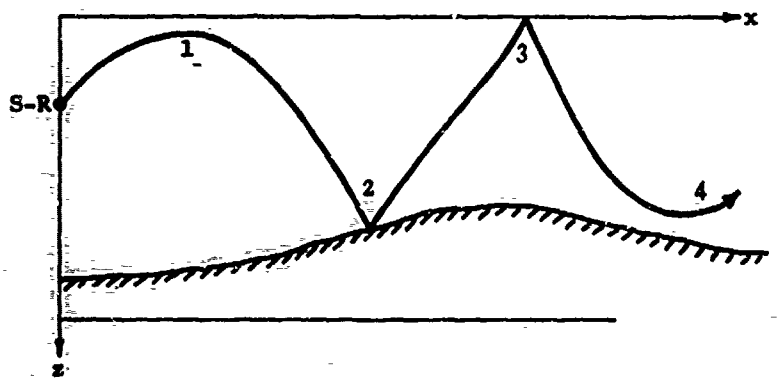

FIG. 3

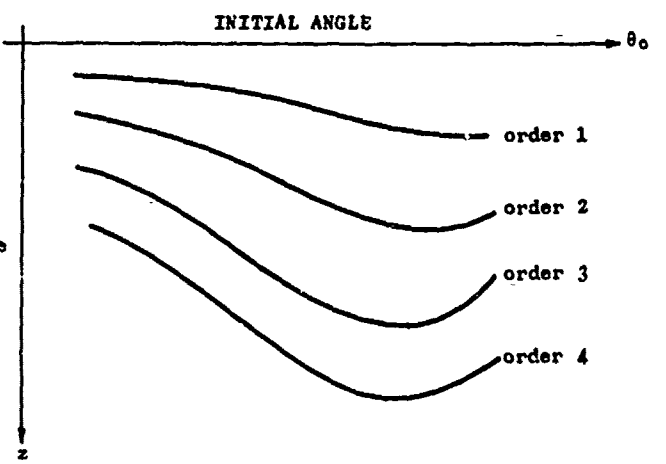

FIG. 4

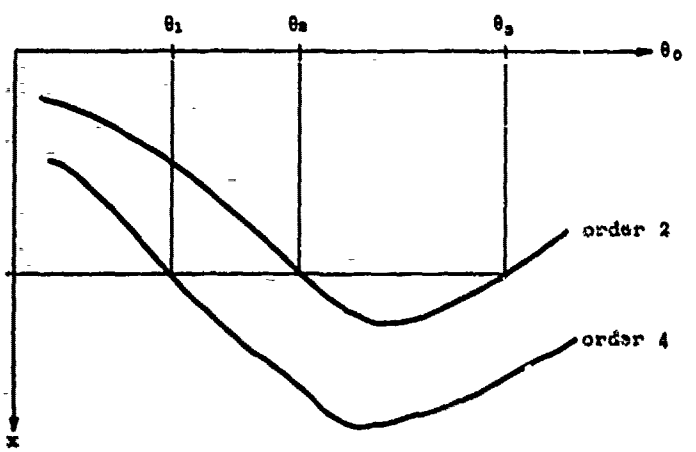

FIG. 5

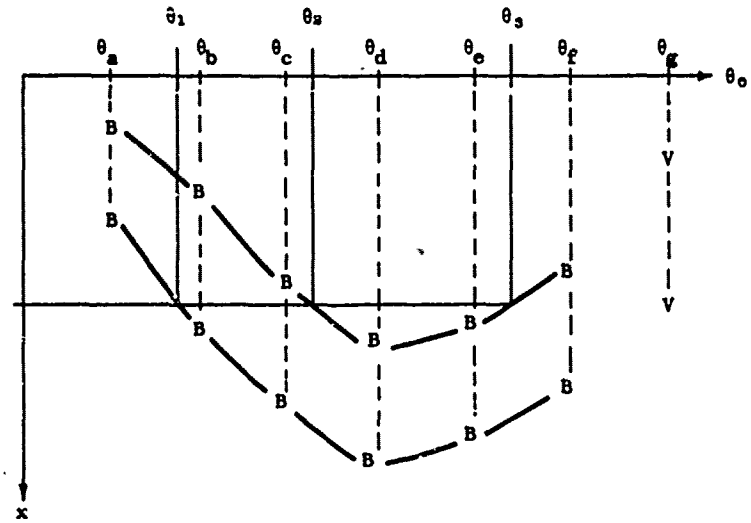

FIG. 6

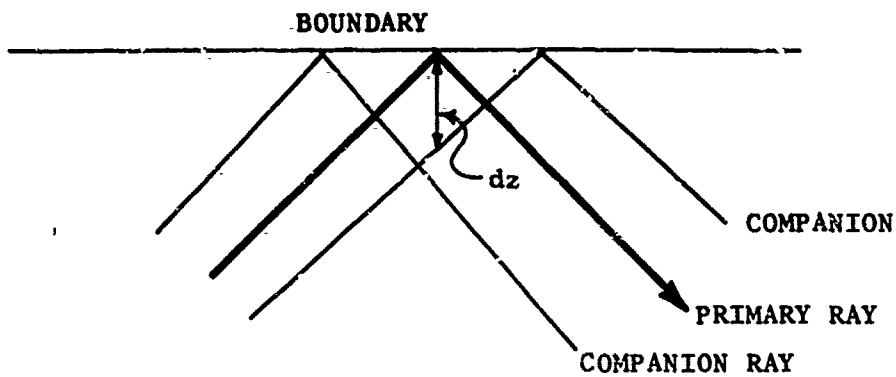

FIG. 7

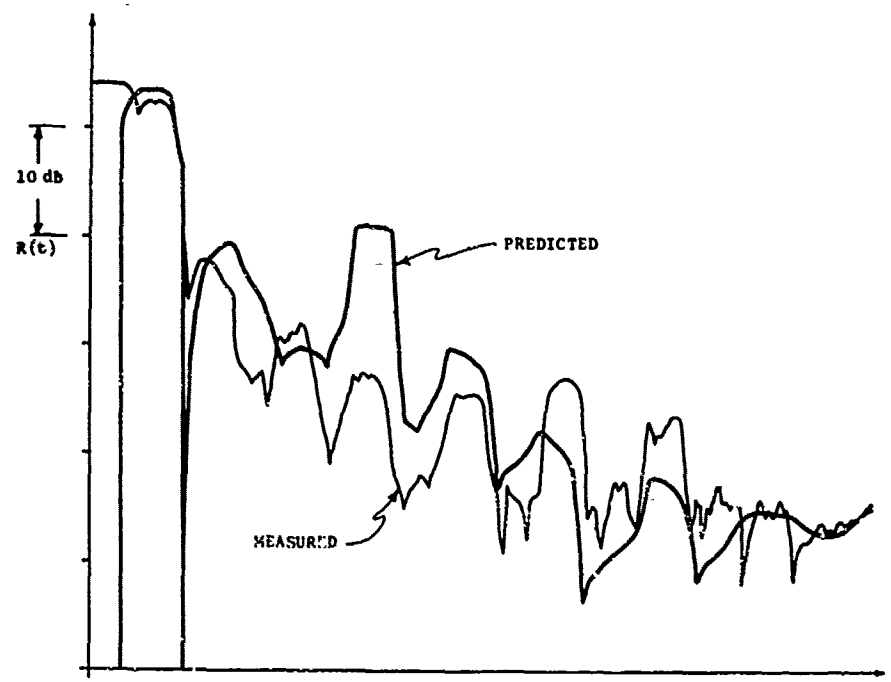

FIG. 8

SESSION 6

APPLICATIONS OF RAY TRACING

Session Chairman : R.H. Prager

Session Secretary : W. Bachmann

ACOUSTIC PROPAGATION MODELS AS VIEWED BY THE SONAR SYSTEMS DESIGNER

by

J.L. Reeves
Naval Ship Systems Command
Washington, D.C., U.S.

ABSTRACT

The purpose of this paper is to consider the efforts performed in the development of ray acoustic propagation analyses from the viewpoint of advanced sonar system design. In particular, those parameters required of such analyses for the enhancement of sonar system design and performance are identified and elaborated upon. A simple ray acoustic shallow water propagation model is used as a vehicle for identitying and relating to a number of areas in which propagation results may be utilized to significantly improve operational sonar system effectiveness. In the development of these examples, the spatial distribution of the acoustic energy together with fluctuations in the received signal energy receive prime consideration. Expanding upon this simple basis, a sonar design concept is developed by analytically incorporating propagation features that can be provided by suitable models.

The orientation of my discussion today is somewhat different from those that have been presented so far in this conference. I intend to talk not as an underwater acoustician actively involved in propagation analysis and the development of ray trace programs.

Rather, from my view point as an engineer faced with the problem of developing sonar systems to operate with maximum efficiency in the ocean medium, I wish to present some of my requirements for information on propagation phenomena.

My reasons for attempting such a presentation are to outline to representatives of the propagation community those aspects of propagation which bear directly on design decisions, and to indicate why simple measures of the energy lost by a signal propagating through the sea are not in themselves sufficient inputs to the sonar design process. In doing this, I hope to indicate to you some specific design-related parameters which characterize propagation phenomena and about which relatively little information exists. Specifically, it is my objective to illustrate why the spatial and temporal behaviour imposed on signals by the medium present inputs to the sonar design process equal in importance to a knowledge of the propagation loss between two points. I hope that this overview will encourage studies in which attention is focused on developing more information about the mechanisms governing these spatial and temporal characteristics which currently are often "washed out" or ignored in analyses directed at developing numbers to characterize average propagation loss.

The general points I wish to consider are outlined in Fig. 1. The usual goals of a programme to develop propagation models, using either ray tracing techniques or normal mode analysis, are twofold, namely:

1. To delineate, on the basis of velocity profiles and other environmental data, the dominant paths via which acoustic signals propagate from source to receiver.
2. To develop a means for estimating the average acoustic power lost by a signal as it propagates between two points. The loss mechanisms involve accounting for geometrical spreading of the wavefront, reflection/scattering, and absorption effects within the medium or at its boundaries.

Once these goals are accomplished, the sonar designer can readily estimate:

1. The average value of the signal present at his array; and
2. The depths at which he can expect high and low levels of signal power.

In general, however, a comprehensive sonar design process requires more detailed knowledge concerning the influences of the medium upon the signal. Specifically, the designer would like to have at his finger tips:

1. The spatial distribution of the signal arrivals at the array.
2. The statistics of both spatial and temporal fluctuations imposed on the signal by the medium; and
3. In the case of short term (transient or pulse) signals, the "impulse response" of the medium; i.e., a measure of the time and frequency dispersion imposed on the original signal.

For the remainder of this paper, I intend to focus on the three areas listed above, and illustrate, by some simple examples, how knowledge of these phenomena may be incorporated into the sonar design process. In particular, I wish to concentrate on the active sonar problem since this area is most urgently in need of more sophisticated techniques.

As a starting point, I would like to consider a simple example to illustrate how a knowledge of the spatial distribution of signal arrivals can impact on the design of a sonar array. The specific case of interest here is one where the impact is greatest, namely, a vertical array for use in a shallow water environment. As used here, the term shallow water implies those instances where propagation takes place over ranges very large relative to water depth, and where the water depth itself is large compared with the wavelength of the signal being propagated.

In such instances (particularly when ranges are such that little energy arrives via a direct path), the signal arrives via multiple surface and bottom reflections. These multiple arrivals imply that the dominant signal energy is distributed over a range of arrival angles rather than being concentrated at a single angle. If this range of angles is known, then the array can be designed to spatially "match" this angular window, and thus insure that maximum signal power is captured by the array.

This can easily be illustrated by use of a very simple ray trace model, which describes the gross features of propagation in a shallow water environment. This model is similar to the one devised by McPherson and Daintith [Ref. 1], and elaborated on by Smith [Ref. 2]. The salient features of this model (which is based on averaging over ray cycles) are shown in Fig. 2.

The details of the model on which the results to be presented are based can be found in the references. Basically, it treats the large number of rays involved in transporting energy from source to receiver as a statistical ensemble. The major features of the propagation mechanisms are preserved, but by use of spatial and temporal averaging over the ranges and depths involved, fine details (i.e., Lloyd's mirror interference phenomena) are smoothed out. However, the fundamental postulates and assumptions which guide the analysis are indicated in the figure.

The postulates are self explanatory; the assumptions are found to be reasonable within the objectives of the analysis, namely, a gross prediction of the propagation loss which preserves the basic sensitivity of the result to the dominant environmental parameters. These are:

1. Water depth.
2. Sound speed profile.
3. Surface loss.
4. Bottom loss.

Although sound velocity profiles are seldom observed to have equal velocity at all depths, the isovelocity model often predicts results close to those observed experimentally in shallow water. The most significant departure from isovelocity behaviour occurs for strong surface ducts and severe upward or downward refraction. The model can, however, be readily extended to include these cases.

The geometry for a simple isovelocity situation is shown in Fig. 3, along with the results of the analysis.

In the isovelocity case β, the loss per cycle from boundary reflection for a ray with initial angle θ, is found to be

$$\beta = b_s\theta + b_b\theta = b(\theta) \quad (\sin\theta = \theta,\ \cos\theta = 1)$$

where

$$b = b_s + b_b \quad .$$

The results of Smith's analysis [Ref. 2] show that the ray cycle method gives the following value of transmission ratio $\tau(r)$ under the isovelocity assumption. (The transmission ratio is the ratio of the intensity at range r to that at 1 yd) and is given by:

$$\tau(r) = \frac{2}{rD}\, e^{-\alpha_v r} \int_0^{\theta_f} e^{-\frac{rb\theta^2}{2D}}\, d\theta$$

The expression in the figure contains twice the integral from 0 (horizontal) to a limiting angle θ_f. For the symmetrical situation, this is equivalent to including all rays from $-\theta_f$ to $+\theta_f$. Note that this integral is of the form of the area under a Gaussian (normal) curve. In their paper, McPherson and Daintith [Ref. 1] obtained a similar isovelocity result by analysing the number of bounces, rather than working with ray cycles. They showed that the result is the same for the sloping bottom case if average depth is used for D. In addition, they derived equations that are quite similar to those shown here for propagation loss under negative gradient conditions.

The distribution of signal arrival angles as determined from the equation for the transmission ratio per radian is shown in Fig. 4.

Note that in isovelocity water the received energy is normally distributed in arrival angle about a mean angle $\vartheta = 0$ with a standard deviation σ that increases with increasing depth and decreases with increased range and bottom absorptivity. The upper limit of the integral for an omnidirectional receiver is $\pi/2$ corresponding to the two cut-off points shown in the figure.

The implications on array design are immediately evident. First, if one designs a vertical array to have a beamwidth of θ_B between say, the 6 dB down points, when steered to the maximum response axis, the choice of θ_B should be dictated by the distribution of signal arrivals as shown in the figure. These, in turn, depend upon the water depth, the range between source and receiver, and the combined bottom and surface losses. While the first two parameters are usually definable for the conditions over which an array must operate, the determination of the surface and bottom losses is not so easily made. However, it is interesting to note that sufficient information for the designer is obtained by developing estimates of average bottom and surface losses over the ocean area of interest. Thus, a useful effort would be to continue work aimed at developing estimates of average bottom and surface losses, parameterized in terms of controlling physical mechanisms (i.e., windspeed, etc.) in areas of interest to the sonar community.

The preceding example results in conclusions which may seem somewhat obvious to people versed in propagation analysis. However, this simple example was intended mainly to illustrate the coupling which exists between the design process and a knowledge of medium effects; the two cannot be separated, nor can simple estimates of energy loss suffice. In this case, the spatial distribution of the energy arrivals impact on design choices; in turn, the design impacts on guiding the propagation analysis by delineating the environmental parameters of importance.

This analysis also points out the types of shallow water propagation models of use to the sonar designer. Essentially, he looks for a model which provides maximum visibility of the physical parameters of the ocean environment which influence sonar performance. In this context, a simple approximate model, which can be rapidly executed may be favoured over an elaborate ray trace model which requires large computer facilities. At the same time, the designer is aware of the limitations of such simple approximate models. In the one employed here, for example, the use of incoherent energy addition of ray paths precludes accounting for spatial phase cancellation effects among rays (e.g., the Lloyd's mirror effect). However, as long as the designer is aware of the model limitations, he can use various sub-models to investigate "fine structure" effects as required. Basically, this amounts to an iterative application of propagation models; i.e., begin with the simplest physical model available, and then expand the analysis through the use of sub-models as the design development dictates.

Of even more relevance to the sonar designer are data concerning the characteristics of fluctuations imposed on the signal by the medium. Sound fluctuations in the ocean are observed for virtually every type of propagation; rface ducts, deep sound channels, sea surface or bottom reflected paths — to name a few. All of these propagation paths can be characterized by an observed mean value of propagation loss around which instantaneous values of transmitted energy are distribute

Too often, modelling efforts are focused on predicting the mean values, with little or no attention given to estimation of the fluctuating components. Yet, often the fluctuations are of primary interest to the sonar designer, in that they impact on his selection of processing times and his estimations of the spatial stability of the signal over the array aperture. Recent work, such as that of Nichols and Young [Ref. 3], and Dyer [Ref. 4] have provided considerable information on the character and statistics of fluctuations; however, more extensive studies are needed if an adequate data base is to be established.

As an example of how such information may be incorporated into the sonar design process, consider the problem of estimating the spatial phase stability of a signal over the aperture of a sonar system. Here, it is important to understand that the degree to which a sonar array can improve signal-to-noise gain and provide directional information is directly related to the degree of stationarity of the phase of the signal wavefront over the array elements. When the array is "steered" to the direction from which the signal arrives, any "jitter" or fluctuations in phase among elements of the array can cause a degradation in performance, in the sense that the signal is not perfectly "in phase" at every element of the array.

This can be illustrated by considering the response of a simple two-element array to a signal arriving from an angle, θ, as shown in Fig. 5. The two identical receivers each generate an output voltage e_o in response to the incoming wave. However, the difference in signal path length between the two receivers results in a spatial phase difference between their outputs. Referenced to the geometric center of the two-element array, the sum of the voltages from the two hydrophones is given as

$$e_T = 2e_o \cos\left(\frac{kd}{2} \sin\theta\right) = 2e_o \cos(\omega\tau)$$

where $k = \frac{2\pi}{\lambda}$, d = element spacing.

Since $k = \omega/c$, where ω is the angular frequency and c the velocity of sound in the medium, the phase term can be written as

$$\cos\left(\frac{\omega d}{c} \sin\theta\right) = \cos\omega\tau$$

where $\tau = \frac{d \sin\theta}{c}$ represents the time delay between constant phase (spatial) arrivals at each hydrophone. Note that when the signal arrives at an angle $\theta = 0$ (i.e. broadside), there is zero time delay, and the output voltage of the array is a maximum; i.e. $2e_o$. Suppose,

however, that fluctuations in the medium produce a fluctuation in the delay time, such that $\tau = \tau_0 + \tau(t)$; i.e. the delay is characterized by a mean value and a fluctuation about that mean. In this case, for a signal incident along maximum response axis ($\theta = 0$), $\tau_0 = 0$, but $\tau(t)$ may be finite. The output of the array in this case is given as

$$e_T = 2e_0 \cos[\omega\tau(t)]$$

where $\tau(t)$ may be treated as a random variable.

To develop an average response we are interested in the expected value of $\cos[\omega\tau(t)]$. This value is given as

$$\langle \cos[\omega\tau(t)] \rangle = \int_{-\infty}^{\infty} p(\tau) \cos \omega\tau \, d\tau$$

where $p(\tau)$ is the probability distribution of the time delay fluctuation. If we assume that the values of $\tau(t)$ are Gaussianly distributed, and have a zero mean, then

$$\langle \cos[\omega\tau(t)] \rangle = \frac{1}{\sqrt{2\pi}\,\sigma_\tau} \int_{-\infty}^{\infty} \cos \omega\tau \, e^{-\tau^2/2\sigma_\tau^2} \, d\tau$$

The result of the integration yielding

$$\langle \cos[\omega\tau(t)] \rangle = e^{-\omega^2\sigma_\tau^2/2} .$$

Since we assumed the amplitudes of the arrivals to be constant, the expected value of the array output voltage is

$$\langle e_T \rangle = 2e_0 \, e^{-\omega^2\sigma_\tau^2/2} .$$

Note that as $\sigma_\tau \to 0$, the array response is maximum. However, as the magnitude of the fluctuations increase, as reflected in increasing values of σ_τ^2 of the value of $\langle e_T \rangle$ decreases from $2e_0$ for "on-beam" arrivals.

Intuitively, one might expect the magnitude of the phase fluctuations to increase in proportion to the separation between elements. Thus, one might assume $\sigma_\tau^2 \alpha d$, i.e. $\sigma_\tau^2 = \gamma d$, where γ is the constant of proportionality. In this case, the expected output voltage of the ideal two-element array is given as

$$\langle e_T \rangle = 2e_0 \, e^{-\gamma \frac{\omega^2 d}{2}} .$$

Note that the degradation in response increase as the frequency, as well as with increased element spacing.

The result derived here, although for a simple, if not trivial, case is illustrative of how such fluctuation information can be used by the sonar designer. The analysis techniques can be readily extended both to include multi-element large arrays, and also to allow for fluctuations in the amplitude of signal arrivals. The main point here, however, is the indication of a need for better measurements of characteristic delay time fluctuations induced by the medium, and most importantly the development of propagation models that incorporate and predict these parameters.

Up to this point, I have been stressing the parameters required of propagation models, in addition to signal attenuation, to produce a driving influence on the sonar design and advanced development process. All too often it seems that the signal processing people proceed independently of the environmental people with the result that the idealizations that appear to perform so well in radar fail to reach expectations in the underwater medium. My message then is that although the question of the best mathematical fit to a sound velocity profile is important, the character of the outputs in both space and time that are obtained from a propagation model are of perhaps greater importance.

As a final example to illustrate this point, I wish to consider a problem in the active sonar area. In general, as the threat becomes more quiet, active sonar must greatly increase its capability to enable more likely detections to occur in a shorter time frame; thereby reducing the threat of counter detection and localization. To achieve this increase in capability in the face of reverberation it appears that more than just an increase in source level will be required. In particular, it seems reasonable that increased gains in signal processing must be obtained. These gains in turn can only result from increased knowledge of the environmental conditions and their effect on the transmitted signal.

Proceeding from this point, let us conceptualize a hypothetical system that might be realizable in the not too distant future. Such a system is shown in block diagram form in Fig. 6. We hypothesize an advanced active sonar sub-system capable of transmitting and receiving sonar signals and displaying the processed results. In addition, we include an environmental measurement sub-system capable of providing real time environmental parameters including measurements of the sound velocity profile. Interfacing these two sub-systems, we envision a ray trace propagation sub-system providing on-site estimates of the signal propagation situation based on the environmental (and historical) inputs. The outputs of the propagation sub-system perhaps with an operator interface dictate the type of sonar transmission mode to be employed, e.g. bottom bounce, direct path, etc., for the mission to be performed and also the type of signal to be transmitted. In addition, the propagation sub-system also determines the type of receiver processing both spatial and temporal to be employed.

To illustrate how these sub-systems might interact, let me consider another simple example, based on some of the propagation modelling that was alluded to earlier in the talk. We assume an environment as depicted in Fig. 7 which might be representative of some generalized area during the winter/early spring months where upward refraction is obtained just below the surface because of the lack

of surface heating. Under the assumption of isogradient conditions, one characteristic of the propagation behaviour is that of a deep surface duct as shown in the figure. If a SVP gradient of 0.025/s is assumed then at short ranges the limiting ray of the duct would reach a vertex of about 200 ft. The rays "trapped" within this limiting ray would be surface-reflected and their energy contribution would arrive after that of the limiting ray. The transmission angle of the limiting ray would be much less than 6°, implying that the surface reflected rays are all reflected at grazing angles less than this value. Since surface reflected paths will undergo very little scattering, at reasonable sea states the sea surface reflection may be considered essentially specular. Under these conditions, the surface-reflected rays will all arrive at essentially the same intensity as that of the non-reflected limiting ray.

The travel time for the limiting ray is the smallest among the duct arrivals and consequently the energy travelling this path is the first to arrive from the duct. The energy travelling e remaining ducted paths will arrive in a non-uniform manner following that of the energy travelling the limiting or refracted-only ray. The order of arrival follows the number of surface reflections. In other words, the energy travelling the one surface reflection path will be following by that travelling the two surface reflection paths, and so on. In terms of our system design, it is envisioned that this type of information would be automatically displayed by our hypothesized ray path computer.

As an approximation for illustrating the method by which the receiver processing might be determined by the ray path computer, let us assume that the ducted multipaths arrive uniformly in time with an equal delay of Δ seconds between each path. If the arrivals are assumed of equal intensity the normalized received signal can be expressed as shown by the equation:

$$s(t) = \frac{1}{N} \sum_{i=1}^{N} \cos(\omega t - \Delta i) \ .$$

In this equation the effects of doppler scattering causing shifts in the received frequency are neglected. The energy envelope of the received signal can easily be expressed by noting that it is of the form of the off-axis response of an equally spaced coherent array [Ref. 5]. In particular, the envelope of $s(t)$ is given by

$$S_e^2 = \left[\frac{\sin(N\omega\Delta/2)}{N\sin(\omega\Delta/2)}\right]^2 .$$

In general there will be a large number of arrivals from the duct, and the delay between arrivals can be considered to approach zero. This fact may be incorporated in the expression by letting $N\to\infty$ while $\Delta\to 0$ with $N\Delta\to\tau$, where τ is the total time delay of the duct. Under these conditions

$$\alpha_c = \left[\frac{\sin(\omega\tau/2)}{\omega\tau/2}\right]^2 \quad ; \quad N\to\infty,\ \Delta\to 0,\ N\Delta\to\tau .$$

This expression is termed the coherency factor and represents the normalized energy arriving via the duct as a function of the transmitted frequency and the duct time delay.

At this point, we require some knowledge of the environment parameters. From the ray trace sub-system, we are able to determine a value for the average duct time delay. If we use the shallow water propagation model referred to earlier in the talk, this is indeed possible. In fact, Smith has shown that for a shallow water isogradient duct, the average duct time delay can be expressed approximately by

$$\tau = \frac{1}{3}\left(\frac{R}{c}\right)\left(\frac{c_b - c_s}{c}\right) .$$

In this equation R is the range of interest, c_s and c_b are the sound velocity values at the source and the vertex of the limiting ray respectively, and c is the nominal velocity of sound in sea water (5000 ft/s). For a SVP gradient of 0.025/s, a depth

difference of 150 ft between the source and the vertex of the limiting ray and for the purpose of illustration a nominal range of 6.5 kyd, then a time delay of 1 ms results.

Given this computation by the propagation sub-system, the sonar operator may determine that the energy transmitted in the duct at least at short ranges is quite concentrated in time. Thus if his sonar can transmit pulse burst transmissions which would generally have pulses long compared to 1 ms he need not concern himself with time dispersion caused by the surface duct transmission. In other words, in this situation he concludes that he need not worry about the time dispersion.

In addition, if all of the reverberation energy associated with the termination of a given pulse decays before the arrival of the next transmitted pulse, then the pulse period within a burst, i.e., the pulse-on to pulse-off duty cycle, should be reasonably stable. All of these results arise from the fact that for a 1 ms duct delay as much as a 100% perturbation caused by medium variations amounts to only a maximum 2 ms delay in the signal time.

At this point, the operator has used the propagation results to indicate the type of propagation to be encountered and the extent of the time delay and in turn has used this information to determine the type of signals he should transmit. Because of the short time delay, he has concluded that gated pulse signals will not be dispersed in time enough to cause them to be distorted greatly. Frequency distortion caused by the multipath situation is another matter of interest to the operator. If he has a range of transmission frequencies available to him he would like to choose a value to minimize the fading characteristics of the signal.

Since the coherency factor has previously been determined this function with the appropriate time delay obtained from the propagation results may be used by the operator to choose from among the frequencies available to him.

Thus, based on calculations provided by the propagation computations the operator may select within the available range, the transmission frequency for which the signal fading is minimized.

The total propagation situation in our example consists of a bottom bounce mode in addition to the surface duct transmission. [See Fig. 7]. In general, the energy arriving via these two paths will interfere and may cause degradation in the total received energy. However, with an adequate ray trace program in the system, it is conceivable that an on-the-spot determination of the arrival time difference between the two paths may be made and that this information could be used to either select an appropriate processing mode to eliminate the effects or by properly assessing the characteristics to use them to advantage. In the former approach, one might select a processor similar to the Rake System in radar which attempts to separate the various energy arrivals and then to coherently recombine them to enhance the total received energy. In the latter technique, by properly assessing the propagation situation, the operator might be able to range on the basis of received signal strength.

Let me consider this latter technique in more detail since it provides a good illustration of incorporating propagation information into the operational problem. Without exact knowledge of bottom topography, it is always difficult to compute the bottom bounce paths; however, a reasonable approach is to assume an essentially flat bottom over the bounce region. If this assumption is made, then for the isogradient case representative calculations indicate that the time delay of the single bottom bounce path relative to the limiting ray (for a gradient of 0.025/s) may be computed to be in the range of 10 ms. This result, of course, is extremely sensitive to parameter changes. However, a good lower bound may be 8 ms with an upper bound as high as 50 ms.

Incorporating this result with the surface channel delay of 1 ms indicates that the total impulse response of the measurement

channel in the short range case we are considering consists of the narrow surface duct response plus a bottom arrival impulse (probably a series of bottom arrivals) delayed 8 ms to 50 ms with respect to the surface arrivals. To keep this example simple let us neglect the multiple bottom bounce arrivals on the basis of energy contributions.

In the duct, the incoherent energy E_{IC} is given by the incoherent addition of the energy of each multipath arrival E_p. This implies that E_{IC} is given by the number of significant arrival paths times the energy per path,

$$E_{IC} = NE_p \ .$$

The coherent energy, on the other hand, is given by

$$E_C = N^2 E_p \alpha_c \ .$$

In this equation α_c is a measure of the coherency. If α_c is 1, the energy arrivals are coherent and maximum energy is obtained. Eliminating N from the two equations results in the equation shown for the coherent energy.

$$E_c = \frac{E_{IC}^2 \alpha_c}{E_p} \ .$$

If one bottom arrival is considered, then it contributes the energy per path E_p modified by the bottom loss factor β. Thus, the ratio of the bottom to duct energy is given by

$$RBD = \frac{E_p/\beta}{E_{IC}^2 \alpha_c / E_p} \ .$$

Since the source is common, the RBD ratio can be expressed in decibels in terms of the duct and bottom path transmission losses. This expression is given below. It expresses the ratio of the bottom to duct energy in terms of the duct and bottom transmission losses, the duct coherency factor and the bottom loss parameter

$$RBD = 2(TL_b - TL_d) - 10 \lg \alpha_c - 10 \lg \beta \ .$$

To utilize this expression, we determine duct and bottom transmission losses from the shallow water (range much greater than depth) propagation loss model of Smith [Ref. 2]. An approximate expression for the transmission loss in an isogradient duct is

$$TL_d = 10 \lg \left(\frac{2\theta_\ell}{L} \frac{e^{-\alpha R_d}}{R_d} \right) .$$

In this equation R_d is the horizontal range between the source and the receiver, α is the volumetric attenuation coefficient as a function of frequency, L is the depth of the duct measured from the surface to the limiting ray, and θ_ℓ is the angle of the limiting ray at the source which is determined by the equation

$$\theta_\ell = \left[\frac{2(c_b - c_o)}{c_o} \right]^{1/2} .$$

Using a sound speed gradient of 0.025/s in these equations and an assumed duct depth of 200 ft, we determine that

$$\theta_\ell = \left(\frac{2(5)}{5000} \right)^{1/2} = \frac{1}{\sqrt{500}} .$$

In addition, for the 200 ft duct we determine the duct transmission loss as

$$TL_d = -28 - 10 \lg R_d - 4.34 \alpha R_d .$$

For the bottom transmission loss assume spherical spreading with a range of essentially the same as that of the duct and a volumetric attenuation α. Thus, the simple spherical spreading loss is

$$TL_b = -20 \lg R_d - 4.34 \alpha R_d .$$

From our previous calculations a representative value of the coherency factor may be determined to be -28 dB. Thus, we may combine our results to obtain the expression for the ratio of the bottom and duct energy,

$$RBD = 2(28 - 10 \lg R_d) + 28 - 10 \lg \beta .$$

Choosing a short horizontal range of 6.5 kyd,

$$RBD = 6 - 10 \lg \beta \ .$$

A reasonable bottom loss value in the range 4 dB to 9 dB may be chosen from Urick [Ref. 6] for a sand type composition. Using this range of values yields the range of RBD values of from 0 dB to -3 dB. Thus, on the basis of these calculations it may be expected that the duct and bottom energy arrivals are of the same order of intensity. This is a significant result for the sonar operator in that it implies that pulse spreading caused by the bottom arrival is of the same order of intensity as that of the duct arrivals.

The combination of the duct and bottom arrivals at a receiver implies a time spreading of an individual pulse and the generation of an interference pattern in the region of time overlap. The magnitude of this interference is most simply investigated by the simple Lloyd's Mirror type of pattern generated by two arrivals of the same frequency. A plot of the expected envelope in the region of overlap is shown in Fig. 8 as a function of operating frequency and the difference between the path arrival times. The curve is also parameterized by the relative intensities of the two arrivals.

An interpretation of this diagram is as follows. Assuming that the energy envelope of the initial pulse arrival is at zero dB (for convenience) when the energy arrives on the second path, an interference pattern is established during the duration of overlap of the two pulses. The magnitude of the envelope during this overlap period is a function of the degree to which the arrivals coherently add (measured by $f\tau$) and their relative intensities (measured in dB) and may be found from the diagram. When time progresses beyond the overlap period, the envelope of the response reduces to that of the second arrival. In terms of the results we have found for the surface duct and bottom path, since the two arrivals are at essentially the same energy, one would expect a relatively continuous pulse with a discontinuity (either an increase or a decrease depending on the $f\tau$ product) during the period of overlap. From

previous calculations the difference between the duct and bottom arrivals can be expected to be on the order of 8 ms to 50 ms. In these ranges one would expect both increases and decreases during the overlap of the duct and bottom arrivals. In addition, of course, the pulse will be spread in time by the later bottom arrival.

Although the computations we have presented may seem somewhat complicated, in reality, of course, they could easily be programmed on a mini-computer. In this manner, the operator could, at least ideally, be presented with an indication of the type of pulse distortion that he might expect and could either alter his frequency or signal shape accordingly.

In summary, I have tried to indicate the importance of propagation models from the view-point of sonar design and future sonar systems. In doing so, I have tried to emphasize that simple predictions of transmission loss are not sufficient for these purposes. Rather, more emphasis must be placed upon the temporal and spatial influences of propagation, the fluctuations encountered, and the interference effects that may occur in transmitted signals. I hope that these remarks may serve to stimulate the direction of future work and operation.

REFERENCES

1. J.D. McPherson and M.J. Daintith, "Practical Model of Shallow-water Acoustic Propagation", J. Acoust. Soc. Am., Vol. 41, April 1967. p.850.

2. P.W. Smith, Jr., "Sound Transmission in Shallow Water; Part I: Analysis", Bolt, Beranek and Newman Inc., Report No. 1563, October 1967.

3. R.H. Nichols and H.J. Young, "Fluctuations in Low-Frequency Acoustic Propagation in the Ocean", J. Acoust. Soc. Am., Vol. 43, 1968, pp. 716-722.

4. I. Dyer, "Statistics of Sound Propagation in the Ocean", J. Acoust. Soc. Am., Vol. 48, 1970, pp. 337-345.

5. F.J. Jackson and R.L. Spooner, "Underwater Communications Environment", Bolt, Beranek and Newman Inc., Arlington, Va., presented at the University of Pennsylvania Symposium on Ocean Engineering, 19-20 November 1970.

6. R.J. Urick, "Principles of Underwater Sound for Engineers", McGraw-Hill Book Co., New York, 1967.

DISCUSSION

When asked whether sonars should not be designed for more general use than just shallow-water operation, the author said that the trend was toward more specialised sonars, otherwise the necessary compromises become too difficult.

PROPAGATION ANALYSIS: USUAL OBJECTIVES

1. DELINEATE DOMINANT PATHS OF ENERGY TRANSMISSION
2. ESTIMATE LOSS IN ENERGY AS SIGNAL PROPAGATION FROM SOURCE TO RECEIVER

PROPAGATION ANALYSIS: ADDITIONAL OBJECTIVES

1. SPATIAL DISTRIBUTION OF SIGNAL ARRIVALS (MULTIPATH EFFECTS)
2. STATISTICS OF SPATIAL AND TEMPORAL FLUCTUATIONS IMPOSED ON SIGNAL BY MEDIUM
3. IMPULSE RESPONSE OF MEDIUM AS IT INFLUENCES SHORT TERM (PULSE OR TRANSIENT SIGNALS)

FIG. 1

SIMPLE SHALLOW WATER PROPAGATION MODEL

REFERENCES: SMITH, P.W. Jr., "SOUND TRANSMISSION IN SHALLOW WATER: PART I: ANALYSIS," BB & N REPORT NO. 1563, OCT. 24, 1967
McPHERSON, J.D., AND JAINTITH, M.J., "PRACTICAL MODEL OF SHALLOW WATER ACOUSTIC PROPAGATION," J. ACOUST. SOC. AM. VOL. 41

RAY CYCLE MODEL (AFTER SMITH)

POSTULATES
1. ENERGY TRAVELS ALONG RAY PATHS
2. ENERGY IS BOTH CONTINUOUSLY ATTENUATED (VOLUME) AND INTERMITTENTLY ATTENUATED (SURFACE + BOTTOM REFLECTION/SCATTERING)
3. ENERGY TRAVELS AT LOCAL SOUND SPEED ALONG RAY

FIG. 2

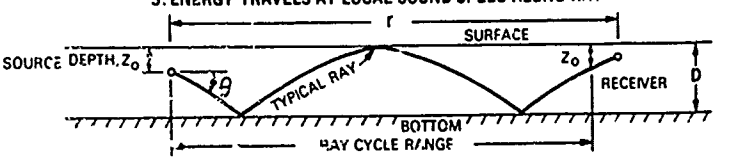

ASSUMPTIONS
1. ONLY RAYS IN WATER CONTRIBUTE (NO BOTTOM REFRACTED PATH)
2. ENERGY SCATTERED TOO FAR OUT OF BEAM ESSENTIALLY LOST
3. BULK OF ENERGY RECEIVED CLUSTERED ABOUT IDEAL RAY PATHS
4. SOURCE-SEQUEN[illegible] OF IMPULSES, RECEIVED SIGNAL $p^2(t)$; i.e. SUPERPOSITION OF ENERGY ARRIVALS (NO INTERFERENCE EFFECTS)

ISOVELOCITY CASE

LOSSES

$\beta = b_s\theta + b_b\theta = b\theta$

$b = b_s + b_b$

b_s = surface loss per ray cycle per radian

b_b = bottom loss per ray cycle per radian

TRANSMISSION LOSS

$N_W = 10 \log \tau$

where

$$\tau = \frac{2}{rD}\, e^{-\alpha_v r} \int_0^{\theta_f} e^{-\frac{rb\theta^2}{2D}}\, d\theta$$

FIG. 3

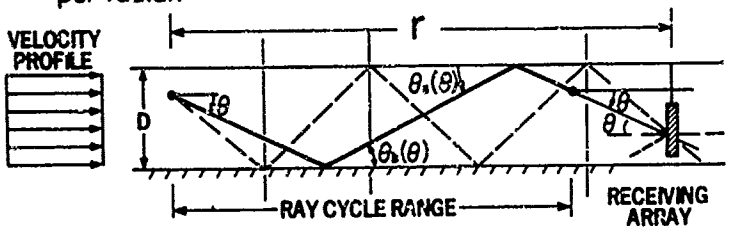

SIGNAL ARRIVAL ANGLES FOR ISOVELOCITY CASE

$$\frac{d\tau}{d\theta} = \frac{2}{rD}\, e^{-\alpha_v r}\, e^{-\frac{\theta^2}{2\sigma_\theta^2}}, \quad \sigma_\theta = \sqrt{\frac{D}{br}}$$

FIG. 4

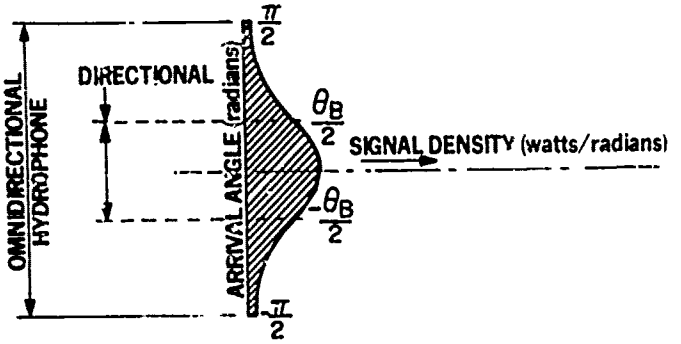

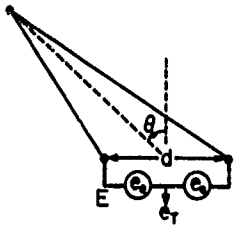

$$k = \frac{2\pi}{\lambda} = \frac{\omega}{c}$$

FIG. 5

$$e_1 = 2e_0 \cos\left[\frac{kd}{2}\sin\theta\right] = 2e_0 \cos[\omega\tau]$$
$$= 2e_0 \text{ when } \tau = 0$$

However, when $\tau = \tau_0 + \tau(t)$

$$\langle e_\tau \rangle = 2e_0\, e^{-\frac{\omega^2\sigma_\tau^2}{2}} = 2e_0 e^{-\frac{\chi\omega^2 d}{2}}$$

for $\tau_0 = 0$

σ_τ^2 = Variance of distribution of $\tau(t)$

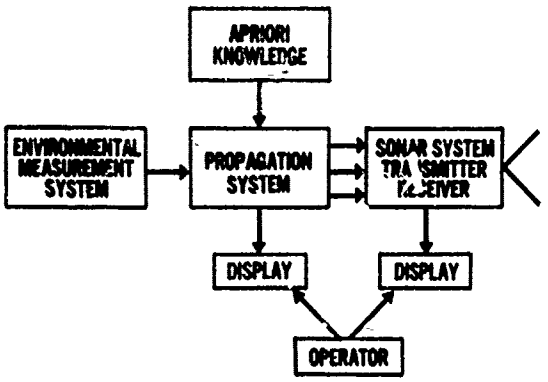

FIG. 6

POSITIVE ISOGRADIENT SHORT RANGE PROPAGATION

FIG. 7

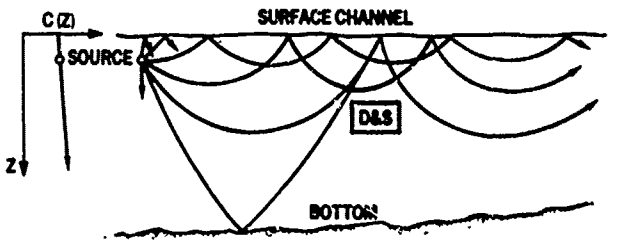

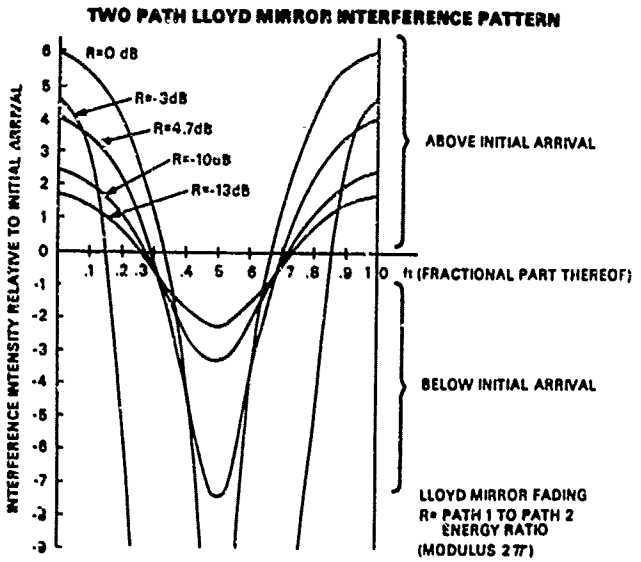

FIG. 8

DETERMINATION OF THE INTENSITY OF SOUND AT ARBITRARY POINTS IN THE SOUND-FIELD OF A SOURCE IN A HORIZONTALLY LAYERED MEDIUM

by

M.J. van der Scheur
Physics Laboratory, T.N.O.,
The Hague, Netherlands

The following method is based on finding all the rays through a point P and to add the corresponding intensities.

Consider a layered medium with a linear depth-velocity profile. The ray-path and the corresponding intensity losses are calculated according to a number of well-known formulae (Fig. 1).

To determine the intensity at P, we add an extra layer through P to the velocity/depth profile. When two rays, leaving the source with starting-angles close to each other, intersect the level through P on both sides of P, there will be generally at least 1 ray with a starting angle between the two mentioned ones, which reach the level at P.

An iterative process will give us the value of θ_o.

Of course we need a set of good starting values for this iterative process. Therefore, we define the characteristic velocities of the depth-velocity profile. These are the greatest velocities of each layer, provided that this value is greater than the velocity at the source-depth, C_B, and greater than all values occurring between the source and the layer considered. The corresponding characteristic values of $K(\theta_o) = \frac{C_B}{\cos\theta_o}$ gives the start angles of the rays, which will turn back just at the limit of a layer.

The horizontal distance between the source and a point on the ray, S, is a function of $K(\theta_o)$: $S = S(K(\theta_o))$. We consider one specified

depth level. S consists of a number of pieces of the type ΔS_1, ΔS_2, ΔS_3 (see Fig. 1). We can write in general

$$S = \sum_{i=1}^{A_1} (\Delta S_1)_i + \sum_{i=1}^{A_2} (\Delta S_2)_i + \sum_{i=1}^{A_3} (\Delta S_3)_i$$

Consider the derivatives of S [Fig. 2]. We see that $\frac{dS}{dK(\theta_0)}$ can be written as the sum of two monotonic functions, one increasing and the other decreasing. From this we can conclude that in the interval between two characteristic values of $K(\theta)$, $\frac{dS}{dK}$ has two zero points: $K(\theta*)$.

Now we add all the values $K(\theta*)$ for which $\frac{dS}{dK} = 0$ to the array of characteristic values $K(\theta)$. This means that in the interval between two successive values of array K, the function of the horizontal distance S at a certain level is monotonic. When two rays with successive values K[i] and K[i+1] intersect the considered level on both sides of P, there will be exactly 1 ray with a starting angle θ between K[i] and K[i+1], intersecting the level in P.

In our computer model the ray path will be symmetric, fixed by three values a, b, c [see Fig. 3].

As you can see, we make a difference between the direct and indirect rays. The n^{th} intersection with the level through P of the ray with value K[i] lies at

$$\text{DISTANCE } (K[i],n) = a + [\tfrac{n}{2}] * b + [\tfrac{n-1}{2}] * c$$

for the indirect rays:

$$\text{INDIST } (K[i],n) = d + [\tfrac{n}{2}] * b + [\tfrac{n-1}{2}] * c$$

K[i]: the array of characteristic starting values.

For every value of n we decide if array K[i] must be completed with values for which $\frac{dS}{dK} = 0$.

Define: $MAX(n) = \max_i DISTANCE(K(i),n)$ $\quad MIN(n) = \min_i DISTANCE(K(i),n)$

When for the horizontal distance between the source and the point P, range P, the following relation holds:

$$MIN(n) \leq \text{range } P \leq MAX(n),$$

then there will be rays intersecting the level considered for the K^{th} time in P.

When we repeat this process for n=1, ..., N both for direct as well as indirect rays, then we will find M rays going through P. For each of these rays we determine the intensity and finally we find for the total transmission loss at P

$$N_{spr} = 10 \log_{10} \left[\sum_{i=1}^{N} \left(\frac{I_o}{I_p} \right)_i \right]$$

Of course there are some restrictions in the present computer model. Except for the restriction of a linear depth-velocity profile the most important assumption is that the sea surface is a flat plate in order to obtain a symmetric ray path. However, there is the possibility of giving an attenuation factor for each surface reflection. For the bottom similar assumptions are made.

When we introduce a waving surface, the simplicity of the computation disappears since the function S becomes much more complicated.

DISCUSSION

The author said that no comparisons had yet been made with measurements.

Transmission loss

$R = \bar{R}(\vartheta_0, k)$: horizontal distance between transmitter and receiver

$$\frac{1}{F} = \frac{\cos\vartheta_0}{\sin\vartheta_n \times R \times \frac{dR}{d\vartheta_0}}$$

Transmission loss in dB $H = 10 \log \left(\frac{R \times \frac{dR}{d\vartheta_0} \times \sin\vartheta_n}{\cos\vartheta_0} \right)$ dB

$k = \frac{c}{\cos\vartheta}$ = constant for 1 ray g : velocity gradient

$k = k(\vartheta_0)$

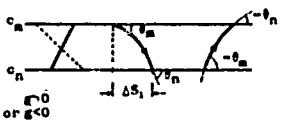

$g \gtrless 0$ or $g < 0$

$$\Delta S_1 = \frac{k}{g}[\sin\vartheta_m - \sin\vartheta_n] = \pm\frac{1}{g}\left[\sqrt{k^2 - c_m^2} - \sqrt{k^2 - c_n^2}\right] \begin{matrix} + \text{ ray down} \\ - \text{ ray up} \end{matrix}$$

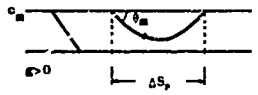

$$\Delta S_2 = \frac{2 \times k}{g} \sin\vartheta_m = \pm\frac{1}{g}\sqrt{k^2 - c_m^2}$$

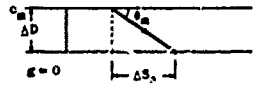

$$\Delta S_3 = \Delta D \times \cot\vartheta_m = \pm\Delta D \times \frac{c_m}{\sqrt{k^2 - c_m^2}}$$

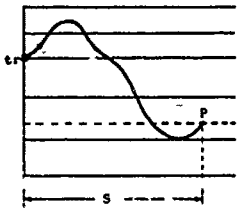

$$S = \sum_{i=1}^{5} (\Delta S_1)_i + \sum_{i=1}^{2} (\Delta S_2)_i + \sum_{i=1}^{0} (\Delta S_3)_i$$

$$\Delta S_1 = \pm\frac{1}{g}\left[\sqrt{k^2 - c_m^2} - \sqrt{k^2 - c_n^2}\right]$$

$$\frac{d(\Delta S_1)}{dk} = \pm\frac{k}{g}\left[\frac{1}{\sqrt{k^2 - c_m^2}} - \frac{1}{\sqrt{k^2 - c_n^2}}\right]$$

$$\frac{d(\Delta S_1)}{dc_m} = \frac{1}{c_m}\frac{d(\Delta S_1)}{dk} = -\Delta D \times \frac{k}{\sqrt{k^2 - c_m^2}}$$

$\frac{d(\Delta S_1)}{dk} < 0$

furthermore : SECOND derivative always POSITIVE
THIRD derivative always NEGATIVE

$\frac{d(\Delta S_1)}{dk}$ is a monotonically increasing function

$$\frac{d(\Delta S_2)}{dk} = \pm\frac{2k}{g}\frac{1}{\sqrt{k^2 - c_m^2}} \quad \text{and} \quad \frac{d(\Delta S_2)}{dk} > 0$$

$\frac{d(\Delta S_2)}{dk}$ is a monotonically decreasing function

$\frac{dS}{dk}$ is a function with two zero-points

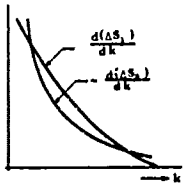

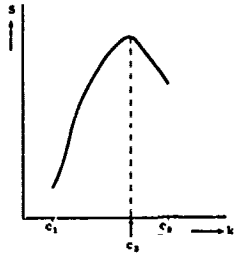

Horizontal distance S as a function of $k(\vartheta_0)$ on a certain depth-level

FIG. 2

FIG. 1

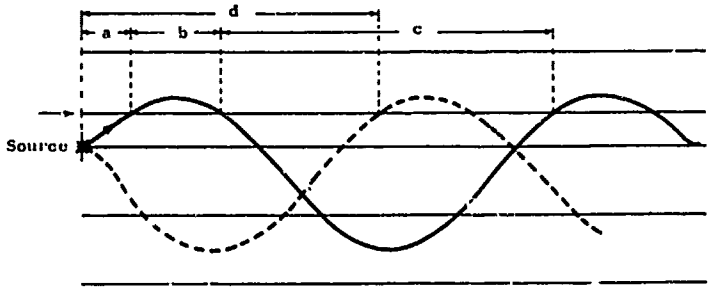

——— Direct Ray

– – – – Indirect Ray

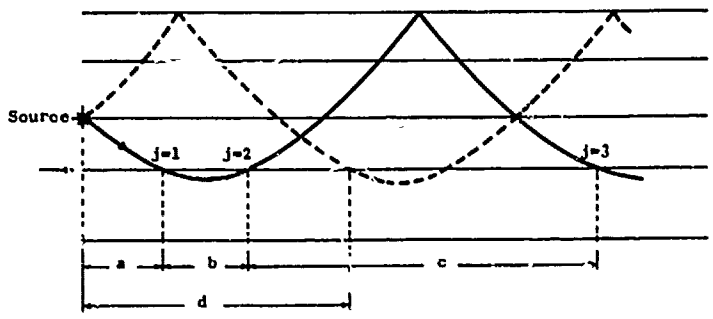

FIG. 3

POSITION AND SHAPE OF THE SURFACE SHADOW ZONE

by

B. de Raigniac
SACLANT ASW Research Centre
La Spezia, Italy

From surface reverberation studies conducted by SACLANTCEN's Target Classification Group*, it has been found necessary to know before any sea experiment the precise position of the first surface shadow zone. Since normal ray tracing programs usually do not answer such a question, a simple computer program has been implemented which, on a small shipborne computer, calculates within seconds: distance, extent and maximum thickness of the shadow zone as a function of the source depth.

From submarine detection trials subsequently performed, it was seen that a more accurate shape of this shadow zone was desirable and an extension of the previous program is underway.

DISTANCE, EXTENT AND THICKNESS OF THE SHADOW ZONE

Figure 1 shows the rays which limit the shadow zone both in range and depth when the source is between the minimum velocity depth and the critical depth. At the surface, the shadow zone is bounded by the rays which have zero grazing angle. The maximum depth of the shadow zone is the depth at which a ray horizontal at source becomes horizontal again. A similar figure would be obtained with a source

* W. Bachmann and B. de Raigniac, "The Calculation of the Surface Backscattering Coefficient of Underwater Sound from Measured Data", SACLANTCEN Technical Memorandum No. 174, November 1971, NATO UNCLASSIFIED

between surface and minimum velocity depth; the shadow zone is then of much larger dimensions. Once the Snell's constant k of the ray is known, the distance to the shadow zone is

$$D = \sum_i R_i \, (\sin \alpha_{i-1} - \sin \alpha_i) \quad , \qquad \text{[Eq. 1]}$$

where R_i is the radius of ray curvature in each layer i, α_{i-1} and α_i are the grazing angles of the ray at the boundaries of the ith layer, and the summation extends over all layers from the source to the surface.

The extent of the shadow zone is given by

$$E = 2 \sum_i R_i \, (\sin \alpha_{i-1} - \sin \alpha_i) \quad , \qquad \text{[Eq. 2]}$$

where the summation is now taken over the layers between the source and the critical depth Z_k .

The maximum thickness of the shadow zone is

$$Z_{max} = Z \Big|_{V = V_s} \qquad \text{[Eq. 3]}$$

where V_s is the sound speed at the source depth.

In Fig. 2 these three quantities are plotted as a function of source depth for a typical summer Mediterranean sound velocity profile.

SHAPE OF THE SHADOW ZONE

Figure 3 gives an idea of the shadow zone as obtained by a conventional ray tracing program. A precise determination of the shape requires a large number of rays and therefore a large amount of computer time is involved, particularly on a small shipborne machine.

An alternative method is to look directly for the rays (in caustics or limiting rays) which delimit the shadow zone. The exact solution is mathematically difficult. The shape is then approximated as the

locus of the points where at closely spaced depths a ray vertexes. As limiting rays may occur when strong negative gradients are predominant, a comparison is performed at each depth between ranges of the vertex points and of intersection of rays vertexing at shallower depth. The points retained are those which indicate a smaller extent of the shadow zone, as indicated in Fig. 4.

Figure 5 shows how the shape of the shadow zone varies as a function of the source depth for the same summer velocity profile. It should be noted how the shape can be complicated and how the single knowledge of distance, extent and maximum thickness may not be sufficient.

In Fig. 6 different shapes are obtained from a typical winter sound velocity profile. It should be noted that the maximum shadow zone depth given by Eq. 3 is not always reached because of limiting rays.

DISCUSSION

In reply to a question, the author reiterated the point that a complete ray tracing was not required to obtain the shape of the shadow zone; the method described being very much simpler than that.

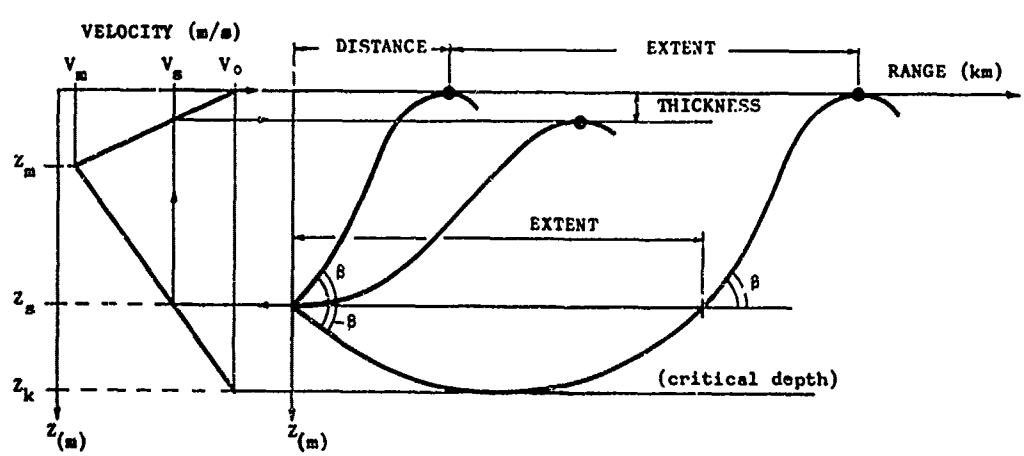

FIG. 1

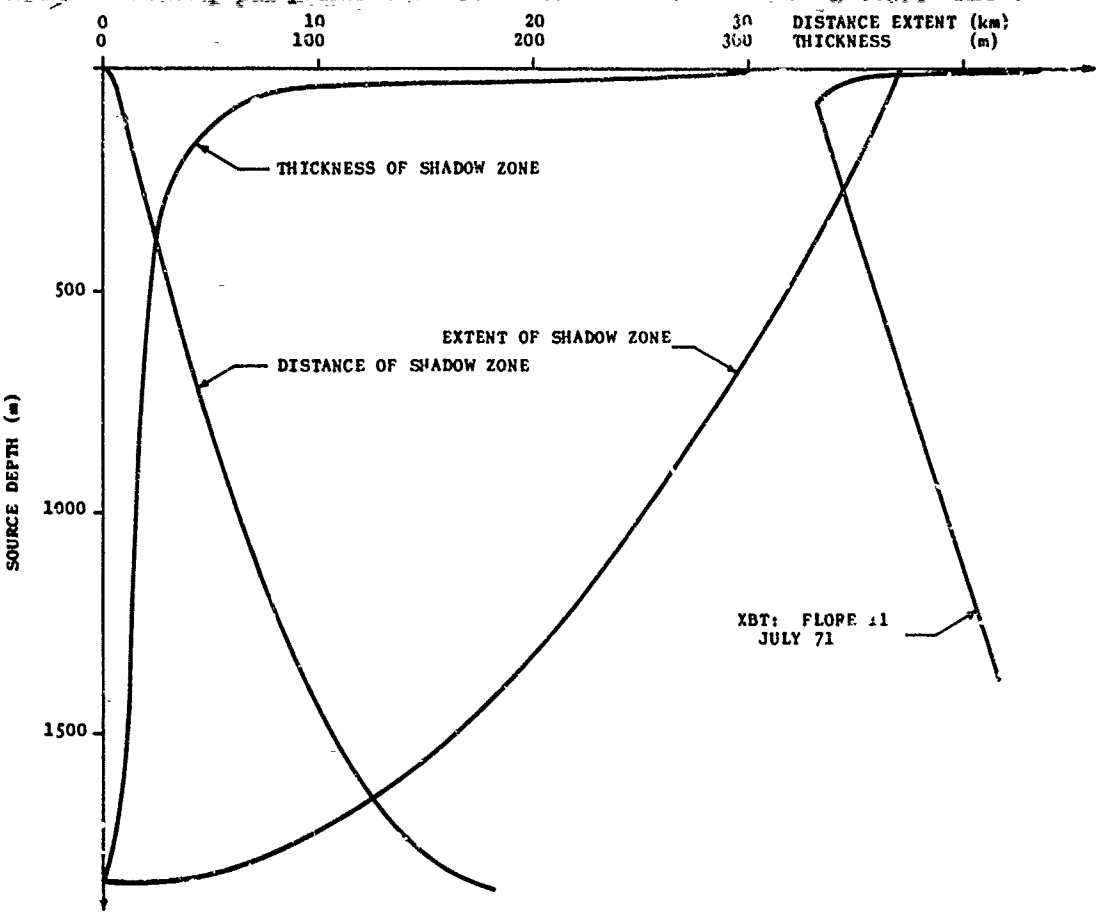
0
0
10
100
20
200
30
300
DISTANCE EXTENT (km)
THICKNESS (m)
THICKNESS OF SHADOW ZONE
EXTENT OF SHADOW ZONE
DISTANCE OF SHADOW ZONE
XBT: FLOPE 1
JULY 71
SOURCE DEPTH (m)
500
1000
1500

FIG. 2

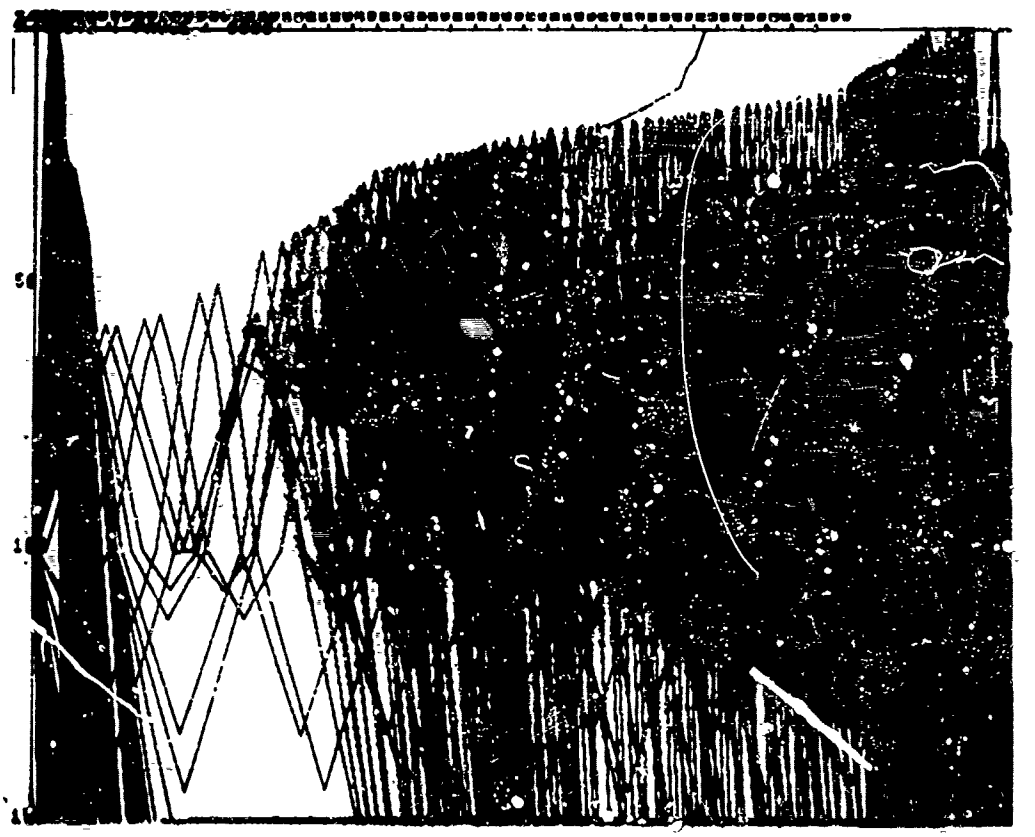

FIG. 3

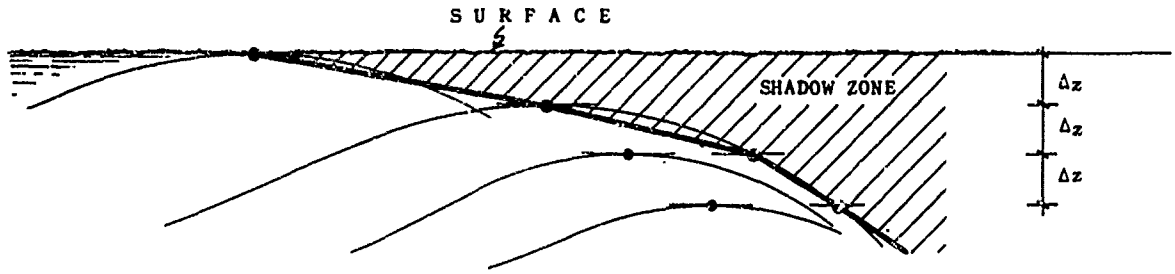

FIG. 4

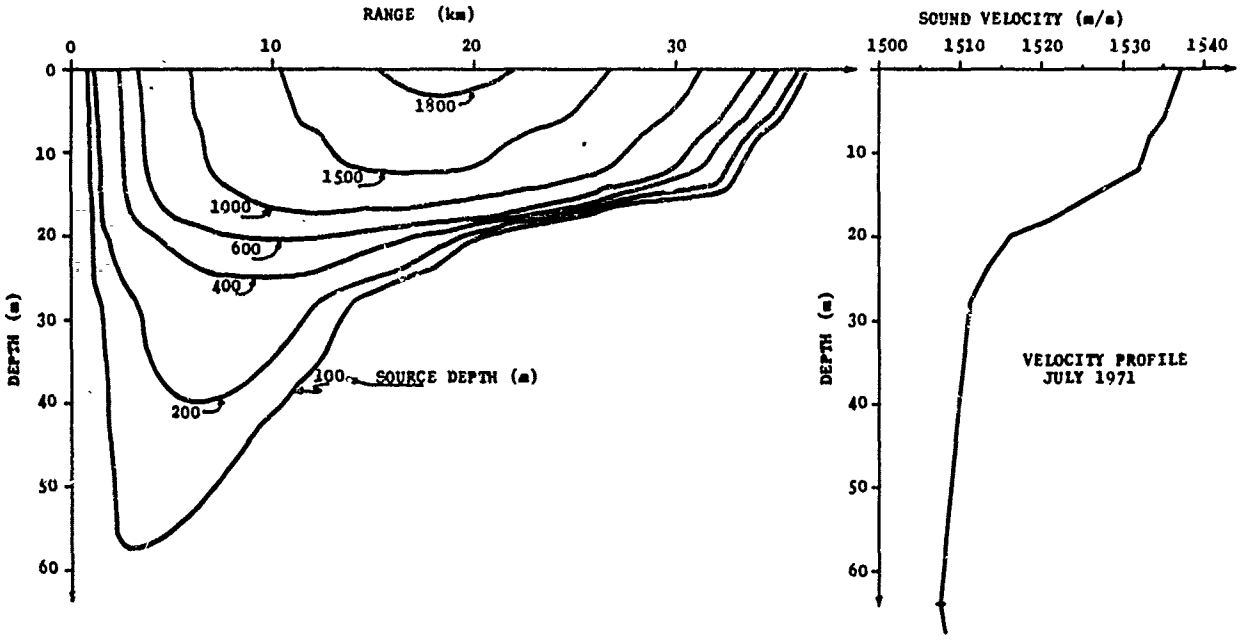

FIG. 5

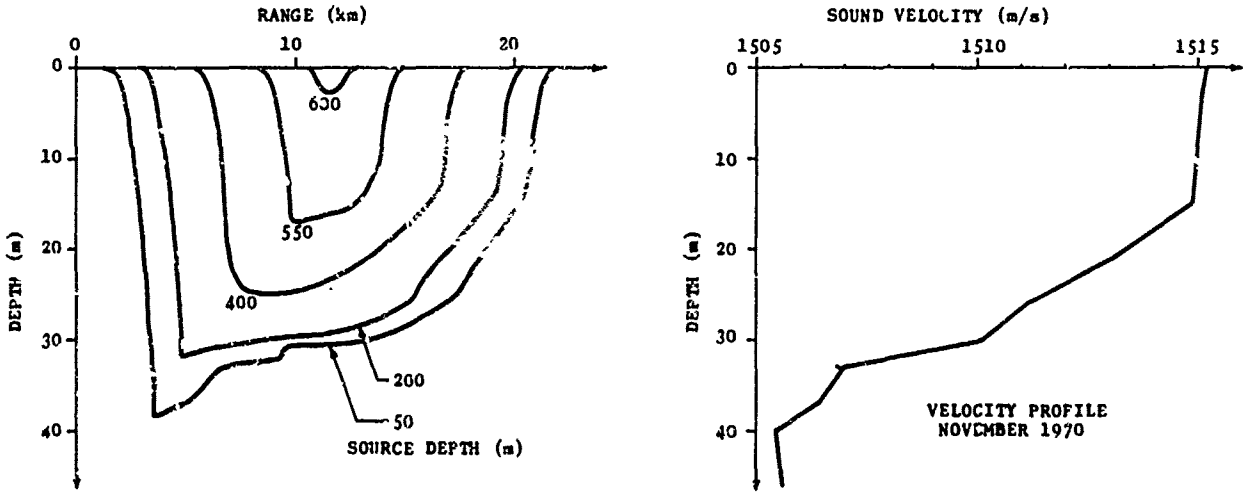

FIG. 6

INFORMAL PRESENTATIONS, CONCLUSIONS AND RECOMMENDATIONS OF THE CONFERENCE

INFORMAL PRESENTATIONS

1. Oceanic-Acoustic Experiments at SACLANTCEN
   by T.D. Allan

2. Acoustic Propagation through Oceanic Fronts
   by M.J. Daintith

SUMMARY AND RECOMMENDATIONS - PERSONAL VIEW

by R.H. Clarke

CONCLUDING GENERAL DISCUSSION

1. OCEANIC-ACOUSTIC EXPERIMENTS AT SACLANTCEN

T.D. Allan (SACLANTCEN, La Spezia, Italy)

Last year, at the Director's suggestion, a project in oceanic-acoustics was set up at the Centre with scientists from at least 3 groups playing some part in the planning and execution of experiments. The project represents a serious effort to break down the older concepts of ASW oceanographers and acousticians following broadly the same research lines but working independently of one another and planning separate cruises. With oceanographers and acousticians working together at sea the acoustic trials benefit from having much more detailed environmental data than usually available in trials while any prediction of sonar conditions that the oceanographer is likely to make from the environmental data can be checked by the acoustician.

The relevance of ray-tracing to this type of research is obvious. It provides the bridge between the observed sound velocity or temperature structure and the predicted sonar conditions with which to compare the observed sonar conditions.

The first oceanic-acoustic cruise was carried out in February 1970 in the N.W. Mediterranean [Fig. 1].

The area chosen for the experiment had been surveyed the previous February during a multi-ship expedition sponsored by the NATO Sub-Committee on Oceanographic Research (MEDOC 69), and it appeared that during winter the Ligurian Sea could be divided into 3 different zones according to the temperature structures shown in Figs. 2 - 4. Acoustic runs were therefore planned as shown by the full lines in Fig. 1. Although hampered by appalling weather the experiment had some success. It certainly showed that acousticians and oceanographers could integrate their programmes with little or no mutual interference.

We were fortunate to be offered the services of one French and two Italian minesweepers besides our own research vessel MARIA PAOLINA. The procedure was planned as follows:

(a) Over the three shorter profiles (10 miles each) the receiving ship, MARIA PAOLINA, was to remain stationary at the end of the profile with hydrophones placed at 25 m, 50 m, 100 m, 200 m and 500 m depth. XBT's to be taken every 10 minutes.

(b) The French minesweeper to act as firing ship opening and closing range on MPG, firing deep and shallow (25 m and 200 m) $\frac{1}{2}$ lb explosive charges every 5 minutes.

(c) The two Italian minesweepers to follow behind the firing ship at distances of $2\frac{1}{2}$ and 5 miles taking XBT's every 10 minutes [see Fig. 5].

(d) Each run to be repeated 3 times in succession.

(e) At the end of the third run the French minesweeper to transmit CW pulses (50 ms pulses at 20 seconds interval, 3.5 kHz) for a period of 1 hour at a fixed range of 10 miles. All four ships to continue to take XBT's every 10 minutes during this time-series experiment.

(f) CW transmissions to be repeated at a range of 5 miles for 1 hour, with the XBT ships again aligned between source and receiver.

(g) For the long profile (20 miles) across the stable and unstable zones the same procedure to be used but with XBT's every 5 minutes. (It might be noted here that the major factor in deciding the time interval between XBT's was simply the total number available to us for the four ships.)

(h) Two self-recording oceanographic buoys with suspended arrays of thermistors (20 from the surface to 300 m) to be situated at positions B_1 and B_2 so that two further temperature inputs would be available along the long profile 2 and one each along profiles 3a and 3b.

As stated, the weather was bad and for more than 80% of the time the minesweepers had to lie in harbour. Not only was the programme severely curtailed but the unusual frequency of high winds contributed to a radically different oceanographic environment in 1970 from that found in 1969.

Of the four acoustic profiles planned, only one complete profile and 1/3 of another (the latter made with two support ships instead of three) could be made. This was a great pity because the procedure went very smoothly at the first attempt. The locations of the XBT measurements are shown in Figs. 6 and 7.

Data Processing and Analysis

All XBT traces were digitised and hence interpolated to provide a temperature reading every 2 m down to 300 m and every 20 m from 300 m to 500 m. Each trace was preceded by an identifying ship number, and distance along the profile from the receiving ship, MARIA PAOLINA.

Through the good offices of Dr J.B. Hersey and Capt P. Wolff, the Fleet Numerical Weather Central, Monterey agreed to carry out the range-dependent ray-tracing required to compare the computed and observed rays from the two sources to the five hydrophones. The following information was requested, firstly, for a ray-trace made with only the BT taken from the firing ship and subsequently for a ray-trace made with 4 simultaneous BT's taken along the profile at the moment of fire:

For each ray:

(i) Path length in metres.

(ii) Travel time in milliseconds to the third decimal place, if possible.

(iii) Propagation loss anomaly, in decibels defined as

$$A = 10 \log_{10} \frac{I}{I_0} + 20 \log_{10} D$$

where I is acoustic intensity at receiver

I_0 is acoustic intensity at 1 m from the source

D is the straight-line distance from source to receiver in metres

(iv) Angle at the source, in degrees measured to the horizontal.

(v) Grazing angle, in degrees, of the surface-reflected rays for each reflection.

This involved a considerable number of ray tracings — over a hundred for the one profile successfully completed as planned.

Although at the time of writing the data analysis is well underway it is, perhaps, too early to try to draw conclusions. There have been some delays caused by working with two computers of different generations but for most of the events we now have plots, for each of ten hydrophone-source combinations, of the various ray paths predicted by four (or more, by moving backwards or forward in time) temperature traces and by the single temperature trace at the firing ship. Similarly all of the observed acoustic data are analysed and plotted for each event. Within a few months we should be able to say how well they match.

A few words on another oceanic-acoustic project carried out again with the help of Monterey. This is an investigation of the acoustic effect of an oceanic front.

Such a front was surveyed in December 1970 by O. Johannessen using the thermistor chain on the LEE (US). Temperature traces measured every 6 minutes along a 45-mile track through the front were digitised and taken to Monterey together with one detailed section of 8 miles in the centre of the frontal region where the sampling interval was 90 seconds.

From these traces, propagation loss has been calculated in both directions through the front (east-west and west-east) for a variety of source and receiver depths and for three frequencies. The computer calculations already show that there are significant differences in propagation loss in the two directions.
In December 1971 it is hoped to measure the effect directly in another joint oceanic-acoustic cruise.

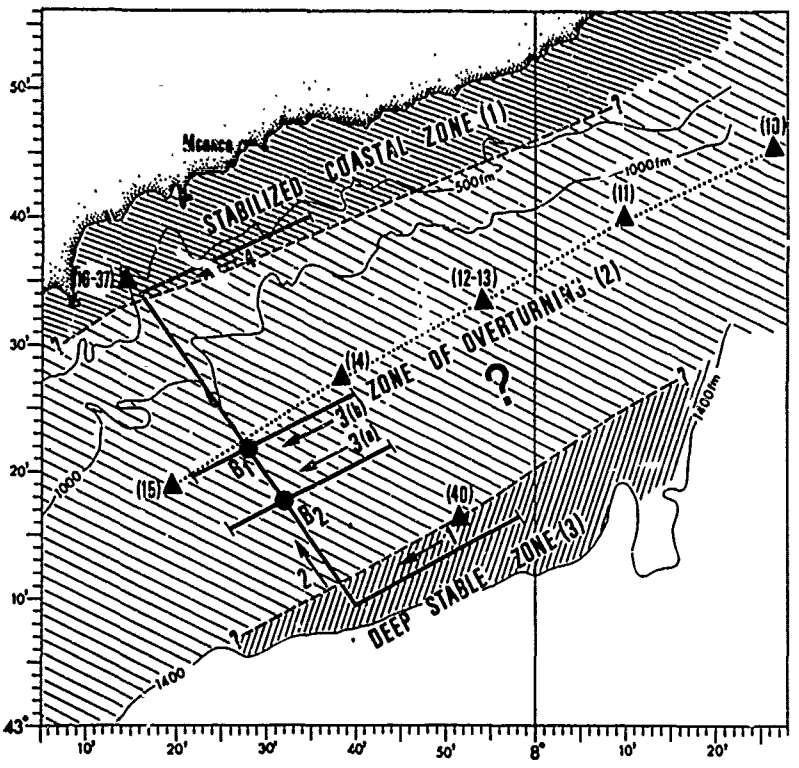

FIG. 1 LOCATION OF ACOUSTIC RUNS PLANNED FOR THE FEBRUARY CRUISE

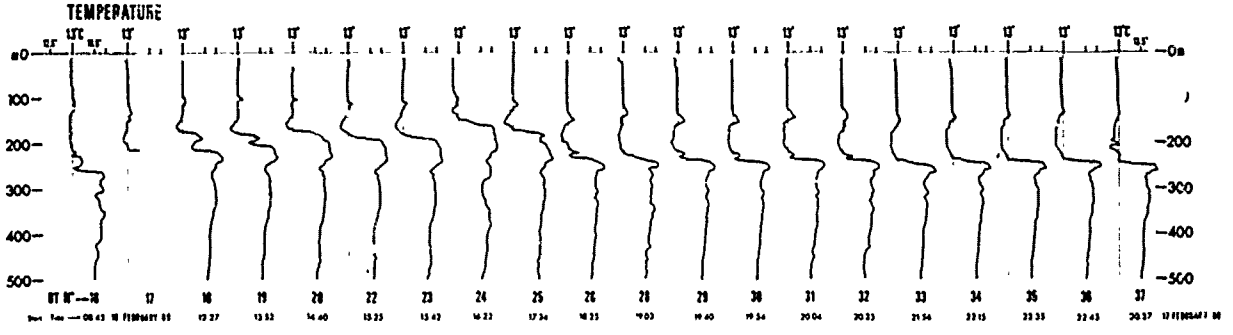

FIG. 2 TEMPERATURE PROFILES TAKEN APPROXIMATELY EVERY HOUR AT ONE STATION IN THE STABILISED COASTAL ZONE (MEDOC 69)

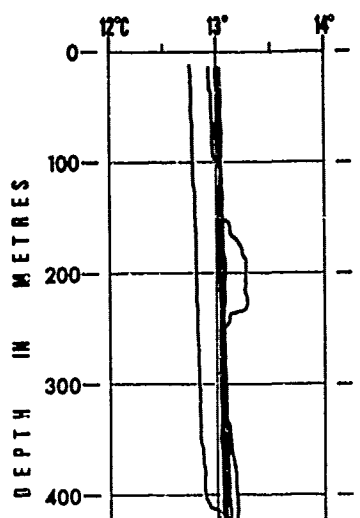

FIG. 3 SUPERIMPOSED TEMPERATURE PROFILES FROM STATIONS IN THE ISOTHERMAL ZONE (MEDOC 69)

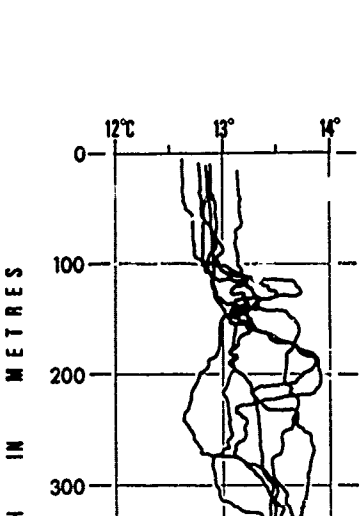

FIG. 4 SUPERIMPOSED TEMPERATURE PROFILES FROM STATIONS IN THE ZONE OF OVERTURNING (MEDOC 69)

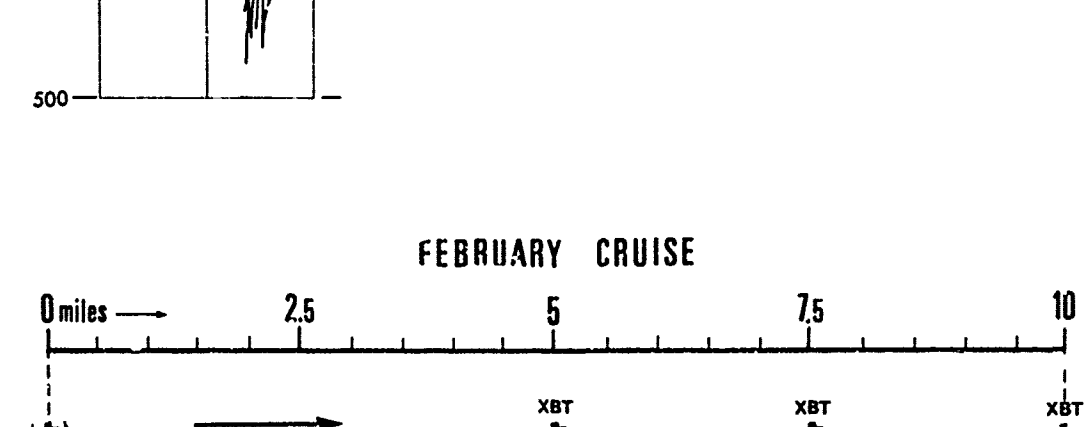

FIG. 5 PLAN FOR THE OCEANOGRAPHIC/ACOUSTIC MEASUREMENTS ALONG THE SHORT RUNS. Each ship to take an XBT every 10 minutes with the firing ship exploding deep and shallow charges every 5 minutes. MARIA PAOLINA stationary at the end of the profile with hydrophones at 5 depths

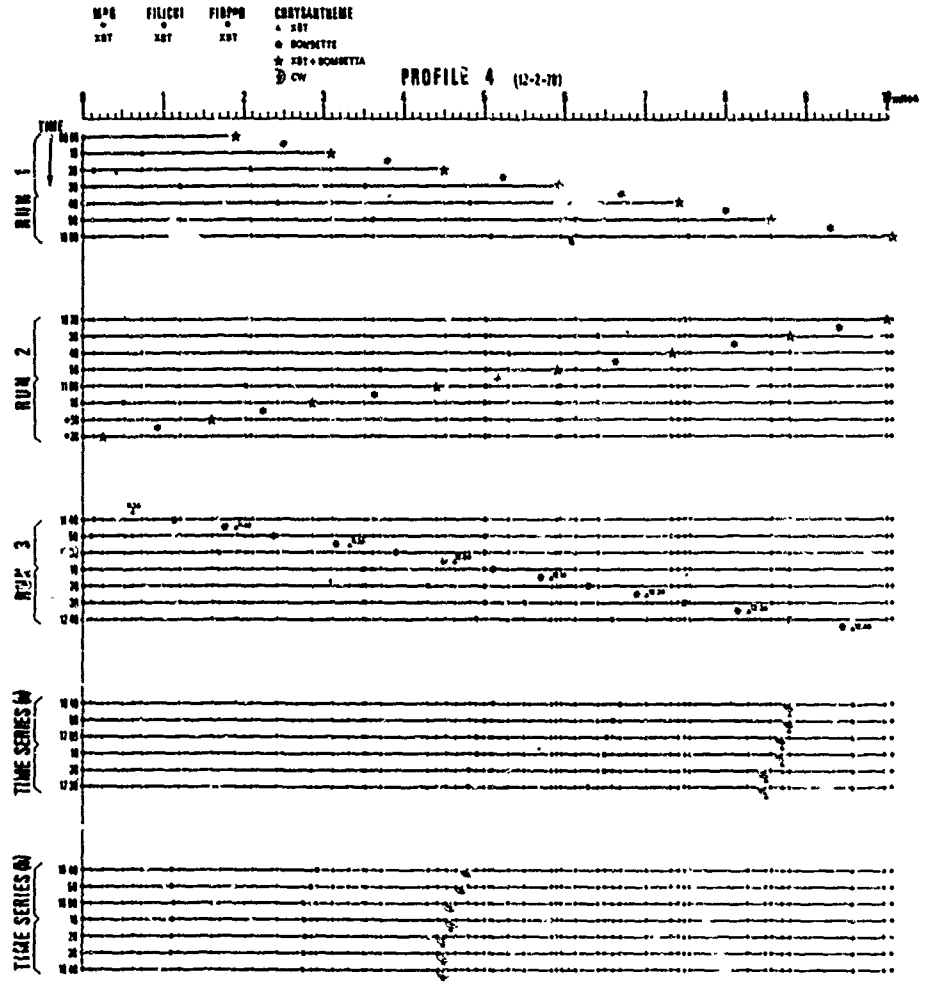

FIG. 6 LOCATION OF XBT MEASUREMENTS ALONG PROFILE 4.
Heavy, full circles indicate an XBT taken at the time shown. Open circles represent history of XBT measurements throughout the acoustic runs.

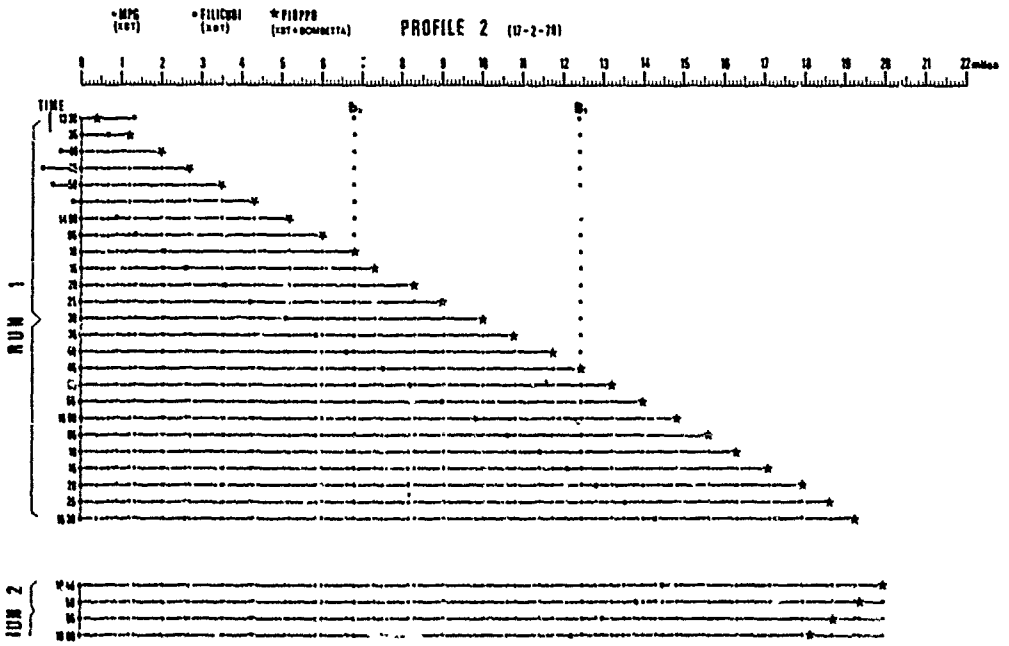

FIG. 7 LOCATION OF XBT MEASUREMENTS ALONG PROFILE 2.
Heavy, full circles indicate an XBT taken at the time shown. Open circles represent history of XBT measurements throughout the acoustic runs.

2. ACOUSTIC PROPAGATION THROUGH OCEANIC FRONTS

M.J. Daintith (A.U.W.E., Portland, Dorset, U.K.)

A résumé was given of recent experiments in the Mediterranean, East of Malta, designed as a preliminary test of the effect of oceanic fronts on acoustic propagation. It was apparent that in certain circumstances the propagation loss was considerably increased by the presence of a front; and it seems likely that the front's presence could lead to significant bearing errors.

SUMMARY AND RECOMMENDATIONS - A PERSONAL VIEW

by

Richard H. Clarke, Conference Secretary

An unfortunate first impression might be that ray tracing is dull, simply because the idea is a very old one. In fact, ray tracing is the single most powerful method available to us for understanding the complexities of sound propagation in the ocean. And gaining this understanding is quite literally all our business. I will take the main topics of the conference in turn, attempt to give a personal summary of what has been presented, and suggest where future research should be directed.

The Ocean

We learned, or were forcefully reminded, that far from being uniform in the horizontal direction there are drastic changes that occur across fronts (analogous to atmospheric fronts), and that these fronts can be found in all oceans and seas. Further than that, the temperature and salinity (and hence the sound velocity) are not continuous in depth but often proceed in steps of isothermal and isohaline water, separated by thin sheets across which the temperature and salinity change abruptly.

As acousticians we must thank the oceanographers for their awkward findings, but press them to give us more detail; both about the fine structure of temperature and salintiy and its global occurrence.

Sound Velocity

That vital link which joins the oceanographer's description of the ocean to the acoustician's has made great strides in the last thirty years or so. But it is obvious that there is much painstaking work to do particularly with regard to pressure and depth. I will come back to this point later, in connection with modified ray theory.

Computations

This subject has reached a satisfactorily advanced stage, in consonance with the enormous and rapid machines that are now available.

I have a very strong feeling, however, that now is the time to stand back and try to fit the computational aspects of ray tracing into a sensible perspective. A good example is the use of a mini-computer: obviously essential in small laboratories, or on board ship, where it is an invaluable tool in conducting fruitful experiments at sea; but equally valuable in computer investigations where the ultimate in accuracy or detail is not required (and would indeed be a hindrance, especially when such things as turn-around time and availability are concerned) such as in O.R. work, tests of ray tracing sensitivity, etc. But my general point is that we should seek a rational balance between such things as computational sophistication, required accuracy, accuracy of input data, computer availability, cost, flexibility — and even decay time of scientists' enthusiasm.

To go back to the beginning: we now have a variety of options with which to fit the sound velocity profile — linear segments, continuous gradients, Epstein segments, polynomials, splines, and so on.

This leads to the fundamental computational question of whether (a) to fit the profile with segments for which there is an

easily obtained solution, or (b) to use something like a spline fit and ask for a differential-equation solution. The linear-segment fit still seems the most convenient choice for mini-computers. But on large computers the choice between (a) and (b) when one looks ahead, say, for the next five years seems much more problematical. Perhaps approach (a) is more suited to plotting rays and calculating travel times, whereas the differential equation approach yields more reliable intensities. It may still be too early to decide the point, but the point nevertheless needs attention.

What does the ocean think of all this? Possibly it feels a bit like a transvestite The sound velocity in a step-structure ocean is a series of linear segments, separated by discontinuities. So, the sound velocity is not necessarily continuous in its zeroth, first, or second – order derivatives. But more of this later.

We did not hear very much about ray-tracing when the sound velocity has a bivariate profile, although we are told that this often is the case in reality. From a computational view point there is again the choice between (a) seeking simple ray solutions in rectangular sections corresponding to particularly chosen forms of profile and (b) seeking differential-equation solutions in regions where the velocity description is made by something like bicubic splines. However, we are not aware of any useful simple solutions, so the differential equation approach looks more promising at the present time.

Finally, with regard to ray tracing computations, what is the general feeling about applying tests in the manner of Moler and Solomon's use of Pederson and Gordon's Epstein profile results? We have recently launched a modest venture at SACLANTCEN in this direction, with beneficial results. Has anayone's experience suggested using Epstein profiles different from that used by Moler and Solomon? It seems that such test programs would be invaluable in the evaluation of ray-tracing programs, regarding not only their accuracy, but also their convenience, speed and cost.

Experiments

Due to the unclassified nature of our discussions in the last few days, there may be many more experiments than we have heard about. Nevertheless, I feel that the experimental validation of ray tracing has hardly started. This is a pity, since the challenge of obtaining consistent and convincing explanations of experimental results is the mainspring of modern science — it would have very beneficial effects on the development of new theories and computational techniques. Of course, one should continually remind onself of the painstaking care required and, with experiments at sea, the sheer physical difficulty of even performing them. And overall, it seemed to me, "the agreement between theory and experiment was encouraging".

But for the future, one can hope for more and better experiments. It would be particularly useful to have many more experiments of the joint acoustic-oceanographic type, such as the experiment just described by T.D. Allan, in which dense spatial and temporal sampling of the temperature structure of the ocean is combined with acoustic propagation experiments, and the acoustic propagation through known fronts just described by M.J. Daintith.

Extensions to Ray Tracing

There appears to have been a considerable increase in understanding of the behaviour of sound fields in the region of caustics, turning points, and shadow boundaries. Some aspects of modified ray analysis are positively seductive. However, these topics are excellent examples of where the acid test of comparison with experiments is essential for future progress to occur; experiments not only in sound propagation but also in the determination of the sound velocity itself at depth.

Theory

I started by admitting that ray theory is an old subject, but the papers on the Riesz Potential and Hamiltonian methods

demonstrated that fresh view points can be taken which may offer the benefit of techniques adopted in other disciplines. They certainly merit very careful consideration. The demonstration of the equivalence of the ray and wave approaches promises advances in the description of propagation in a medium with statistically defined properties.

It was encouraging to hear of efforts being made to put quantitative limits on the oft-quoted conditions for the validity of ray theory. Obviously a great deal more needs to be done in this direction, with particular attention paid to the obliquity of the ray, as well as the scale size of the irregularities in terms of acoustic wavelength.

A related topic is the validity of ray tracing at the discontinuous sheets separating the layers of a step-structure ocean. Of course, these discontinuities are physically large gradients, which can be viewed as discontinuities under certain conditions of sheet thickness to wavelength ratio and ray angle. But it is important to know what these conditions are; and what happens when the conditions are violated.

We heard a little about what we might expect when a sound-velocity profile, or other oceanographic feature, is specified statistically. This is an important avenue that has hardly been entered. Though difficult, statistical approaches must be used to deal honestly with the real ocean. Perhaps the most promising first step is to examine the sensitivity of ray tracing to perturbations in the gradient or other features of the profile, and then to extend this to statistically specified profiles, either by analytical or numerical means.

Applications

The application of ray tracing to reverberation modelling is obviously receiving considerable attention, with encouraging agreement with observations.

It was salutary to be reminded that the most important channel of our work lands up on the desk of the sonar systems designer, and extremely useful to have stated with such clarity his requirements.

CONCLUDING GENERAL DISCUSSION

The Medium

There was very little reaction by the meeting to the oceanographers' revelations concerning the step-like structure of the sound speed. A plea was made for more salinity data in these investigations.

It was pointed out that it was necessary for acousticians to specify the fineness of detail required in oceanographic measurements.

Conventional Ray Tracing

The considerable fraction of the discussion devoted to the various aspects of conventional ray tracing indicated a general concern with a need to refine present methods. Some of the points raised in this connection were:

Is it possible to obtain reliable answers while still employing a linear-segment approximation to the sound-speed profile, either by taking a sufficiently large number of segments, or by smoothing the output in some suitable manner?

There is a possible danger in the use of spline fits to sound-speed data that it might sometimes introduce artificial wiggles in the sound-speed profile, perhaps leading to local gradients of sign opposite to the actual gradient, for example. The opposing view was put that "splines are fine", provided that one works with sufficient data points and takes care with the end conditions.

An alternative approach to making a rational fit to sound-speed data was that the fit should be continuous up to, and including, the second derivative, but that the correct morphology should be retained — presumably judged on oceanographic grounds.

The possibility was mentioned of finding the eigenrays by the direct numerical application of Fermat's principle, as an alternative to the "shooting" method.

A variety of profiles, for which there are analytical solutions is available from L.P. Solomon, Tetra Tech., Inc., 1911 Fort Meyer Drive, Suite 601, Arlington, Virginia 22209, U.S These could be useful for testing ray tracing programs.

Range-Dependent Ray Tracing

A recurring theme during the discussion was the need to extend present ray tracing capability to bivariate sound-speed profiles, and eventually to trivariate profiles. But there were no clear ideas put forward as to how this could best be achieved.

Current methods include simply dividing the range into blocks, each block having a sound speed that depends on depth only, and then proceeding with the usual univariate methods within each block. Another technique is to divide the range between given profiles into triangular sections, the ray paths within each section then being circular arcs. Both these techniques suffer from implying oceanographically unacceptable sound-speed structures in regions between the given profiles.

Mention was made of the Hudson Laboratories technique employing a special form of double Taylor series expansion (linear variation in range, linear plus curvature term in depth) specifying the sound speed in the region between two given profiles. There is also the possibility of representing the bivariate sound speed in terms of doubly-cubic spline functions. In both these cases the ray tracing could then be accomplished by numerically solving the ray differential equations.

Statistical Aspects and Profile Sensitivity

A difficult problem, but one requiring urgent attention, is that of allowing for the effect of the variability of the sound-speed profile. This can be viewed as a problem of the sensitivity of ray tracing to certain perturbations of the sound-speed profile. Or it can be viewed as a statistical problem, requiring the statistics of the output of ray tracing given the statistics of the input profile(s).

The sensitivity problem is important when considering the adequacy of proposed methods of curve fitting to the given sound-speed data points.

A major difficulty with the statistical problem is that of posing the problem properly. For example, if one starts with a mean profile (obtained by averaging a large collection of profiles) this profile may be devoid of all the features (such as layer depth) which are known to affect the sound propagation drastically. Therefore, some method should be found by which the essential character of the profiles is preserved. In other words, one should work with a "typical" profile, rather than with a strictly "mean" profile.

But more significant than working with mean values, the second-order statistics of the ray tracing output are an important measure of the variability caused by variations of the sound-speed profiles as inputs to ray tracing programs.

General Points

The opinion was expressed that insufficient attention had been paid to the final objectives of ray tracing in an ASW context. If we are not approaching anything of value, we might as well stop now and turn our attention to potentially more fruitful subjects, such as loudspeaker design!

Two drastic alternatives to the present highly computer-orientated approach to the solution of underwater sound propagation problems were proposed. One was to replace computers by mathematicians who would be cheaper, and whose task would be to develop alternative and more amenable theoretical approaches. The other alternative was to de-emphasize computers and mathematicians, and to accentuate in compensation experiments at sea. In other words, it might be easier and more reliable to use the Oceanic analogue computer.

There is, naturally, a bias of American interests towards low-frequency, long-range propagation, whereas SACLANTCEN interest is concentrated more on relatively short ranges at sonar frequencies. Thus the outcome of modified ray theory appears to be of greater interest to the former than to the latter; although some intriguing discrepancies between experiment and conventional ray theory at the shorter ranges need to be scrutinized in the light of modified ray theory.